Robust Trajectory Tracking of Mobile Manipulators Based On Extended State Observer and Nonlinear Control

by

Mhmed ALGRNAODI

THESIS PRESENTED TO ÉCOLE DE TECHNOLOGIE SUPÉRIEURE
IN PARTIAL FULFILLMENT FOR THE DEGREE OF
DOCTOR OF PHILOSOPHY
Ph.D.

MONTREAL, "FEBRUARY 17, 2026"

ÉCOLE DE TECHNOLOGIE SUPÉRIEURE
UNIVERSITÉ DU QUÉBEC

BOARD OF EXAMINERS

THIS THESIS HAS BEEN EVALUATED

BY THE FOLLOWING BOARD OF EXAMINERS

Prof. Maarouf Saad, Thesis supervisor
Department of Electrical Engineering, École de technologie supérieure

Prof. Mohamad Saad, Thesis Co-Supervisor
School of Engineering, Université du Québec en Abitibi-Témiscamingue (UQAT)

Prof. Raouf Fareh, Thesis Co-Supervisor
Department of Electrical Engineering, University of Sharjah, Sharjah, UAE

Prof. Christian Belleau, Chair, Board of Examiners
Department of Mechanical Engineering, École de technologie supérieure

Prof. Vahé Nerguizian, Member of the Jury
Department of Electrical Engineering, École de technologie supérieure

Prof. Yassine Kali, External Examiner
School of Engineering, Université du Québec en Abitibi-Témiscamingue (UQAT)

Prof. Azeddine Kaddouri, External Independent Examiner
Department of Electrical Engineering, Université de Moncton

THIS THESIS WAS PRESENTED AND DEFENDED

IN THE PRESENCE OF A BOARD OF EXAMINERS AND THE PUBLIC

ON "JANUARY 26, 2026"

AT ÉCOLE DE TECHNOLOGIE SUPÉRIEURE

ACKNOWLEDGEMENTS

First and foremost, I would like to express my deepest gratitude to my supervisor, Prof. Maarouf Saad, for his invaluable guidance, encouragement, and insightful supervision throughout my doctoral journey. His scientific rigor, patience, and constant support have been the cornerstone of this work.

My sincere appreciation also goes to my co-supervisors, Prof. Mohamad Saad and Prof. Raouf Fareh, for their constructive advice, continuous encouragement, and many fruitful discussions that have greatly enriched both the theoretical and experimental aspects of this research.

I would like to extend my heartfelt thanks to Prof. Yassine Kali, whose assistance in the laboratory, collaboration on improving the journal papers, and significant contributions to this research were truly invaluable. His guidance and support were essential to the success of this work.

I am also honoured by the presence of all the members of the examination board, whose insightful comments and recommendations have greatly improved the quality and clarity of this dissertation. I wish to express my sincere gratitude to Prof. Christian Belleau, Prof. Vahé Nerguizian, and Prof. Azeddine Kaddouri for taking the time to help me progress as a researcher and for kindly agreeing to serve on my Ph.D. examination committee.

Special thanks are extended to my colleagues and friends at the GREPCI Laboratory at ÉTS for their collaboration, friendship, and continuous motivation throughout my research years. Their support created a stimulating and pleasant working environment.

Finally, I dedicate this achievement to my beloved family: my wife Amina; my children Hamam, Harith, Fares, and Asser; and my loving parents. In particular, this work is dedicated to the memory of my father, who devoted his life to our family, and to my supportive brothers and sisters. Their love, patience, and unwavering encouragement have been the driving force behind this accomplishment and a constant source of strength through every challenge.

Suivi de trajectoire des manipulateurs mobiles basé sur la commande non linéaire et l'observateur d'état étendu

Mhmed ALGRNAODI

RÉSUMÉ

Cette thèse de doctorat propose et valide expérimentalement des stratégies de commande non linéaire basées sur des observateurs d'état étendus pour le suivi de trajectoire en temps réel de manipulateurs mobiles (MM) opérant dans des environnements incertains et dynamiques. Les approches développées visent à surmonter les limitations des méthodes de commande conventionnelles dans la gestion du couplage non linéaire, des incertitudes paramétriques et des perturbations externes, qui affectent significativement la stabilité et la précision de suivi des manipulateurs mobiles.

Les manipulateurs mobiles combinent la dextérité des bras robotiques ayant plusieurs degrés de liberté avec la mobilité des plateformes à roues, élargissant ainsi leur espace de travail opérationnel et permettant des applications dans l'automatisation industrielle, l'assistance médicale et l'exploration planétaire. Cependant, leur dynamique complexe et couplée, caractérisée par des contraintes non holonomes et des sous-systèmes interconnectés, rend le suivi de trajectoire une tâche particulièrement difficile. Cette recherche aborde ces défis en développant un cadre unifié observateur-contrôleur qui garantit des performances de suivi de trajectoire robustes, de haute précision et à temps fixe.

La première partie de la recherche introduit un schéma de commande par rejet actif de perturbations non linéaire (NADRC), dans lequel un observateur d'état étendu non linéaire (NESO) estime les perturbations totales provenant des incertitudes du modèle et des perturbations externes, tandis qu'un contrôleur PD non linéaire assure un suivi de trajectoire précis. La deuxième contribution propose une commande par mode glissant terminal rapide non singulier basée sur un observateur d'état étendu (ESO–NFTSMC) pour les manipulateurs mobiles couplés à n degrés de liberté (DDL). Cette conception élimine les singularités, améliore la réponse transitoire et compense les perturbations globales en temps réel, atteignant une convergence en temps fini avec un niveau de réticence (chattering) réduit. Enfin, la troisième et principale contribution développe une commande par mode glissant terminal à temps fixe (FTSMC) intégrée avec un observateur d'état étendu à temps fixe (FESO). Ce cadre assure la convergence vers la trajectoire désirée dans une limite de temps prédéfinie, indépendante des conditions initiales, tout en maintenant la robustesse face aux incertitudes et au bruit de mesure.

Toutes les approches proposées sont analysées mathématiquement en utilisant la théorie de la stabilité de Lyapunov et validées expérimentalement sur une plateforme de manipulateur mobile à 5 DDL (Mob-ETS) développée à l'ÉTS. Les résultats en temps réel démontrent des performances progressivement sophistiquées, allant du suivi fluide et robuste du NADRC à la convergence rapide en temps fini de l'ESO-NFTSMC, et culminant avec la convergence vérifiée en temps fixe du cadre FTSMC-FESO. Tous les contrôleurs montrent une excellente précision

de suivi et une forte robustesse contre les perturbations externes dans une variété de conditions de fonctionnement.

Dans l'ensemble, cette recherche établit un cadre de commande complet et vérifié expérimentalement pour le suivi de trajectoire robuste et à temps garanti des manipulateurs mobiles, apportant une contribution significative au domaine de la commande robotique non linéaire et posant les bases pour de futures extensions vers la coordination multi-robots et la conception d'observateurs adaptatifs à temps fixe.

Mots-clés: Commande par rejet actif de perturbations, mode glissant terminal rapide non linéaire, stabilité à temps fixe, contrôleur découplé, manipulateur mobile, incertitude de modélisation, perturbations externes, observateur d'état étendu non linéaire

Robust Trajectory Tracking of Mobile Manipulators Based On Extended State Observer and Nonlinear Control

Mhmed ALGRNAODI

ABSTRACT

This doctoral thesis proposes and experimentally validates Extended State Observer(ESO) based nonlinear control strategies for real-time trajectory tracking of mobile manipulators (MMs) operating in uncertain and dynamic environments. The developed approaches aim to overcome the limitations of conventional control methods in handling nonlinear couplings, parameter uncertainties, and external disturbances, which significantly affect the stability and tracking precision of mobile manipulators.

Mobile manipulators combine the dexterity of multi-link robotic arms with the mobility of wheeled platforms, thereby expanding their operational workspace and enabling applications in industrial automation, medical assistance, and planetary exploration. However, their complex coupled dynamics, characterized by nonholonomic constraints and interconnected subsystems, make trajectory tracking a highly challenging task. This research addresses these challenges by developing a unified observer–controller framework that guarantees robust, high-precision, and fixed-time trajectory tracking performance.

The first part of the research introduces a Nonlinear Active Disturbance Rejection Control (NADRC) scheme, in which a Nonlinear Extended State Observer (NESO) estimates the total disturbances arising from model uncertainties and external perturbations, while a nonlinear proportional-derivative (PD) controller ensures accurate trajectory tracking. The second contribution proposes an Extended State Observer-based Non-Singular Fast Terminal Sliding Mode Control (ESO-NFTSMC) for n-DoF coupled mobile manipulators. This design avoids singularities, enhances transient response, and compensates for lumped disturbances in real-time, achieving finite-time convergence with reduced chattering. Finally, the third and principal contribution develops a Fixed-Time Terminal Sliding Mode Control (FTSMC) integrated with a Fixed-Time Extended State Observer (FESO). This framework ensures convergence to the desired trajectory within a predefined time bound, independent of initial conditions, while maintaining robustness to uncertainties and measurement noise.

All proposed approaches are mathematically analyzed using Lyapunov stability theory and experimentally validated on a 5-DoF mobile manipulator platform (Mob-ETS) developed at ÉTS. The real-time results demonstrate progressively sophisticated performance, from the smooth and robust tracking of the NADRC to the fast, finite-time convergence of the ESO-NFTSMC, and culminating in the verified fixed-time convergence of the FTSMC-FESO framework. All controllers show excellent tracking accuracy and strong robustness against external disturbances under a variety of operating conditions.

Overall, this research establishes a comprehensive and experimentally verified control framework for robust and time-guaranteed trajectory tracking of mobile manipulators, providing a significant

contribution to the field of nonlinear robotic control and laying the foundation for future extensions to multi-robot coordination and adaptive fixed-time observer designs.

Keywords: Active disturbance rejection control, nonlinear fast terminal sliding mode, fixed-time stability, decoupled controller, mobile manipulator, modeling uncertainty, external disturbances, nonlinear extended state observer

TABLE OF CONTENTS

LIST OF TABLES

LIST OF FIGURES

LIST OF ABBREVIATIONS

ADRC	Active Disturbance Rejection Control
CFTSM	Continuous Fast Terminal Sliding Mode
CTC	Computed-Torque Controller
DH	Denavit-Hartenberg
DoF	Degree(s) of Freedom
ESO	Extended State Observer
FESO	Fixed-Time Extended State Observer
FTSMC	Fixed-Time Terminal Sliding-Mode Control
GREPCI	Research Group in Power Electronics and Industrial Control (ÉTS Laboratory)
IK	Inverse Kinematics
MIMO	Multi-Input Multi-Output
MM	Mobile Manipulator
MMs	Mobile Manipulators
Mob-ÉTS	Mobile Manipulator Experimental Platform at ÉTS
MP	Mobile Platform
MPC	Model Predictive Control
MR	Manipulator Robot
NADRC	Nonlinear Active Disturbance Rejection Control
NESO	Nonlinear Extended State Observer

NFTSM	Non-Singular Fast Terminal Sliding Mode
NFTSMC	Non-Singular Fast Terminal Sliding-Mode Control
NPD	Nonlinear Proportional Derivative
PD	Proportional–Derivative Control
PID	Proportional-Integral-Derivative
RM	Robotic Manipulator
RNN	Recurrent Neural Network
RTW	Real-Time Workshop
SISO	Single Input–Single Output
SMC	Sliding-Mode Control
SSR	Self-Stable Region
TSM	Terminal Sliding Mode
UAV	Unmanned Aerial Vehicle
WMM	Wheeled Mobile Manipulator
WMP	Wheeled Mobile Platform

LIST OF SYMBOLS AND UNITS OF MEASUREMENTS

C	Coriolis and centrifugal matrix
$e, \dot{e}$	Tracking error and its derivative
$f(\theta, \dot{\theta})$	Total disturbance function including nonlinear dynamics
G	Gravitational torque vector
$J_e(q)$	End-effector Jacobian matrix
k_i, k_s, k_d	Control gains (proportional, sliding, and derivative)
M	Symmetric and positive definite inertia matrix
M^{-1}	Inverse of the inertia matrix
q_v	Mobile platform generalized coordinates
s	Sliding surface variable
t_f	Fixed-time convergence bound $[s]$
T_{max}	Maximum predefined convergence time $[s]$
$V(e)$	Lyapunov candidate function
V_e	End-effector velocity vector [m/s]
x_1, x_2, x_3	State variables used in the observer and controller design
z_1	Observer state variables [rad]
χ	Derivative of the lumped disturbance term
η	Fixed-time gain coefficient
$\theta, \dot{\theta}, \ddot{\theta}$	Joint coordinate, velocity, and acceleration vectors [rad], [rad/s], [rad/s^2]

θ_a	Robotic arm generalized coordinates [rad]
θ_d	Desired trajectory components
τ	Control input torque vector $[N \cdot m]$
τ_d	External disturbance and model uncertainty torque $[N \cdot m]$
$\hat{f}$	Estimated total disturbance by ESO or FESO
λ, α, β	Positive control gains in sliding mode laws

INTRODUCTION

The field of robotics has undergone a significant transformation, evolving from fixed industrial manipulators confined to structured factory floors to intelligent, mobile platforms capable of performing complex tasks in uncertain and dynamic environments. A key development in this evolution is the mobile manipulator (MM), a robotic system that integrates a wheeled mobile base with a multi-degree-of-freedom (DoF) manipulator arm (Li & Ge (2013); Yamamoto & Yun (1994)). This synergistic combination fundamentally extends the robot's reachable workspace, merging the rapid, large-scale motion of the mobile platform with the precise, dexterous manipulation of the arm (Yamamoto & Yun (1994)). This capability has unlocked a wide range of applications, including advanced manufacturing, infrastructure inspection, field logistics, hazardous environment maintenance (e.g., nuclear facilities), assistive healthcare, and planetary exploration.

However, the integration of these two distinct robotic subsystems introduces significant control challenges. The system dynamics are characterized by strong, nonlinear base-arm couplings (Yamamoto & Yun (1996)), the presence of nonholonomic motion constraints on the mobile platform (Li & Ge (2013)), and a high degree of sensitivity to model uncertainties and external disturbances (Zhong, Kobayashi, Hoshino & Emaru (2013)). These factors include friction, wheel slip, unmodeled terrain interactions, and unknown payload variations, all of which complicate motion planning and degrade the accuracy of trajectory tracking (Chung & Velinsky (1998)).

Conventional model-based control strategies, such as the computed-torque method and feedback linearization, can theoretically provide excellent performance, but their efficacy is contingent upon the availability of an accurate dynamic model (Slotine & Li (1991)). In practice, the performance of these controllers often degrades substantially as unmodeled dynamic effects accumulate. While linear controllers like the Proportional-Integral-Derivative (PID) and its variants remain

popular due to their simplicity, they face inherent limitations. It is particularly challenging for these linear methods to deliver the fast convergence and high resilience required to handle the large uncertainty sets and strong nonlinearities common in MM applications (Åström & Hägglund (1995)).

These limitations have provided a strong motivation for research into nonlinear robust control. Among the various approaches, Sliding Mode Control (SMC) has emerged as a powerful technique due to its property of invariance with respect to a class of matched uncertainties and bounded disturbances (Utkin (1977); Drakunov & Utkin (1992); Choi, Baek, Lee, Lee & Han (2020)). However, classical SMC is often affected by chattering, a high-frequency oscillation in the control signal that can excite unmodeled dynamics and cause mechanical wear (Levant (2010); Xian, Shen, Chen & Feng (2022); Liu *et al.* (2025a,b)). To enhance transient performance, Terminal Sliding Mode (TSM) methods were developed to achieve finite-time convergence. Refinements such as Non-Singular Fast Terminal SMC (NFTSMC) were introduced to avoid singularities and accelerate convergence (Feng, Yu & Man (2002); Yang & Yang (2011); Liu, Chen & Huang (2019); Kim, Ahn, Hu & You (2023)). Nevertheless, a key limitation persists: this finite-time convergence is dependent on the initial system error, making the settling time difficult to predict (Polyakov (2011)).

In parallel, the Active Disturbance Rejection Control (ADRC) framework offers a compelling, model-light alternative (Han (2009)). A core component of ADRC is the Extended State Observer (ESO) , which is essential for this technique. The ESO augments the system's state vector with an additional state representing a lumped "total disturbance" (Gao (2006b)). This total disturbance term encompasses all uncertainties: unmodeled dynamics, parameter variations, and external perturbations. By estimating this augmented state online, the ESO enables real-time compensation with minimal model knowledge. This strategy allows the ESO to approximate the system disturbance, thereby improving the control system's robustness and

efficiency (Huang & Xue (2014)). When this disturbance estimation strategy is combined with Sliding Mode Control (SMC), the ESO is used for feed-forward compensation of the estimated disturbance. This compensation reduces the magnitude of the disturbance that the robust switching component must overcome, thereby mitigating chattering while preserving the inherent robustness of the design (Cui, Jin, Chang, Zuo & Zhao (2022)).

This doctoral thesis is dedicated to the development, analysis, and experimental validation of a unified observer-controller framework for the trajectory tracking of mobile manipulators (MMs). The research progresses systematically through three manuscript-style chapters, each building upon the last to address the core challenges of uncertainty, convergence, and robustness. The investigation begins by establishing a robust baseline using a Nonlinear Active Disturbance Rejection Control (NADRC) framework, which employs a Nonlinear Extended State Observer (NESO) for smooth disturbance compensation. Building on this, the second stage develops an ESO-based improved Non-singular Fast Terminal Sliding Mode (ESO-NFTSM) controller, integrating the observer to achieve chattering-reduced, finite-time convergence. The research culminates in the principal contribution: a novel Fixed-Time Terminal Sliding Mode Controller (FTSMC) integrated with a Fixed-Time Extended State Observer (FESO). This advanced framework is designed to guarantee system convergence within a prescribed time bound that is explicitly independent of the initial conditions (Polyakov (2011); Zuo (2015)), enhancing the predictability and safety of the MM's operation.

Each stage of the research includes the derivation of a control-oriented dynamic model for the MM (Li & Ge (2013)), a Lyapunov-based stability analysis of the proposed controller (Slotine & Li (1991)), and experimental validation on a 5-DoF Mob-ÉTS MM. The results show progressive improvements in tracking accuracy and robustness as the controller structure evolves from NADRC to ESO–NFTSM and finally to FTSMC–FESO. This work is grounded in foundational results from variable-structure systems (Utkin (1977); Shtessel, Edwards, Fridman & Levant

(2014)), finite-time and fixed-time stability (Polyakov (2011); Zuo (2015)), and disturbance-observer and ADRC methodologies (Han (2009); Huang & Xue (2014)).

A particular emphasis is placed on comparing the three proposed controllers under similar conditions. For each design, the controller is implemented in real-time on the Mob-ÉTS MM, and its performance is evaluated in terms of tracking error, convergence speed, and robustness to modeling uncertainties and external disturbances. These comparative studies highlight the advantages and trade-offs of the NADRC, ESO–NFTSM, and FTSMC–FESO schemes, and they clarify how the additional complexity introduced at each stage translates into measurable gains in closed-loop performance.

CHAPTER 1

RESEARCH PROBLEM

The trajectory tracking control of mobile manipulators (MMs) presents a multifaceted challenge that stems from the inherent complexity of integrating a nonholonomic mobile base with a multi-degree-of-freedom manipulator. Despite significant advances in nonlinear control, three critical and interrelated problems remain unresolved in the context of real-time, high-performance applications.

The first critical problem is the robust handling of complex, lumped uncertainties without relying on high-gain control. MMs are subject to significant "total disturbances," which include strong, state-dependent dynamic coupling between the base and the arm (Yamamoto & Yun (1994, 1996)), unknown friction forces, payload variations, and external environmental perturbations. Traditional robust controllers, such as standard Sliding Mode Control (SMC), address this by employing large switching gains to overpower the upper bound of these uncertainties. However, this approach exacerbates the phenomenon of chattering. Chattering not only degrades tracking precision but also risks exciting unmodeled high-frequency dynamics and causing severe mechanical wear to the actuators, rendering such controllers impractical for physical deployment (Shtessel *et al.* (2014)).

The second problem concerns the predictability of convergence time. While finite-time control strategies, such as Non-singular Fast Terminal SMC (NFTSMC), ensure convergence within a finite time, the settling time remains dependent on the initial system states (Feng *et al.* (2002); Yu, Yu, Shirinzadeh & Man (2005)). This dependency creates a significant limitation for safety critical or time-constrained tasks, as a larger initial error results in a longer convergence time. Achieving fixed-time stability is therefore essential. A fixed-time controller guarantees that the system state converges to the equilibrium within a pre-defined time bound that is strictly independent of the initial conditions (Polyakov (2011); Zuo (2015)), providing a necessary guarantee for reliable robotic operation. Furthermore, existing observer-based solutions often

lack this fixed-time convergence property for the estimation error itself, creating a limitation in the overall system performance.

The third and perhaps most challenging problem is the complexity of designing a decoupled control law for a highly coupled nonlinear system. Most advanced control frameworks for MMs result in complex, coupled control laws that are computationally intensive and difficult to tune (Li & Ge (2013); Zhong *et al.* (2013)). There is a lack of control architectures that can effectively decouple the dynamics of the mobile base and the manipulator robot (MR) while simultaneously ensuring robust, fixed-time performance for both subsystems. Developing a decoupled fixed-time controller that integrates with a fixed-time observer to handle the coupled dynamics as part of the lumped disturbance remains a significant gap in the literature (Polyakov (2011)).

Addressing these three problems: robust disturbance rejection without chattering, guaranteed convergence time independent of the initial conditions, and effective decoupling of complex mobile manipulator (MM) dynamics constitutes the central research problem of this thesis.

1.1 Research Motivation

The motivation for solving this tripartite problem stems from the expanding role of MMs in critical, real-time applications where performance and reliability are paramount.

Motivation for Robustness: In environments like advanced manufacturing, logistics, or hazardous site maintenance, the robot must handle unknown payloads, navigate varied terrain, and interact with an unstructured world (Li & Ge (2013)). A controller that relies on an exact model will fail. An observer-based approach that actively estimates and rejects disturbances in real-time (Gao, Hu & Jiang (2001)) is essential for reliable operation.

Motivation for Fixed-Time Convergence: In applications such as assistive healthcare, collaborative human-robot assembly, or tasks in time-critical industrial processes, predictability is safety. Knowing with certainty that a robot will recover from a tracking error (regardless of its

magnitude) within a predefined, non-negotiable time bound is a powerful performance and safety guarantee (Polyakov (2011)) that finite-time or asymptotic controllers cannot provide.

Motivation for Chattering Mitigation: To ensure the longevity, precision, and reliability of the physical hardware (i.e., the motors, gears, and structure of the Mob-ÉTS MM), the control signal must be smooth. Chattering-aware design, achieved by integrating observers to reduce switching gain requirements (Shtessel *et al.* (2014)), is what makes advanced control theory practical and deployable on real-world robots.

1.2 Research Objectives

The overall objective of this research is to design, analyze, and experimentally validate a unified, observer-based nonlinear control framework that provides robust, chattering-reduced, and time-bounded trajectory tracking for MMs. The specific, progressive objectives are:

- To design and validate a Nonlinear Active Disturbance Rejection Control (NADRC) scheme. This involves developing a Nonlinear Extended State Observer (NESO) to estimate and compensate for the "total disturbance" (Han (2009)) and integrating it with a nonlinear Proportional-Derivative (NPD) controller (Gao (2006b)). The objective is to establish a robust, chattering-free baseline and validate its real-time performance on the five-degree-of-freedom (5-DoF) MM.
- To develop an observer-based Non-Singular Fast Terminal Sliding Mode (NFTSM) controller for finite-time convergence. This objective involves designing an NFTSM controller (Yang & Yang (2011)) and augmenting it with an ESO (Yang, Li & Yu (2012)) to improve tracking accuracy and robustness against uncertainties (Li, Ge & Wang (2008)). The goal is to achieve faster, finite-time error convergence while using the observer to mitigate the chattering typically associated with NFTSM (Levant (2010)).
- To create a composite Fixed-Time Terminal Sliding Mode (FTSMC) controller with a Fixed-Time Extended State Observer (FESO). This is the principal objective of the thesis. It requires the design of a novel decoupled, fixed-time nonlinear sliding surface (Zuo (2015)) and a corresponding fixed-time Extended State Observer (ESO) (Basin, Yu & Shtessel

(2017)). The objective is to formally prove, via Lyapunov analysis (Slotine & Li (1991)), that the closed-loop system states converge to their desired trajectories within a fixed time, independent of initial conditions.

- To provide comprehensive experimental validation and comparative analysis. A final objective is to implement all three proposed controllers on the 5-DoF Mob-ÉTS MM hardware, tune them according to the developed theory, and rigorously evaluate their trajectory tracking performance (in both Cartesian and joint spaces) against each other and against baseline controllers.

1.3 Main Contributions

This doctoral thesis provides a coherent and experimentally validated progression of observer-based nonlinear controllers, culminating in a fixed-time control framework for MMs. The primary contributions, directly resulting from the original research conducted for this dissertation, are:

- Design and Experimental Validation of a Nonlinear ADRC for a 5-DoF MM (Journal Paper I, Chapter 4). A complete NADRC framework is developed and implemented on the 5-DoF Mob-ÉTS MM. A NESO is designed to estimate the lumped total disturbance, which is then actively compensated in the control law. The controller structure, stability analysis, and real-time experiments demonstrate that the proposed NADRC–NESO scheme achieves accurate trajectory tracking and good robustness to modeling uncertainties and external disturbances, while avoiding chattering.
- Composite ESO–NFTSM Control with Chattering Reduction and Finite-Time Convergence (Journal Paper II, Chapter 5). Building on the NADRC–NESO framework as a robust reference controller, a composite controller that combines an extended state observer with an NFTSM law is proposed. The ESO provides an online estimate of the lumped disturbances, which is used within the control input to reduce the required switching gain of the NFTSM law. This design achieves finite-time convergence of the tracking error with significantly reduced chattering compared to a conventional NFTSM controller. The complete design

procedure, Lyapunov-based analysis, and experimental results on the Mob-ÉTS MM are presented and compared against the reference NADRC–NESO controller.

- Decoupled Fixed-Time Observer–Controller Framework (FTSMC–FESO) for MMs (Journal Paper III, Chapter 6): The principal contribution of the thesis is a FTSMC integrated with a FESO. A coupled sliding surface is constructed using the inertia matrix to obtain a control law that is suitable for the coupled MM dynamics while remaining straightforward to implement. Fixed-time stability of the closed-loop system, including the observer error dynamics, is established, and the convergence-time bound is shown to be independent of the initial conditions. Experimental validation on the Mob-ÉTS MM confirms fixed-time convergence, high tracking accuracy, and strong robustness to disturbances, demonstrating a clear improvement over the robust reference controller and the ESO–NFTSM design.
- Comprehensive Experimental Comparison and Implementation Guidelines. The three proposed controllers (i) NADRC,(ii) ESO–NFTSM, and (iii) FTSMC–FESO are implemented and tested under comparable conditions on the same experimental platform. Their performance is systematically compared in terms of tracking error, convergence speed, and robustness to uncertainties and disturbances. Based on these results, the thesis provides practical guidelines for tuning, implementation, and selection of the appropriate controller structure for different performance and complexity requirements in real-time MM applications.

1.4 Outline of Thesis

Following the Introduction and the research problem presented in Chapter 1, this dissertation is organized into six main chapters, followed by a concluding chapter. The structure of the remaining chapters is summarized as follows:

- Chapter 1 – Research Problem: This chapter presents the research background, defines the research problem, states the motivation and objectives, and outlines the main contributions of the thesis.
- Chapter 2 – Background and Literature Review: This chapter reviews the main concepts and prior work on mobile manipulator modeling, nonlinear control, disturbance observation, and finite-time and fixed-time stability. It also identifies the research gaps that motivate the contributions of this thesis.

- Chapter 3 – System Modeling and Approach of Control: This chapter presents the complete kinematic and dynamic modeling of the 5-DoF Mob-ÉTS mobile manipulator and reformulates the equations into a control-oriented form that is used in all subsequent controller designs.
- Chapter 4 – Trajectory Tracking for Mobile Manipulator Based on Nonlinear Active Disturbance Rejection Control: This chapter introduces the NADRC–NESO baseline controller, including its design, Lyapunov-based stability analysis, and experimental validation on the Mob-ÉTS platform.
- Chapter 5 – ESO-Based Improved Non-Singular Fast Terminal Sliding Mode for Mobile Manipulators: This chapter develops the ESO–NFTSM controller, integrating the ESO with a non-singular fast terminal sliding surface to achieve finite-time convergence with reduced chattering, and validates the method experimentally.
- Chapter 6 – Fixed-Time ESO-Based Decoupled Terminal Sliding Mode for Mobile Manipulator: This chapter presents the main contribution of the thesis, the FTSMC–FESO framework. It provides the fixed-time stability analysis, details the decoupled controller structure, and reports experimental results that demonstrate fixed-time convergence and enhanced robustness.

Finally, the Conclusion and Recommendations chapter summarizes the main findings of the thesis, discusses how the research objectives and contributions have been achieved, and outlines several directions for future work.

CHAPTER 2

BACKGROUND AND LITERATURE REVIEW

2.1 Overview

This chapter provides a comprehensive review of the foundational literature and recent advances pertinent to the trajectory tracking control of mobile manipulators (MMs). The primary objective is to establish the academic context for this thesis by systematically examining the key challenges, the evolution of control solutions, and the current state-of-the-art. The control of MMs is a formidable problem, defined by the complex interplay of multi-body dynamics, nonholonomic constraints, and pervasive, unstructured uncertainties (Li & Ge (2013); Yamamoto & Yun (1994, 1996)).

This review is structured to build a logical argument for the research presented in this thesis. We begin by defining the control problem itself, analyzing the dynamic modeling of MMs and the characteristics that make them challenging to control. Following this, we trace the evolution of control strategies, from classical linear methods and model-based nonlinear approaches to the introduction of robust Sliding Mode Control (SMC), paying close attention to the practical limitations that have driven innovation, such as model dependency and the chattering phenomenon (Slotine & Li (1991)).

This review then transitions to two advanced theoretical frameworks that form the basis of this dissertation. The first framework is rooted in the "model-light" strategy of observer-based and disturbance-rejection control, with a specific focus on the Active Disturbance Rejection Control (ADRC) framework and its core component, the Extended State Observer (ESO) (Han (2009); Gao (2006b)). The second framework concerns the temporal performance of controllers, charting the progression of stability theory from finite-time stability, exemplified by Non-singular Fast Terminal SMC (NFTSMC) (Yang & Yang (2011)), to the more robust and predictable concept of fixed-time stability (Polyakov (2011); Zuo (2015)).

Finally, we synthesize these fields by reviewing recent literature at their intersection, identifying the specific, unresolved gaps in the trajectory tracking control of MMs. This

chapter concludes by summarizing these gaps, which directly motivate the novel, three-stage contributions of this dissertation.

2.2 Modeling and Dynamic Characteristics of Mobile Manipulators

A mobile manipulator (MM) is a robotic system composed of a serial-link manipulator mounted on a wheeled mobile platform (WMP) (Li & Ge (2013)). This architecture provides a synergistic combination of the large-workspace mobility of the platform and the dexterous manipulation capabilities of the arm. However, this integration creates a unified dynamic system that is far more complex than the sum of its parts. The accurate mathematical modeling of this system is the foundational step for any advanced control design.

The dynamic model of an n-degree-of-freedom (N-DoF) MM is typically derived using the Lagrangian formulation. When considering the nonholonomic constraints of the wheeled platform, the Lagrange-d'Alembert formulation is often employed (Chung & Velinsky (1998); Yu & Chen (2002)). The resulting equations of motion are characterized by three fundamental challenges for control design:

1. Nonlinear Coupling: The system exhibits strong, nonlinear dynamic coupling between the platform and the manipulator (Yamamoto & Yun (1994, 1996)). The motion of the manipulator arm induces reaction forces and torques on the mobile base, and conversely, the platform's movement introduces inertial disturbances to the manipulator. This interplay results in highly coupled, state-dependent, and non-diagonal inertia ($M(q)$) and Coriolis/centrifugal ($C(q, \dot{q})$) matrices (Zhong *et al.* (2013); Li & Ge (2013)).
2. Nonholonomic Constraints: In the case of a differential-drive mobile platform (MP), the kinematic model is subject to nonholonomic constraints that arise from the ideal pure-rolling, no lateral-slip assumption at the wheel ground contact (Li & Ge (2013); Klancar, Zdesar, Blazic & Skrjanc (2025)). These constraints can be written as non-integrable velocity relations $A(q_v)\dot{q}_v = 0$, which restrict the instantaneous motion of the platform (e.g., prohibiting sideways motion) without restricting the set of reachable configurations. As a consequence, the kinematic model is nonholonomic and effectively underactuated, which makes stabilization by smooth, time-invariant state-feedback non-trivial (Walsh,

Tilbury, Sastry, Murray & Laumond (1994)). In practice, small amounts of slip may occur; while these effects violate the ideal constraints, they are typically treated as unmodeled dynamics or disturbances to be rejected by the controller.

3. Pervasive Uncertainties and Disturbances: The mathematical model is only an approximation. In any real-time application, the controller must contend with significant uncertainties (Zhong *et al.* (2013)). These can be categorized as:
   - Structured (Parametric) Uncertainties: Inaccuracies in model parameters, such as link masses, moments of inertia, and unknown or time-varying payloads.
   - Unstructured Uncertainties: Highly complex, time-varying, and unmodeled dynamics, such as nonlinear friction (stiction, viscous) in the joints and wheel-ground interface, actuator dead-zones, and structural flexibilities (Xing, Li & Yang (2025)).
   - External Disturbances: Unknown forces from the environment, such as variations in terrain, bumps, wheel slip (Sebastian & Ben-Tzvi (2019)), and physical contact forces.

For robust control design, these varied and unknown terms are often lumped into a single "total disturbance" vector, f_{total}. The central challenge of robust control is to design a controller τ that achieves accurate trajectory tracking despite the presence of this large, unknown, and time-varying f_{total}.

2.3 Classical and Nonlinear Control Approaches

Given the complex dynamics described above, the evolution of control strategies for MMs has moved from simple linear methods to highly robust nonlinear frameworks.

2.3.1 Classical Linear Control (PD/PID)

Proportional-Derivative (PD) and Proportional-Integral-Derivative (PID) controllers are the bedrock of industrial control due to their simplicity and intuitive tuning (Åström & Hägglund (1995)). However, their performance is fundamentally limited when applied to highly nonlinear and coupled systems like MMs. A linear controller with fixed gains cannot effectively compensate for the highly nonlinear, state-dependent dynamics. High gains may be used to "overpower" the nonlinearities, but this leads to high control effort, potential

instability, and poor performance in the presence of large, varying disturbances (Su, Sun, Ren & Mills (2006)).

2.3.2 Model-Based Nonlinear Control

To directly address the system's nonlinearities, model-based strategies like the computed-torque controller (CTC) (also known as feedback linearization) were developed (Slotine & Li (1991)). This approach uses an exact mathematical model to cancel out the nonlinear dynamics, ideally reducing the control problem to a simple, linear, and decoupled one. The critical flaw of CTC is its absolute reliance on a perfect model. In practice, the uncertainties and disturbances are non-zero, the cancellation is incomplete, and the controller's performance degrades significantly (Zhong *et al.* (2013)).

2.3.3 Adaptive Control

To address parametric uncertainties (e.g., unknown payload mass), adaptive control was introduced. These controllers augment the control law with an online parameter estimator that updates the model parameters in real-time (Andaluz, Roberti, Toibero & Carelli (2012); Li *et al.* (2008)). While effective for slowly varying parameters, adaptive control struggles with unstructured, time-varying disturbances (like friction or slip) and can be computationally expensive.

2.3.4 Sliding Mode Control (SMC)

To solve the problem of both structured and unstructured uncertainty, SMC emerged as a dominant robust control technique (Utkin (1977)). SMC is a variable structure control method that uses a discontinuous control law to force the system's state trajectory onto a predefined sliding manifold and maintain it there. The key property of SMC is that once on the manifold, the system dynamics become invariant to a class of matched uncertainties and disturbances.

However, SMC suffers from a major practical drawback: chattering (Levant (2010)). The high-frequency switching of the discontinuous control law is a high-frequency, discontinuous signal. This chattering can excite unmodeled high-frequency dynamics (like joint flexibility), cause excessive wear on actuators, and degrade steady-state tracking precision (Young,

Utkin & Ozguner (1999)). This chattering problem is a primary motivator for the advanced, observer-based approaches that form the core of this thesis.

2.4 Observer-Based and Disturbance-Rejection Control

This section reviews the first major theoretical framework of this thesis, which presents an alternative to both model-based (CTC) and high-gain robust (SMC) control. The central idea is to actively estimate the "total disturbance" in real-time and cancel it, following a "model-light" approach.

2.4.1 The Active Disturbance Rejection Control (ADRC) Framework

Proposed by Han (2009), ADRC is a control philosophy built on the idea that the controller's main job is to compensate for disturbances. It redefines the control problem by lumping all internal model uncertainties (parametric, coupling, friction) and external disturbances into a single "total disturbance" term, $f(t)$ (Gao (2006a)). The core of ADRC consists of two main components: an ESO to estimate $f(t)$, and a state-feedback controller (often a nonlinear Proportional-Derivative (NPD) to use that estimate and control the simplified plant.

2.4.2 The Extended State Observer (ESO)

The key innovation of ADRC is the ESO (Gao (2006b)). The ESO augments the system's state vector with a new state, $x_{n+1} = f$, which represents the total disturbance. The ESO is then designed for this augmented system to estimate all original states plus this new disturbance state, $\hat{f}$. For a second-order system like a robot joint, $\ddot{\theta} = f + b_0\tau$, the state is augmented to $x_1 = \theta$, $x_2 = \dot{\theta}$, and $x_3 = f$. The control law is then a simple feedforward cancellation plus a nominal controller:

$$\tau = (\tau_0 - \hat{x}_3)/b_0 \tag{2.1}$$

The closed-loop system becomes $\ddot{\theta} = f + b_0\big((\tau_0 - \hat{x}_3)/b_0\big) = (f - \hat{x}_3) + \tau_0 \approx \tau_0$. The system is "linearized-by-cancellation," but the cancellation term $\hat{x}_3 = \hat{f}$ is provided by the observer, not a mathematical model. This approach has been shown to be extremely robust and practical

(Huang & Xue, 2014). Often, the ESO is designed with nonlinear gains (a Nonlinear ESO, or NESO) to achieve faster and more accurate estimation (Pu, Yuan, Yi & Tan (2015)).

2.4.3 Synergy of ESO and SMC

The ESO provides a powerful and elegant solution to the chattering problem in SMC (Shtessel *et al.* (2014); Yang *et al.* (2012)). Instead of a high-gain switching law $K \cdot \text{sgn}(s)$ designed to overcome the entire disturbance f, a composite ESO-SMC controller uses the disturbance estimate $\hat{f}$. The control law becomes:

$$\tau = \tau_0 - \hat{f} - K \cdot \text{sgn}(s) \tag{2.2}$$

Since the ESO cancels the majority of the disturbance ($\hat{f} \approx f$), the robust gain K only needs to be large enough to handle the observer's estimation error, $\tilde{f} = f - \hat{f}$. Because the estimation error $\tilde{f}$ is typically much smaller than the total disturbance f, K can be significantly reduced. This massive reduction in the switching gain directly leads to a massive reduction in chattering. This synergistic combination achieves both high robustness and a smooth control signal.

2.5 Finite-Time and Fixed-Time Control Theories

This section reviews the second theoretical foundation of the thesis, which concerns the temporal performance and convergence speed of the controller. While the ADRC framework effectively handles uncertainties, standard observers typically guarantee only asymptotic convergence. In high-dynamic robotics, this is often insufficient; the observer estimation must converge significantly faster than the controller dynamics to ensure stability. Therefore, it is necessary to incorporate finite-time and fixed-time stability theories to guarantee precise estimation and tracking within a bounded time.

2.5.1 From Asymptotic to Finite-Time Stability

Traditional controllers (PID, CTC) provide asymptotic stability, where the tracking error $e(t)$ converges to zero. While stable, this convergence can be slow. For high-performance robotics, a stronger guarantee is desired.

Finite-Time Stability ensures that the system states reach the equilibrium (e.g., $e = 0$) in a finite time, T, and stay there (Bhat & Bernstein (2000)). This provides faster convergence and improved robustness. In SMC, this is achieved using nonlinear surfaces like Terminal Sliding Mode (TSM). However, classical TSM suffers from a singularity problem (Feng *et al.* (2002)). To solve this, Non-singular Terminal Sliding Mode (NTSM) and Non-singular Fast Terminal SMC (NFTSMC) were developed (Yang & Yang (2011)). NFTSMC, in particular, ensures fast, singularity-free, finite-time convergence and is a state-of-the-art method (Boukattaya, Mezghani & Damak (2018)).

2.5.2 From Finite-Time to Fixed-Time Stability

A critical limitation of finite-time stability remains: the convergence time T is a function of the initial conditions, $T(x_0)$. A larger initial error will result in a longer (though still finite) settling time. This lack of predictability is a drawback for safety-critical or time-sensitive robotic tasks. Fixed-Time Stability is a stronger property that solves this. A system is fixed-time stable if it is finite-time stable and the convergence time T is bounded by a constant T_{max} that is independent of the initial conditions (Polyakov (2011)). This means the controller guarantees convergence within, for example, 2 seconds, regardless of whether the initial error is 1 degree or 100 degrees. This provides the ultimate level of predictability. Fixed-time stability is achieved by designing control laws or sliding surfaces that combine terms with fractional and polynomial powers (Zuo (2015)). This concept can also be applied to observers, creating Fixed-Time Extended State Observers (FESO) that also guarantee convergence independent of the initial estimation error (Basin *et al.* (2017)).

2.6 Recent Advances in Trajectory Tracking of Mobile Manipulators

The advanced control concepts from Sections 2.4 and 2.5 have been increasingly applied to the MM trajectory tracking problem, often in combination with other modern techniques. Recent work has explored learning-based methods, such as neural networks, to approximate the unknown dynamics and uncertainties (Khan, Li & Chen (2020); Zhang, Liu & Yang (2023)). Model Predictive Control (MPC) has also been applied to handle constraints and optimize performance (Li, Yang & Su (2016); Su, Li & Yang (2025)). While powerful, these

methods often introduce significant computational complexity or require extensive training data.

The ADRC and advanced SMC approaches, by contrast, offer a computationally-lighter, non-learning-based alternative. However, a review of the literature reveals specific gaps:

- ADRC/ESO for MMs: Applications of ADRC to MMs are often limited to simulation (Ren, Zhang, Ma & Wei (2018); Wei *et al.* (2017)) or subsystems. Rigorous experimental validation of a nonlinear ADRC (NADRC) on a fully-coupled, physical MM platform is lacking.
- NFTSM for MMs: While NFTSM has been applied to various robots, its application to MMs is less common. When used, the chattering problem persists. The synergistic combination of an ESO with NFTSMC, experimentally validated on an MM to explicitly solve chattering while achieving finite-time convergence, is not well-established.
- Fixed-Time Control for MMs: This is an emerging research front. The application of fixed-time control to complex, coupled MMs, especially a composite FTSMC+FESO framework, to provide initial-condition-independent convergence is a significant open problem (Zhang, Wang, Hou & Li (2019); Cui *et al.* (2022)).

2.7 Summary of Literature Gaps

Based on the preceding review, this thesis is motivated by several clear and significant gaps in the existing literature:

- Lack of Rigorous Experimental Validation for NADRC on MMs: While ADRC is a powerful "model-light" theory, its practical application and experimental validation on complex, fully-coupled, nonholonomic MMs for high-performance trajectory tracking is not sufficiently demonstrated in the literature.
- Unaddressed Chattering in Finite-Time MM Control: While NFTSM offers fast, finite-time convergence, its direct application to MMs is hindered by its inherent chattering. The synergistic combination of an ESO with NFTSMC, experimentally validated on MM hardware to simultaneously achieve finite-time convergence and chattering suppression, is a clear and necessary contribution.

- Absence of Fixed-Time Control for MM Trajectory Tracking: The convergence time of all existing finite-time controllers for MMs depends on the initial tracking error. There is a complete gap in the literature regarding a controller that provides a guaranteed, predictable convergence time bound independent of initial conditions (i.e., fixed-time stability), especially one paired with a fixed-time observer and validated on real-time applications.
- Need for Decoupled, Robust Control Laws: Many advanced controllers for MIMO systems like MMs result in complex, coupled control laws. The design of a fixed-time framework that also achieves a decoupled control law for easier tuning and implementation is a significant and unaddressed challenge.

2.8 Chapter Summary

This chapter reviewed the main control strategies for trajectory tracking of MMs. We began by establishing the significant challenges inherent in the system's dynamics: strong nonlinear coupling, nonholonomic constraints, and lumped uncertainties. We then discussed the main categories of control approaches for mobile manipulators, including model-based nonlinear methods and robust sliding-mode control, and pointed out their limitations in terms of model dependence and chattering.

Next, we introduced the three theoretical foundations that form the basis for the developments in this thesis: (i) Active Disturbance Rejection Control and Extended State Observers, which enable uncertainty compensation with limited model information; (ii) Non-Singular Fast Terminal Sliding Mode, which achieves fast finite-time convergence; and (iii) fixed-time stability theory, which provides convergence guarantees that are independent of the initial conditions.

Our review of recent advances at the intersection of these fields identified critical, unaddressed gaps: a lack of rigorous experimental validation for advanced ADRC and observer-based NFTSM on MMs, and the complete absence of a fixed-time, observer-based control framework that ensures predictable convergence time. The following chapters of this thesis will directly address these three gaps by designing, analyzing, and experimentally validating a progressive series of three advanced controllers.

The remainder of this thesis addresses these gaps by designing, analyzing, and experimentally validating three observer-based nonlinear controllers for a 5-DoF MM: a NADRC–NESO reference controller, an ESO–NFTSM controller with finite-time convergence and reduced chattering, and a fixed-time FTSMC–FESO framework that provides guaranteed, initial-condition-independent convergence.

CHAPTER 3

MODELING SYSTEM AND APPROACH OF CONTROL

3.1 Overview

This chapter presents the complete mathematical derivation of the mobile manipulator (MM) model used throughout this thesis. A rigorous, physics-based model is the foundation for developing and simulating high-performance controllers and for understanding the system's inherent properties. Unlike the literature survey in Chapter 2, the objective here is to derive the specific kinematic and dynamic equations for the five-degree-of-freedom (5-DoF) Mob-ÉTS experimental MM (Brahmi *et al.* (2016)).

The derivation begins with a formal description of the system, its coordinate frames, and its kinematic structure (Li & Ge (2013); Henein, Aboul-Seoud & El-Metwally (2022)). We then derive the nonholonomic constraints governing the mobile platform and the complete forward kinematics of the manipulator arm (Brahmi *et al.* (2016). Using the Lagrange-d'Alembert formulation, the full dynamic equations of motion are systematically derived (Li, Ge & Ming (2007); Zhong *et al.* (2013)). A key step is the mathematical elimination of the nonholonomic constraint forces, which yields the reduced, or constraint-free, dynamic model that is essential for control design (Li & Ge (2013)). Finally, this reduced model is rearranged into a "control-oriented" state-space form. This final formulation explicitly isolates the "total disturbance" term, which is the foundational step for designing the Extended State Observers (ESOs) and all subsequent control laws in this thesis (Han (2009); Gao (2006b)).

3.2 System Description, Coordinates, and Frames

The experimental platform used in this work is the Mob-ÉTS MM, a 5-DoF MM. It consists of a 3-DoF serial-link manipulator arm mounted centrally on a 2-DoF differential-drive wheeled mobile platform (WMP) (Brahmi *et al.* (2016)). This configuration combines the large-workspace mobility of the platform with the dexterous manipulation capabilities of the arm. To describe the system's configuration (as shown in Figure 3.1), we establish several key coordinate frames:

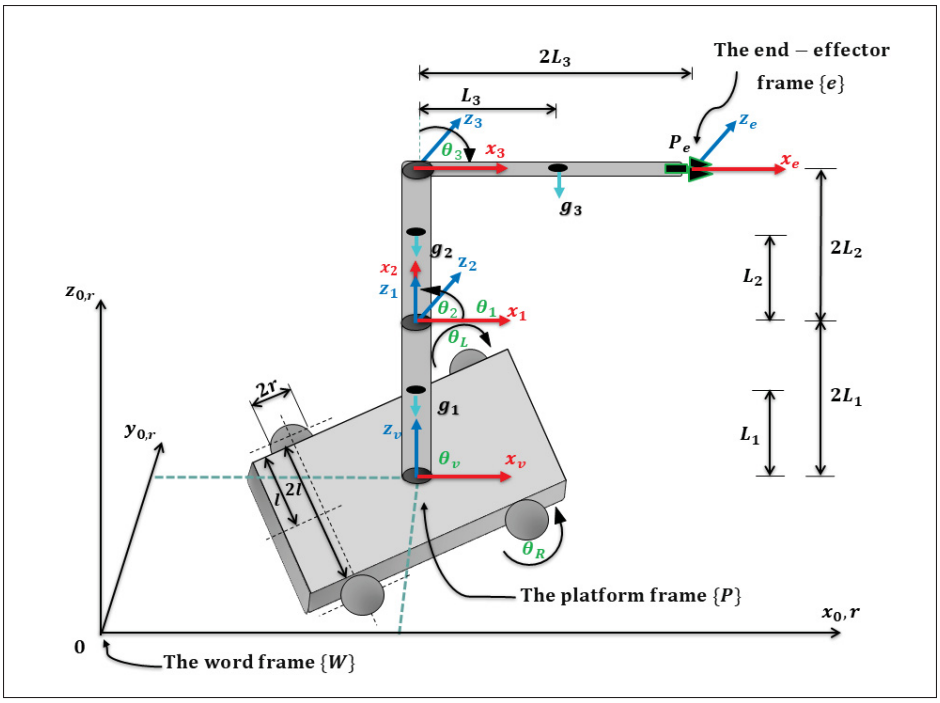

Figure 3.1 Schematic of the 5-DoF Mobile Manipulator (Mob-ÉTS)

- World Frame $\{W\}$: This is the fixed, global reference frame for all motions, denoted in the figure as $\{0, r\}$ with axes $(x_{0,r}, y_{0,r}, z_{0,r})$.
- Platform Frame $\{P\}$: This frame is attached to the mobile base and moves with it. It is denoted as $\{v\}$ and is centered on the platform's wheel axle, with the x_v axis pointing forward.
- Link Frames $\{L_i\}$: A series of frames, $\{1\}$, $\{2\}$, and $\{3\}$, are attached to the manipulator robot (MR) to describe its posture, corresponding to the joint angles θ_1, θ_2, and θ_3. The end-effector frame $\{e\}$ is located at the tool tip, P_e.

The entire system's configuration is described by a 6-dimensional vector of generalized coordinates, $q \in \mathbb{R}^6$ (Brahmi *et al.* (2016)):

$$q = [q_v^T, \theta_a^T]^T = [X_v, Y_v, \phi_v, \theta_1, \theta_2, \theta_3]^T \tag{3.1}$$

where $q_v = [X_v, Y_v, \phi_v]^T$ is the pose of the mobile platform (MP) (vehicle) in the world frame (its X_v, Y_v position and orientation angle ϕ_v), and $\theta_a = [\theta_1, \theta_2, \theta_3]^T$ is the vector of the manipulator's joint angles (arm).

3.3 Kinematic Modeling

The kinematic model describes the geometry of the system's motion, relating the joint-space velocities to the task-space velocities. This derivation is a critical prerequisite for the dynamic modeling, as it provides the transformation matrices needed to eliminate constraints.

3.3.1 Mobile Platform Kinematics and Nonholonomic Constraint

The differential-drive WMP is subject to a nonholonomic constraint, which is a velocity-level constraint that is not integrable. This constraint arises from the physical assumption that the wheels roll purely on the ground plane (Li & Ge (2013); Klancar *et al.* (2025)). This imposes a restriction on the platform's world-frame velocity vector, $\dot{q}_v = [\dot{X}_v, \dot{Y}_v, \dot{\phi}_v]^T$. The velocity component perpendicular to the robot's heading must be zero, which is expressed as:

$$\dot{Y}_v \cos(\phi_v) - \dot{X}_v \sin(\phi_v) = 0 \tag{3.2}$$

The constraints of the mobile platform are presumed to be independent such that they can be written in the standard matrix form $A(q_v)\dot{q}_v = 0$ (Li *et al.* (2007)):

$$A(q_v)\dot{q}_v = 0 \tag{3.3}$$

where $A(q_v)$ is the constraint matrix:

$$A(q_v) = [-\sin(\phi_v) \quad \cos(\phi_v) \quad 0] \tag{3.4}$$

Although q_v has three dimensions, its motion is restricted to only 2-DoF. We can therefore define a full-rank matrix $S(q_v) \in \mathbb{R}^{3\times2}$ that spans the null-space of $A(q_v)$, such that (Li & Ge (2013)):

$$S^T(q_v)A^T(q_v) = 0 \tag{3.5}$$

This matrix maps the two independent base velocities, $\dot{\eta} = [v_v, w_v]^T$ (where v_v is the linear velocity and w_v is the angular velocity), to the 3-dimensional generalized velocity vector $\dot{q}_v$:

$$\dot{q}_v = S(q_v)\dot{\eta} \tag{3.6}$$

where:

$$S(q_v) = \begin{bmatrix} \cos(\phi_v) & 0 \\ \sin(\phi_v) & 0 \\ 0 & 1 \end{bmatrix} \tag{3.7}$$

While $\dot{\eta}$ represents the independent velocities of the platform, the system is ultimately driven by the motors on the right and left wheels. Let θ_R and θ_L denote the angular positions of the left and right wheels, respectively, and let $\dot{\theta}_R$ and $\dot{\theta}_L$ denote their corresponding angular velocities. The mobile platform (MP) wheel-rate vector is then defined as $\dot{\theta}_v = [\dot{\theta}_R, \dot{\theta}_L]^T$. The relationship between these wheel velocities and the platform velocities $\dot{\eta}$ is given by the standard differential-drive kinematic map (Klancar *et al.* (2025)):

$$\dot{\eta} = R\,\dot{\theta}_v \tag{3.8}$$

where R is the wheel-to-base transformation matrix:

$$R = \begin{bmatrix} \frac{r}{2} & \frac{r}{2} \\ \frac{r}{2l} & \frac{-r}{2l} \end{bmatrix} \tag{3.9}$$

Here, r is the wheel radius and $2l$ is the track width (distance between the wheels).
To formulate the final kinematic model, we need a direct mapping from the actuated wheel velocities $\dot{\theta}_v$ to the world-frame velocities $\dot{q}_v$. This is found by substituting Eq. (3.8) into Eq. (3.6):

$$\dot{q}_v = S(q_v)\dot{\eta} = S(q_v)(R\,\dot{\theta}_v) = H(q_v)\dot{\theta}_v \tag{3.10}$$

where $H(q_v) \in \mathbb{R}^{3\times2}$ is the wheel-to-world transformation matrix (Li & Ge (2013)). Based on the user's provided text, this matrix is defined as:

$$H(q_v) = S(q_v)R = \begin{bmatrix} \frac{r}{2}cos(\phi_v) & \frac{r}{2}sin(\phi_v) & \frac{r}{2l} \\ \frac{r}{2}cos(\phi_v) & \frac{r}{2}sin(\phi_v) & \frac{-r}{2l} \end{bmatrix}^T \tag{3.11}$$

Differentiating Eq. (3.10) with respect to time gives the platform's generalized acceleration, which is essential for the dynamic model derivation:

$$\ddot{q}_v = \dot{H}(q_v)\dot{\theta}_v + H(q_v)\ddot{\theta}_v \tag{3.12}$$

3.3.2 Manipulator Kinematics and Whole-Robot Jacobian

The previous section defined the kinematics of the MP, culminating in the matrix $H(q)$ (Eq. 3.10) that maps the actuated wheel velocities $\dot{\theta}_v$ to the platform's velocity in the world frame $\dot{q}_v$. We now extend this model to include the 3-DoF MR to describe the motion of the end-effector, P_e.

3.3.2.1 Forward Kinematics and Task-Space Definition

The MP consists of 3 links with 3 actuated revolute joints, $\theta_a = [\theta_1, \theta_2, \theta_3]^T$. The objective is to control the 6-DoF pose of the end-effector, $P_e \in \mathbb{R}^6$, which includes its 3D position (x, y, z) and 3D orientation (e.g., Euler or RPY angles) in the fixed world frame $\{W\}$. The end-effector's pose is a function of the entire 6-dimensional generalized coordinate vector $q = [q_v^T, \theta_a^T]^T$. This relationship is found by chaining the homogeneous transformations from the world frame to the platform frame, and then from the platform frame to the end-effector frame:

$$T_e^W(q) = T_P^W(q_v) \cdot T_e^P(\theta_a) \tag{3.13}$$

where:

- $T_P^W(q_v)$ is the 4×4 homogeneous transformation matrix from the platform frame $\{P\}$ to the world frame $\{W\}$, constructed from the platform's pose $q_v = [X_v, Y_v, \phi_v]^T$.

- $T_e^P(\theta_a)$ is the 4×4 homogeneous transformation matrix from the end-effector frame $\{e\}$ to the platform frame $\{P\}$. This is the standard forward kinematics of the 3-DoF manipulator, typically derived from Denavit-Hartenberg (DH) parameters, and is a function of only the joint angles θ_a. The complete set of DH parameters for the manipulator is provided in (Li & Ge (2013)).

From the final transformation matrix $T_e^W(q)$, we extract the 6-DoF pose vector $P_e \in \mathbb{R}^6$. We denote by f_{FK} the forward kinematics mapping $P_e = f_{\text{FK}}(q)$, which maps the generalized coordinates q of the MM to its end-effector pose in the world frame.

3.3.2.2 Whole-Robot Velocity Model and Jacobians

For control design, we require the end-effector velocity $V_e \in \mathbb{R}^6$, consisting of the linear and angular velocity components expressed in the world frame. This relationship is obtained from the differential kinematics, which map the generalized joint velocities to the end-effector velocity through the whole-robot Jacobian $J_e(q) \in \mathbb{R}^{6\times6}$ (Brahmi *et al.* (2016); Li & Ge (2013)).

The differential kinematic relation is:

$$V_e = J_e(q)\dot{q} = \begin{bmatrix} J_v(q) & J_a(q) \end{bmatrix} \begin{bmatrix} \dot{q}_v \\ \dot{\theta}_a \end{bmatrix} \tag{3.14}$$

which separates the contributions of the mobile platform and the robotic arm:

- $J_a(q) \in \mathbb{R}^{6\times3}$ is the manipulator Jacobian, mapping the joint velocities ($\dot{\theta}_a$) to the end-effector's velocity.
- $J_v(q) \in \mathbb{R}^{6\times3}$ is the platform Jacobian, mapping the platform's generalized velocities ($\dot{q}_v$) to the end-effector's velocity.

3.3.2.3 Reduced (Independent) Jacobian

The velocity vector $\dot{q}$ is 6-dimensional, but it is not a vector of independent velocities due to the nonholonomic constraint. The entire system is controlled by only 5 independent (actuated) velocities: $\dot{\theta} = [\dot{\theta}_v^T, \dot{\theta}_a^T]^T = [\dot{\theta}_R, \dot{\theta}_L, \dot{\theta}_1, \dot{\theta}_2, \dot{\theta}_3]^T$.

To derive the dynamic model and the final control law, we must relate the 6-DoF end-effector velocity V_e directly to this 5-dimensional independent velocity vector $\dot{\theta}$. We first define a full transformation matrix $S_{full}(q_v) \in \mathbb{R}^{6\times5}$ that maps $\dot{\theta}$ to $\dot{q}$ by combining the platform kinematics (Eq. 3.12) with the manipulator kinematics:

$$\dot{q} = \begin{bmatrix} H(q_v) & 0_{3\times3} \\ 0_{3\times2} & I_{3\times3} \end{bmatrix} \begin{bmatrix} \dot{\theta}_v \\ \dot{q}_a \end{bmatrix} = S_{full}(q_v)\,\dot{\theta} \tag{3.15}$$

This matrix $S_{full}(q_v)$ is the same transformation matrix that will be used to derive the reduced dynamic model in the next section. By substituting this into the velocity model, we get:

$$V_e = J_e(q)\dot{q} = J_e(q)(S_{full}(q_v)\,\dot{\theta} \tag{3.16}$$

We can now define the Reduced Jacobian (or Independent Jacobian) $J_r(q) \in \mathbb{R}^{6\times5}$:

$$J_r(q) = J_e(q)S_{full}(q_v) \tag{3.17}$$

This gives the final, crucial kinematic relationship for this thesis:

$$V_e = J_r(q)\,\dot{\theta} \tag{3.18}$$

This equation maps the 5 actuated velocities ($\dot{\theta}_R, \dot{\theta}_L, \dot{\theta}_1, \dot{\theta}_2, \dot{\theta}_3$) directly to the 6-DoF velocity of the end-effector in the world frame. The 6×5 dimension of $J_r(q)$ highlights a key characteristic of this system: it is underactuated in the task space, meaning it has fewer independent controls (5) than the number of task-space coordinates it must manage (6). This makes analyzing system singularities and generating trajectories more complex (Li & Ge (2013)).

3.3.2.4 Inverse Kinematics for Trajectory Generation

The control strategies developed in this thesis are formulated in joint space. Accordingly, the control objective is to ensure that the system's five independent generalized coordinates namely the joint positions, velocities, and accelerations θ, $\dot{\theta}$, and $\ddot{\theta}$ track the corresponding

desired joint space references θ_d, $\dot{\theta}_d$, and $\ddot{\theta}_d$. These reference signals are generated by applying inverse kinematics to the desired task-space motion and differentiating the resulting joint trajectory to obtain consistent velocity and acceleration signals.

However, tasks for a mobile manipulator are typically defined in the 6-DoF Cartesian task space as a desired end-effector trajectory $P_{e,d}(t)$. Therefore, an inverse kinematics (IK) solver is required as a preliminary step to map the desired Cartesian-space trajectory $P_{e,d}(t)$ into the corresponding 5-dimensional joint-space trajectory $\theta_d(t)$.

Solving the inverse kinematics for this system amounts to finding $q(t)$ such that $FK(q(t)) = P_{e,d}(t)$, subject to the nonholonomic constraint $A(q_v)\dot{q}_v = 0$. This constitutes a constrained and generally nonlinear optimization problem, which is often addressed using numerical methods Li & Ge (2013); Henein *et al.* (2022).

Within the scope of this thesis, it is assumed that a feasible and sufficiently smooth joint-space reference trajectory $\theta_d(t)$ has been generated offline by an IK solver. The primary objective of the control laws developed in Chapters 4, 5, and 6 is to ensure that the actual system state $\theta(t)$ tracks $\theta_d(t)$ with high precision and robustness.

3.4 Dynamic Modeling with Constraint Elimination

With the kinematic relationships established, we now derive the dynamic model of the MM. This model describes the relationship between the actuator torques and the system's resulting motion (acceleration). The derivation follows the Lagrange-d'Alembert formulation, which systematically accounts for the system's energies and the nonholonomic constraints.

3.4.1 Lagrange Formulation with Constraints

We derive the dynamic model for the entire 6-DoF system using the Lagrangian formulation (Li & Ge (2013)). First, we formulate the total kinetic energy $K(q, \dot{q})$ and total potential energy $P(q)$ of the system (platform and links). The Lagrange-d'Alembert equations of motion are given by:

$$\frac{d}{dt}\left(\frac{\partial \mathcal{L}}{\partial \dot{q}}\right) - \frac{\partial \mathcal{L}}{\partial q} = B(q)\tau - A^T(q)\lambda - \tau_{\text{dist}} \tag{3.19}$$

This expands to the full, constrained dynamic model, which captures the complete physics of the coupled system (Li *et al.* (2007, 2008)):

$$M(q)\ddot{q} + C(q,\dot{q})\dot{q} + G(q) + \tau_d = B(q)\tau - A^T(q)\lambda \tag{3.20}$$

Here, $M(q)$ is the 6×6 coupled inertia matrix, $C(q,\dot{q})$ is the 6×6 coupled Coriolis/centrifugal matrix, and $G(q)$ is the 6×1 gravity vector. These terms are highly nonlinear and capture the complex dynamic coupling between the arm and the base Yamamoto & Yun (1996); Zhong *et al.* (2013)). The term τ is the 5×1 vector of input torques (2 for wheels, 3 for joints), $B(q)$ is the input matrix, τ_d represents all external disturbances and unmodeled forces like friction, and $A^T(q)\lambda$ is the 6×1 vector of nonholonomic constraint forces.

3.4.2 Constraint Elimination and Reduced Dynamics

The full dynamic model is not suitable for control design because it includes the unknown constraint force vector $A^T(q)\lambda$. To obtain a usable model, these constraint forces must be eliminated. This is achieved by projecting the system's dynamics onto the allowable (unconstrained) directions of motion (Li & Ge (2013)).

In the previous section, we defined the 5-dimensional vector of independent (actuated) velocities as $\dot{\theta} = [\dot{\theta}_R, \dot{\theta}_L, \dot{\theta}_1, \dot{\theta}_2, \dot{\theta}_3]^T$. We also derived the full transformation matrix $S_{full}(q_v) \in \mathbb{R}^{6\times5}$ that maps these independent velocities to the 6-dimensional generalized velocities $\dot{q}$:

$$\dot{q} = S_{full}(q_v)\dot{\theta} \tag{3.21}$$

where: $S_{full}(q_v) = \begin{bmatrix} H(q_v) & 0_{3\times3} \\ 0_{3\times2} & I_{3\times3} \end{bmatrix}$

This matrix $S_{full}(q_v)$ spans the null-space of the constraint matrix $A(q)$, meaning $A(q)$ $S_{full}(q_v) = 0$. By pre-multiplying the full dynamic model by $S_{full}(q_v)^T$, the constraint term is eliminated:

$$S_{full}(q_v)^T A^T(q)\lambda = (A(q)S_{full}(q_v))^T\lambda = 0 \tag{3.22}$$

This projection yields the reduced (or constraint-free) dynamic model of the 5-DoF system. We substitute $\dot{q} = S_{full}(q_v)\dot{\theta}$ and its derivative $\ddot{q} = \dot{S}_{full}(q)\dot{\theta} + S_{full}(q_v)\ddot{\theta}$ into the projected equation:

$$S_{full}^T M(\dot{S}_{full}\dot{\theta} + S_{full}\ddot{\theta}) + S_{full}^T C(S_{full}\dot{\theta}) + S_{full}^T G + S_{full}^T \tau_d = S_{full}^T B\tau \tag{3.23}$$

Grouping terms by $\ddot{\theta}$ and $\dot{\theta}$ gives the final reduced dynamic model:

$$\bar{M}(\theta)\ddot{\theta} + \bar{C}(\theta,\dot{\theta})\dot{\theta} + \bar{G}(\theta) + \bar{\tau}_d = \bar{\tau} \tag{3.24}$$

where the reduced matrices are defined as:

- $\bar{M}(\theta) = S_{full}^T M S_{full}$ (the 5×5 reduced inertia matrix)
- $\bar{C}(\theta,\dot{\theta}) = S_{full}^T(M\dot{S}_{full} + CS_{full})$ (the 5×5 reduced Coriolis/centrifugal matrix)
- $\bar{G}(\theta) = S_{full}^T G$ (the 5×1 reduced gravity vector)
- $\bar{\tau}_d = S_{full}^T \tau_d$ (the 5×1 reduced disturbance vector)
- $\bar{\tau} = S_{full}^T B\tau$ (the 5×1 reduced input torque vector)

This equation, which governs the 5 controllable degrees of freedom, is the foundation for all control design in this thesis.

3.4.3 Structural Properties of the Dynamic Model

The reduced dynamic model possesses two critical properties that are essential for the Lyapunov-based stability analysis of advanced controllers (Li *et al.* (2008)):

1. Symmetry and Positive-Definiteness: The reduced inertia matrix $\bar{M}(\theta)$ is symmetric and positive-definite (i.e., $\bar{M} = \bar{M}^T > 0$) for all q.
2. Skew-Symmetry: The matrix $(\dot{\bar{M}} - 2\bar{C})$ is skew-symmetric. This implies $z^T(\dot{\bar{M}} - 2\bar{C})z = 0$ for any vector $z \in \mathbb{R}^5$. This property is crucial for proving that the derivative of quadratic Lyapunov functions (e.g., $V = \frac{1}{2}s^T\bar{M}s$) contains no destabilizing terms from

the model's own dynamics, which greatly simplifies stability analysis for sliding-mode control.

3.5 Control-Oriented Formulation for ESO Design

For the design of the observers (NESO, ESO, FESO), it is essential to isolate the "total disturbance" term. We begin with the reduced dynamic model:

$$\bar{M}(\theta)\ddot{\theta} + \bar{C}(\theta, \dot{\theta})\dot{\theta} + \bar{G}(\theta) + \bar{\tau}_d = \bar{\tau} \tag{3.25}$$

We now solve for the acceleration $\ddot{\theta}$:

$$\ddot{\theta} = \bar{M}^{-1}(\theta)\left(\bar{\tau} - \bar{C}(\theta, \dot{\theta})\dot{\theta} - \bar{G}(\theta) - \bar{\tau}_d\right) \tag{3.26}$$

As established in Chapter 2, it is impractical to model all these terms perfectly. The matrices $\bar{M}$, $\bar{C}$, and $\bar{G}$ are highly complex, and $\bar{\tau}_d$ is, by definition, unknown. Following the ADRC philosophy, we define a nominal, known (or estimated) part of the model, $\bar{M}_0$, and lump everything else into a single vector, f, the "total disturbance". The dynamic equation is then rewritten as:

$$\ddot{\theta} = f + D(\theta)\bar{\tau} \tag{3.27}$$

where:

- $f = \bar{M}^{-1}(-\bar{C}\dot{\theta} - \bar{G} - \bar{\tau}_d) + (\bar{M}^{-1} - \bar{M}_0^{-1})\bar{\tau}$
- $D(\theta) = \bar{M}_0^{-1}(\theta)$

The term f conveniently collects all model uncertainties, nonlinear coupling terms, friction, and external disturbances into a single, aggregated disturbance vector. $D(\theta)$ is the nominal control input matrix, which is assumed to be known (or, at minimum, a constant estimate D_0 can be used).

This final, control-oriented formulation is the foundation for all controllers designed in this thesis. The objective of the ESO, NESO, and FESO in the subsequent chapters will be to provide a real-time estimate, $\hat{f}$, of the unknown disturbance term f, allowing the control law $\bar{\tau}$ to be designed to cancel it.

3.6 Chapter Summary

This chapter has presented the complete derivation of the 5-DoF Mob-ÉTS MM. We began by defining the system's coordinates and kinematic structure. We derived the nonholonomic constraint of the mobile base and the reduced, independent Jacobian. Using the Lagrange-d'Alembert formulation, we derived the full equations of motion and then mathematically eliminated the constraint forces to arrive at the 5-DoF reduced dynamic model. Finally, we rearranged this model into a control-oriented state-space formulation, $\ddot{\theta} = f + D(\theta)\bar{\tau}$, which isolates the "total disturbance" f. This final model and its stated properties form the mathematical basis for the design and stability analysis of the advanced controllers in Chapters 4, 5, and 6.

CHAPTER 4

TRAJECTORY TRACKING FOR MOBILE MANIPULATOR BASED ON NONLINEAR ACTIVE DISTURBANCE REJECTION CONTROL

Mhmed Algrnaodi[1], Maarouf Saad[1], Mohamad Saad[2], Raouf Fareh[3], Abdelkarim Brahmi[1]

[1] Department of Electrical Engineering, École de technologie supérieure,
1100 Notre-Dame Ouest, Montréal, QC, Canada
[2] School of Engineering, Université du Québec en Abitibi-Témiscamingue (UQAT), QC, Canada
[3] Department of Electrical Engineering, University of Sharjah, Sharjah, UAE

Article published in "International Journal of Modelling, Identification and Control"
January 2022

Abstract

This paper designs a nonlinear active disturbance rejection control (ADRC) to solve the trajectory tracking problem of a mobile manipulator (MM) in the presence of parameters' uncertainties, and nonlinear dynamics coupling effects of the MM system. The control scheme consists of a nonlinear extended state observer (NESO) and a nonlinear proportional derivative (PD) controller. Based on the Lagrange formulation, a dynamical model of the MM is formulated, where external disturbances and modeling uncertainties are assumed to be part of the "total disturbance" which is estimated with an observer and rejected on-line in the control law. Since the proposed controller cannot be performed unless the full transformed state vector of the system model is available, an NESO is designed to estimate the transformed state vector as well as the uncertainties. The nonlinear PD controller utilizes the state estimated by the NESO, and the effect of uncertainties is cancelled on-line by the control input. Experimental results of the MM proposed tracking controller show its validity and efficiency.

Keywords:Active disturbance rejection control, mobile manipulator, modeling uncertainty, external disturbances, nonlinear extended state observer.

4.1 Introduction

Nowadays, robots can carry out complex tasks. Modern applications require more advanced functionalities to accomplish the desired tasks. For this reason, robotic systems have an ongoing need to improve and develop their functional systems, to prompt or adapt their reactions to unpredicted circumstances. These missions, which require robots with a major capability for mobility, adeptness and manipulability of the robotic system, have certain advantages in many applications. Mobile manipulators (MMs) provide enormous opportunities to achieve wide tasks which are not achieved by the fixed-base manipulators or by the mobile base alone. An N-degree of freedom (N-DoF) MM is a robotic system composed of a serial-link manipulator mounted on a wheeled mobile platform. Due to different dynamics, there is a combined interaction between both dynamics of MMs.

The trajectory tracking control of the MM is an incorporated system comprising the end-effector of the arm and the mobile base to follow their desired trajectories. In addition, to obtain better control performance, it is realistic to take into consideration the trajectory tracking problem with nonlinearity, uncertainties, external disturbances, and coupling effects. The control scheme of the MM trajectory tracking is still a challenging problem and has attracted considerable attention in the control field.

Many researchers have developed various methods for real-time applications in trajectory tracking control. The modeling and compensation of dynamic interactions in effect between both subsystems of the MM have been the focus of research (Yamamoto & Yun (1994, 1996); Yu & Chen (2002)). Also, these authors considered a modular method to calculate the dynamical equations of a N-link MM. The Lagrange-d'Alembert formulation was used to develop the nonholomonic equations of motion of a MM in (Chung & Velinsky (1998)). The tracking control problem utilizing the overall dynamical model was considered in (Walsh *et al.* (1994)), including the redundancy between the robot manipulator and the mobile platform.

In recent years, several tracking control approaches have been devoted to solve the trajectory tracking problem for MMs, such as input-output linearization (Chung & Velinsky (1998)), adaptive fuzzy combined with backstepping (Zhong *et al.* (2013)), adaptive sliding mode backstepping (Dong (2002)), adaptive control (Andaluz *et al.* (2012)), robust adaptive control

(Li *et al.* (2008); Peng, Yu & Wang (2014); Chen, Song, Li, Sun & Ai (2013)), and Recurrent Neural Network (RNN) (Khan *et al.* (2020)). Despite good tracking performance, most of the proposed controls were validated in simulation. Moreover, decentralized control methods have been applied to solve the trajectory tracking problem for MMs (Fareh, Brahmi, Saad, Saad & Bettayeb (2017); Brahmi, Saad, Gauthier, Zhu & Ghommam (2019); Savino, Pimenta, Shah & Adorno (2020)). In these works, the dynamics of the whole system was divided into two subsystems, and control laws were developed based on each subsystem. To achieve an excellent performance in trajectory tracking applications, the controller needs complete information on the robot dynamics. In practice, this is challenging and the obtained model may be considered with uncertainties, disturbances, and nonlinearities. In general, the tracking control algorithms of MMs are mainly divided into two different approaches that can be found in the literature. One approach considers the MM as a single system and the controller is developed for the whole system, which is termed centralized control. The other approach is called decentralized control. In this case, the MM is considered as two subsystems: the mobile base and the manipulator.

Traditional control schemes based on PD controllers (Castañeda, Luviano-Juárez & Chairez (2014)) have been successfully achieved in robot applications. The PD-based controller is applied without including the coupling effects. Therefore, its execution is influenced by disturbances. In order to obtain an excellent control performance in trajectory tracking applications, advanced control actions are needed to minimize the tracking error (Su *et al.* (2006)).

As an alternative, the ADRC technique does not depend on complete model information for the system, and the total disturbances, including both external disturbances and dynamic uncertainties, are estimated on-line by an extended state observer (ESO). In the ADRC scheme, the ESO is the most commonly used estimation method (Xing, Jeon, Park & Oh (2011); Radke & Gao (2006)).

The ADRC scheme consists of an ESO-based feedback control. The essence of ADRC is to handle out the whole effects of the total disturbances in a nonlinear system. In ESO, the total disturbances are considered as an extended system state which is estimated along with

the original state variables (Castañeda *et al.* (2014)). Furthermore, these total disturbances are actively canceled by a designed feedback controller in the robot's dynamics. Therefore, using an ESO, the ADRC becomes more robust against the total disturbances of the model system due to the accurate estimation of the complete state, as well as uncertainties. These advantages have been used to design ADRC controllers for tracking control problems and have been successfully validated by numerous applications in (Xue, Madonski, Lakomy, Gao & Huang (2017); Talole, Kolhe & Phadke (2009); Guo & Zhao (2016)).

The ADRC approach was designed for an omnidirectional mobile robot in (Fu, Li, Wang & Zhang (2018)). The experimental results illustrated good control accuracy and robustness with modeling nonlinearities and external disturbance. In (Sebastian & Ben-Tzvi (2019)), the path tracking performance of autonomous tracked vehicles was improved using an ADRC method to handle the effect of slip in an online manner. The proposed method has shown reliable trajectory tracking through experiments over the flat and uneven terrain conditions using the tracked skid-steer mobile robot. An ADRC design technique was developed for compass-like biped robots in (Song, Tang, Wang & Yan (2018)). A proposed control strategy was implemented by integrating the ADRC and linearization. A series of numerical simulations illustrated that the ADRC has an excellent disturbance rejection effect. In (Song, Li, Yu, Wang & Ruan (2008)), ADRC has been implemented for control of tracked robots on stairs. This approach allows the robot to maintain a smooth and precise tracking and effectively overcome the disturbance, as shown in simulation results. In (Jiuhong, Xuewen & Sanyou (2007)), ADRC has been designed for a rock drilling robot joint hydraulic drive system. The simulation results illustrate the robustness of the designed approach to the system parameter uncertainties with disturbances. An ADRC method was implemented for the planar vertical take-off and landing aircraft in (Xu, Zhang & Hu (2019b)). A novel reconfigurable control method was proposed by ADRC to counteract the adverse effects when actuator faults occur. The obtained results from the simulation confirm the effectiveness and performance of the proposed controller. Moreover, steady high performance can be achieved. ADRC was also presented for a flexible link manipulator to follow required trajectories in the joint space (Fareh, Al-Shabi, Bettayeb & Ghommam (2019)). The simulation and

experimental results show effective performance of the designed control. In (Zhao, Li, Liu & Cheng (2017)), an ADRC approach was employed for a one-link manipulator system driven by pneumatic artificial muscles. Experimental results demonstrate the validity and the tracking advantages of the designed method.

In MM systems, ADRC was employed for position/force control of a holomonic constrained MM in the joint space (Wei *et al.* (2017)). Simulation results illustrated the convergence of the trajectory and the constrained force to their desired trajectory. In (Ren *et al.* (2018)), an ADRC approach was applied for trajectory tracking control of an omnidirectional MM under external disturbances and unknown system dynamics. Simulation results showed the robustness and effectiveness of the proposed method. However, there is strong coupling between mobile and manipulator subsystems. It is more meaningful to consider disturbance rejection in a complete MM system. To the best of our knowledge, there is little research with experimental results on the design of ADRC for MMs, which motivates us to carry out the current research.

Most of the ADRC schemes mentioned above use linear ESO to estimate total disturbances. Furthermore, all the previous studies of MM systems based on ADRC controller have performed validation with simulations only.

Based on its control design, ADRC is easily implemented and needs very little knowledge about plant dynamics. In the design of the nonlinear ADRC controller for complex systems, there are remarkable efforts to solve the problem of stability analysis. Where the ADRC contributes the complexity can be reduced by grouping all the external disturbances and nonlinearities into a generalized term (Gao (2006b); Ahi & Haeri (2018)). Moreover, with the theoretical progress in the study of the convergence and estimate error analyses of the NESO, it was proved by the self-stable region (SSR) theory that the estimated states can convergence the actual states (Huang (1999); Huang & Han (2000)). Recently, Li, Xia, Qi & Wan (2018) proved and analyzed the convergence of the discrete-time NESO. In (Wu & Chen (2012, 2014)), analysis of nonlinear ADRC-based control system was presented. The stability and the convergence of the ADRC method were studied in (Qi, Li, Xia & Gao (2017); Aguilar-Ibañez, Sira-Ramirez & Suarez-Castanon (2017); Huang & Xue (2014)).

In this paper, a nonlinear ADRC technique is designed and applied in the control scheme for an MM system in real-time application. This proposed control is employed to follow a desired trajectory in the Cartesian space. Nonlinearities, modeling uncertainty, and external disturbances are regarded as the "total disturbance" and are assumed to be unknown. The main contributions of this paper are as follows:

(1) This paper provides strong mathematical modeling based on the coupled dynamics of the Mobile platform and the manipulator (MM) in the presence of modeling uncertainties and external disturbances based on Lagrangian approach.

(2) An NESO-based nonlinear PD controller compensation scheme is introduced to obtain good trajectory tracking control performances for an MM system.

(3) Compared with the previous research works, real-time application of the ADRC method is done for an MM that greatly improves MM's ability to suppress continuous disturbances under a complex nonlinear dynamical model.

(4) Accurate trajectory tracking experimental results taking into account total disturbances, such as nonlinearities, modeling uncertainty, and disturbances show the validity of the proposed method.

The reminder of this paper is organized as follows. A brief description of the kinematic and dynamical models of the MM system, and the control objective are shown in Section II. Section III presents the control design of the ADRC method. Section IV provides experimental results, which illustrate the validation and effectiveness of the proposed control. Finally, conclusions are given in Section V.

4.2 Description of Mobile Manipulator

This section briefly describes the kinematic model and derives the dynamical model of the N-DoF MM in the Cartesian space. The Lagrangian technique is considered for the MM system (Li & Ge (2013)). The system is illustrated in Figure 4.1, where a three-link robotic manipulator is mounted upon the center of a wheeled mobile robot. In the mobile platform, the two front wheels are active, and the two rear wheels are passive. In addition, the full MM system has 5-DoF, where the manipulator is subjected to a holonomic constraint, and the mobile base is subjected to a nonholonomic constraint.

4.2.1 Kinematic

In most robot applications, the desired trajectory is defined in the Cartesian space. P_e illustrates the position/orientation vector of the MM end effector as shown in Figure 4.1. The MM can be described by the generalized coordinates $q = [q_v^T, q_a^T]^T$ where $q_v = [X_v, Y_v, \phi_v]^T$ and $q_a = [\theta_1, \theta_2, \theta_3]^T$ with $q_v \in R^{n_v}$ and $q_a \in R^{n_a}$ are the state vectors of the mobile robot and the manipulator, respectively, and $n = n_v + n_a$. The relation between the generalized coordinates of the MM, its derivative $\dot{q} \in R^n$, and the end effector velocity, $V_e \in R^n$, is described as follows (Brahmi *et al.* (2016)):

$$V_e = J_e(q)\dot{q} \tag{4.1}$$

where $J_e(q) \in R^{n \times n}$ is the Jacobian matrix and $\dot{q} = [\dot{q}_v^T, \dot{q}_a^T]^T$ with $\dot{q}_v = [\dot{X}_v, \dot{Y}_v, \dot{\phi}_v]^T$ is the linear/angular velocity of the mobile robot, and $\dot{q}_a = [\dot{\theta}_1, \dot{\theta}_2, \dot{\theta}_3]^T$ is the joint velocity vector of the robot manipulator.

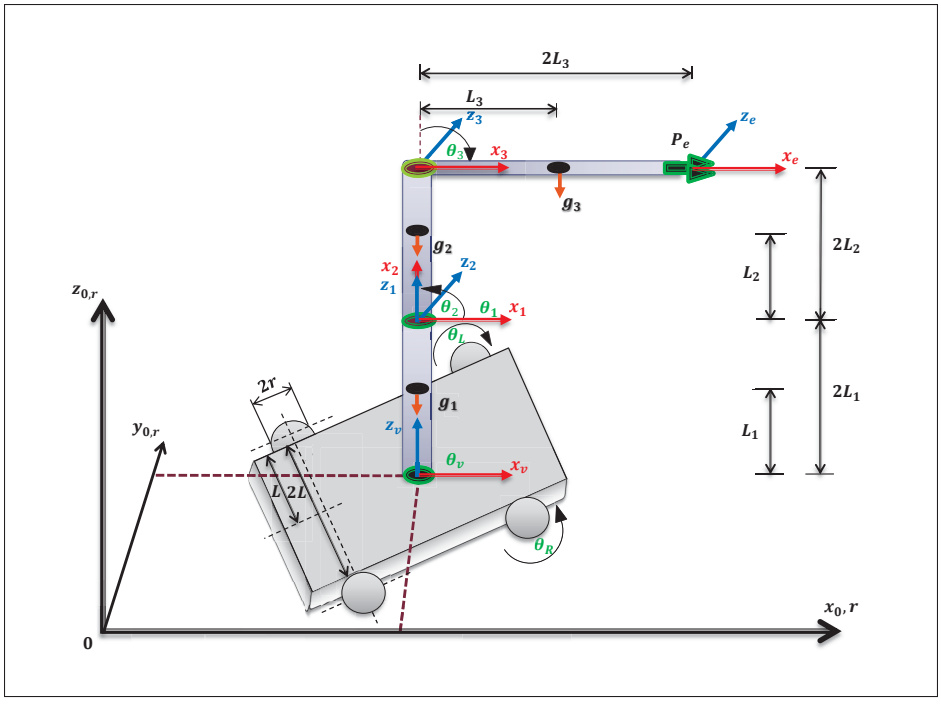

Figure 4.1 The system of 5-DoF MM

4.2.2 Dynamic Model

Using the Lagrangian technique, the mathematical model of the whole MM system is obtained by the following equation (Li *et al.* (2007)):

$$M(q)\ddot{q} + C(q,\dot{q})\dot{q} + G(q) + \tau_d = B(q)\tau - A^T(q)\lambda \tag{4.2}$$

where $M(q)\in R^{n\times n}$ is the positive definite inertia matrix, $C(q,\dot{q})\in R^{n\times n}$ is the centrifugal and Coriolis matrix, $G(q)\in R^n$ is the vector of gravity terms, q, $\dot{q}$ and $\ddot{q}$ represent the position, velocity and acceleration vectors, respectively, of the MM system, $\tau_d\in R^n$ is the vector of external disturbances, $B(q)\in R^{n\times r}$ is the full rank input transformation matrix with $r = r_v + r_a$, $\tau\in R^r$ is the input control vector, $A(q)\in R^{r\times n}$ is a constraint matrix, $\lambda\in R^r$ is the constraint force, and are represented as:

$$M(q) = \begin{bmatrix} M_v & M_{va} \\ M_{av} & M_a \end{bmatrix}, C(q) = \begin{bmatrix} C_v & C_{va} \\ C_{av} & C_a \end{bmatrix},$$
$$G(q) = \begin{bmatrix} G_v \\ G_a \end{bmatrix}, \tau_d = \begin{bmatrix} \tau_{dv} \\ \tau_{da} \end{bmatrix}, B(q) = \begin{bmatrix} B_v & 0 \\ 0 & B_a \end{bmatrix},$$
$$\tau = \begin{bmatrix} \tau_v \\ \tau_a \end{bmatrix}, A = \begin{bmatrix} A_v & 0 \\ 0 & 0 \end{bmatrix}, \lambda = \begin{bmatrix} \lambda_v \\ \lambda_a \end{bmatrix}.$$

The constraints of the mobile platform are presumed to be independent such that:

$$A(q_v)\dot{q}_v = 0 \tag{4.3}$$

where $A(q_v)\in R^{l\times n_v}$ is the kinematic constraint matrix and $l = n_v - m$ is the number of non-integrable constraints.

Assume $S(q_v)\in R^{n_v\times(l-n_v)}$ to be the orthocomplement of $A(q_v)$, and (Li & Ge (2013)):

$$S^T(q_v)A^T(q_v) = 0 \tag{4.4}$$

where $S(q_v) = [S_1(q_v), ..., S_{(n_v-l)}(q_v)]^T\in R^{n_v\times(n_v-l)}$. Remark that $S^T S$ is of full rank.

From the constraints (4.3) and (4.4), let the auxiliary vector $\dot{\eta} \in R^{n_v - l}$, such that:

$$\dot{q}_v = S(q_v)\dot{\eta} \tag{4.5}$$

which is the kinematic model of the nonholomonic mobile subsystem. Differentiating (4.5) yields

$$\ddot{q}_v = \dot{S}(q_v)\dot{\eta} + S(q_v)\ddot{\eta} \tag{4.6}$$

where $S(q_v) = \begin{bmatrix} \cos(\phi_v) & \sin(\phi_v)) & 0 \\ 0 & 0 & 1 \end{bmatrix}^T$, and $\dot{\eta} = [v_v, w_v]^T$ with v_v as the linear velocity and w_v as the angular velocity of the mobile platform.

Let $\dot{\theta}_R$ and $\dot{\theta}_L$ be the angular velocities of the right and left wheels, respectively, where the velocity vector of the mobile platform is denoted as $\dot{\theta}_v = [\dot{\theta}_R, \dot{\theta}_L]^T$. Then, the kinematic model of nonholomonic system can be expressed as:

$$\dot{\eta} = R(q_v)\dot{\theta}_v \tag{4.7}$$

where $R(q_v) = \begin{bmatrix} \frac{r}{2} & \frac{r}{2} \\ \frac{r}{2L} & \frac{-r}{2L} \end{bmatrix}$.

Thus,

$$H(q_v) = S(q_v)R(q_v) = \begin{bmatrix} \frac{r}{2}cos(\phi_v) & \frac{r}{2}sin(\phi_v) & \frac{r}{2L} \\ \frac{r}{2}cos(\phi_v) & \frac{r}{2}sin(\phi_v) & \frac{-r}{2L} \end{bmatrix}^T \tag{4.8}$$

Considering equations (4.4), (4.5), and (4.6), the term of the nonholomonic constraint $A^T(q)\lambda$ can be eliminated from equation (4.2). Then, the dynamic model in equation (4.2) can be reformulated as:

$$\overline{M}(\theta)\ddot{\theta} + \overline{C}(\theta, \dot{\theta})\dot{\theta} + \overline{G}(\theta) + \overline{\tau}_d = \overline{\tau} \tag{4.9}$$

where $\theta = [\theta_v^T, \theta_a^T]^T$ are the generalized coordinates with $\theta_v = [\theta_R, \theta_L]^T$ being the angular position of the mobile platform, and $\theta_a = q_a = [\theta_1, \theta_2, \theta_3]^T$ being the joint position of the robot manipulator, $\dot{\theta} = [\dot{\theta}_R, \dot{\theta}_L, \dot{\theta}_1, \dot{\theta}_2, \dot{\theta}_3]^T$, where $\dot{\theta}_a = [\dot{\theta}_1, \dot{\theta}_2, \dot{\theta}_3]^T$ is the joint velocities

of the robot manipulator,

$$\overline{M}(\theta) = \begin{bmatrix} H^T M_v H & H^T M_{va} \\ M_{av} H & M_a \end{bmatrix},$$

$$\overline{C}(\theta) = \begin{bmatrix} H^T M_v \dot{H} + H^T C_v H & H^T C_{va} \\ M_{av} \dot{H} + C_{av} H^T & C_a \end{bmatrix},$$

$$\overline{G}(\theta) = \begin{bmatrix} H^T G_v \\ G_a \end{bmatrix}, \overline{\tau}_d = \begin{bmatrix} H^T \tau_{dv} \\ \tau_{da} \end{bmatrix},$$

$$\overline{\tau} = \overline{B}\tau, \overline{B} = \begin{bmatrix} H^T B_v & 0 \\ 0 & B_a \end{bmatrix}.$$

The model uncertainty and the state vector of the MM are unknown and had to be exactly estimated for the controller design. The mathematical model given in equation (4.9) has the following properties (Li *et al.* (2008)):

property 1: $\overline{M}$ is a positive definite matrix.

property 2: $S = \dot{\overline{M}} - 2\overline{C}$ is a skew symmetric matrix, i.e. $\forall z \in R^n$, we have $z^T(\dot{\overline{M}} - 2\overline{C})z = 0$.

4.2.3 Control Objective

The main objective of this research is to design an ADRC controller for the MM represented by equation (4.9), so that the manipulator's effector position P_e tracks the desired positions P_d defined in the Cartesian space. The inverse kinematics are used to obtain the joint space desired trajectory θ_d from the Cartesian position/orientation trajectory P_d. The aim of the controller is to generate a set of torque inputs to ensure that the measured position vector θ of the robot tracks the desired joint trajectory θ_d, and to eliminate the effect of the "total disturbance" by introducing an ESO.

With the above notations, the control objective can be formulated so as to design the control input $\tau = [\tau_v^T, \tau_a^T]^T$, where $\tau_v = [\tau_R, \tau_L]^T$ and $\tau_a = [\tau_1, \tau_2, \tau_3]^T$ are the control inputs for the mobile base and the manipulator, respectively, such that:

$$\lim_{t \to \infty} ||\theta - \theta_d|| = \lim_{t \to \infty} ||\dot{\theta} - \dot{\theta}_d|| = 0$$

where, $\theta_d \in R^{5\times1}$ and $\dot{\theta}_d \in R^{5\times1}$ are the desired joint angular position and velocity of the MM, respectively.

4.3 ADRC Design

In this paper, ADRC is used to control the MM by addressing the issue of uncertainties and estimation of state variables. The proposed control involves two steps. The first step is to design the NESO, in order to have an estimate of the uncertainties, as well as the exact state vector. The second step is to integrate the NESO with a nonlinear PD controller to compensate for the estimated uncertainties. During the dynamic compensation of the estimated uncertainties, the system model is reduced to a double integrator. A nonlinear PD controller is then sufficient to control it. The NPD controller and NESO parameters are the gains of the controller, K_p and K_d and the bandwidth of the NESO w_0. Compared to other control methods, the ADRC concept of PD or NPD is a more powerful and easier method to use and tune parameters than PID. Also, the ADRC control model makes the response faster and reduces the overshoot. The ADRC performs with PD much better than PID as mentioned in (Gao *et al.* (2001)).

The MM mathematical model in equation (4.9) can be rewritten as:

$$\ddot{\theta} = f + \overline{M}_0 \, \overline{\tau} \tag{4.10}$$

Define

$$f = \overline{M}_0[-\overline{C}(\theta, \dot{\theta})\dot{\theta} - \overline{G}(\theta) - \overline{\tau_d}\,] \tag{4.11}$$

where $\overline{M}_0 = \overline{M}^{-1}$, and $f = [f_{\theta_R}; f_{\theta_L}; f_{\theta_1}; f_{\theta_2}; f_{\theta_3}]$ is considered as the "total disturbance" of the five joints, including the uncertain dynamics, the external disturbances and the dynamic coupling effects between the robot manipulator and the mobile base.

4.3.1 NESO Design

The NESO is an observer that can estimate the state of the system as well as the "total disturbance". Its merit is that it is simpler to implement, and independent of the dynamical model of the plant (Gao *et al.* (2001)).That is, the fundamental mechanism of ADRC is to

estimate and compensate for the total disturbance via its observer (Huang & Xue (2014)). From the idea of ADRC theory, the total disturbances are expanded as an extended state $f(t) = x_3$ for system in equation (4.12) which is estimated and compensated by the observer and a controller, respectively (Zhao, Cheng & Wang (2018)).

In the present context, by defining $x_1 = \theta$, $x_2 = \dot{\theta}$, and $x_3 = f(t)$ as the state variables of the system, x_3 is the extended state vector.

The robot dynamic system in equation (4.10) can be rewritten in state-space form as:

$$\begin{cases} \dot{x}_1 = x_2 \\ \dot{x}_2 = x_3 + \overline{M}_0\,\overline{\tau} \\ \dot{x}_3 = h \end{cases} \tag{4.12}$$

where $x_3 = f(x_1, x_2, w)$, is a multivariable function of both the state and external "total disturbances" (w), and h is the derivative of f and is the unknown part required for the implementation of the control law $\overline{\tau}$.

Defining $\hat{f}$ as the estimation of f, a simplistic approach to estimate f in equation (4.10) is (Gao *et al.* (2001)):

$$\hat{f}(x_1, x_2, w) = -(\overline{M}_0\,\overline{\tau} - \dot{x}_2) \tag{4.13}$$

which needs the measurement or estimation of the acceleration $\dot{x}_2$.

Assumption 1: The total disturbance $f(t)$ is assumed to be continuously differentiable and bounded.

The ESO proposed in (Han (2009)) is a nonlinear observer employed to estimate f. From equation (4.12), we construct a nonlinear state observer, denoted as NESO, in the form of:

$$\begin{cases} \varepsilon_1 = \hat{x}_1 - \theta \\ \dot{\hat{x}}_1 = \hat{x}_2 - \beta_1\,\varepsilon_1 \\ \dot{\hat{x}}_2 = \hat{x}_3 - \beta_2\,f_1(\varepsilon_1) + \overline{M}_0\,\overline{\tau} \\ \dot{\hat{x}}_3 = -\beta_3\,f_2(\varepsilon_1) \end{cases} \tag{4.14}$$

where $\varepsilon_1 \in R^{5\times1}$ is the observer's error for the state $x_1 \in R^{5\times1}$, $\hat{x}_i \in R^{5\times1}$ are the observer's output and are the estimation of states $x_i \in R^{5\times1}$; $\beta_i \in R^{5\times5}$ are the observer's gains with $i = 1, 2, 3$; $f_1(\varepsilon_1) \in R^{5\times1}$ and $f_2(\varepsilon_1) \in R^{5\times1}$ are two different nonlinear functions applied to increase the convergence speed of the observer's signals with

$$f_1(\varepsilon_1) = [fal_{11}(\varepsilon_{11}, \alpha_1, \delta), fal_{12}(\varepsilon_{12}, \alpha_1, \delta), ..., fal_{1j}(\varepsilon_{1j}, \alpha_1, \delta)]^T \tag{4.15}$$

and

$$f_2(\varepsilon_1) = [fal_{21}(\varepsilon_{11}, \alpha_2, \delta), fal_{22}(\varepsilon_{12}, \alpha_2, \delta), ..., fal_{2j}(\varepsilon_{1j}, \alpha_2, \delta)]^T \tag{4.16}$$

where $j = 1, 2, 3, 4, 5$, and the following nonlinear functions are selected as (Han (2009)):

$$fal_{1j}(\varepsilon_{1j}, \alpha_1, \delta) = \begin{cases} |\varepsilon_{1j}|^{\alpha_1} \, sign(\varepsilon_{1j}), & |\varepsilon_{1j}| > \delta \\ \varepsilon_{1j}/\delta^{1-\alpha_1}, & |\varepsilon_{1j}| \leq \delta \end{cases} \tag{4.17}$$

$$fal_{2j}(\varepsilon_{1j}, \alpha_2, \delta) = \begin{cases} |\varepsilon_{1j}|^{\alpha_2} \, sign(\varepsilon_{1j}), & |\varepsilon_{1j}| > \delta \\ \varepsilon_{1j}/\delta^{1-\alpha_2}, & |\varepsilon_{1j}| \leq \delta \end{cases} \tag{4.18}$$

where α_1, α_2, and δ are positive parameters to be predetermined, $\varepsilon_{1j} \in R^{5\times1}$ is five variable errors for the state $x_i \in R^{5\times1}$. To enhance the numerical properties of ADRC method, Han [2009] explored various nonlinear mechanisms and proposed to use (4.17) and (4.18) to replace $|\varepsilon_{1j}|^{\alpha_1} \, sign(\varepsilon_{1j})$. This function fal_{1j} introduces a small linear region in the gain function. The use of nonlinear function fal_{1j} in (4.14) can make the observer more efficient. It is a nonlinear gain function to prevent excessive gain when an error is small, which was known to cause high frequency chattering in some simulation studies as shown in (Gao *et al.*

(2001)). And

$$\begin{cases} \beta_1 = diag(3w_0, 3w_0, 3w_0, 3w_0, 3w_0) \\ \beta_2 = diag(3w_0^2, 3w_0^2, 3w_0^2, 3w_0^2, 3w_0^2) \\ \beta_3 = diag(w_0^3, w_0^3, w_0^3, w_0^3, w_0^3) \end{cases} \tag{4.19}$$

where w_0 is the observer bandwidth and $w_0 = 3w_c$ where w_c is a design parameter to be determined (tuned) (Gao (2006b)). For the nonlinear ADRC framework, this nonlinear function plays an important role due to its characteristics of "big error, small gain; small error, big gain " when α_1 and $\alpha_2 < 1$. When α_1 and $\alpha_2 = 1$, this nonlinear function turns into a linear one (Pu *et al.* (2015)).

The architecture of the ADRC controller for the 5-DoF MM is shown in Figure 4.2.

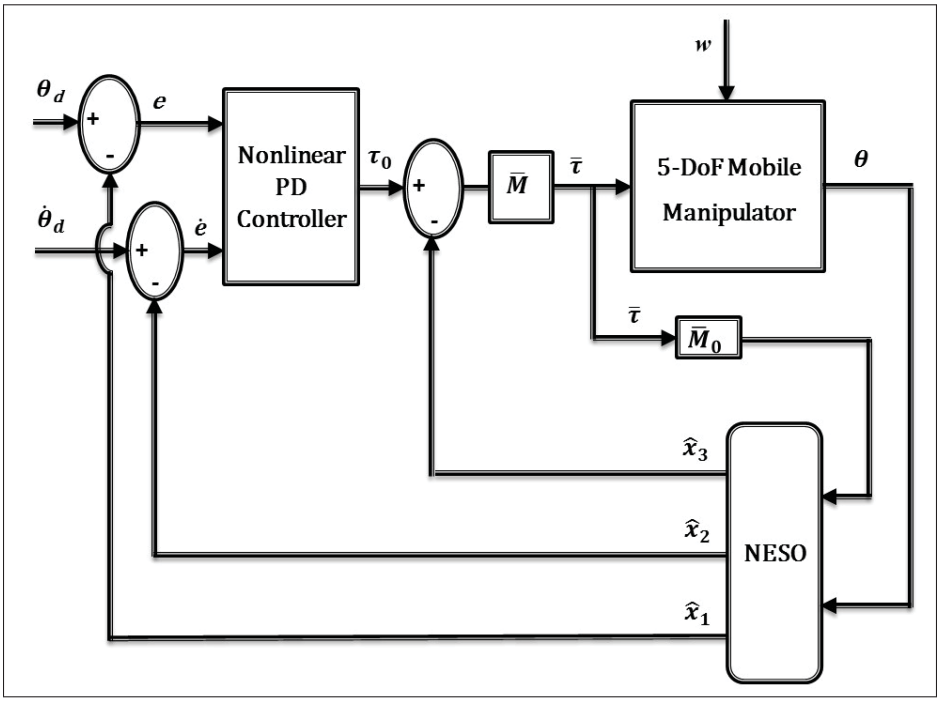

Figure 4.2 Structure of the ADRC controller for 5-DoF MM

4.3.2 Controller Design

Once the NESO has been designed and an appropriate estimation has been obtained, its outputs will track θ, $\dot{\theta}$, and $\ddot{\theta}$, respectively. By cancelling the total effect of f using the observer estimation $\hat{f}$, the ADRC actively compensates for f in the robot system while ensuring acceptable trajectory tracking. The control law is defined as:

$$\tau = \overline{M}(\tau_0 - \hat{f}) \tag{4.20}$$

The system model in equation (3.10) then becomes:

$$\ddot{\theta} = f - \hat{f} + \tau_0 \tag{4.21}$$

We suppose that $f - \hat{f} \cong 0$, this yields to $\ddot{\theta} \approx \tau_0$, which can be easily controlled. The NESO output $\hat{x}_3$ is the estimate of the generalized disturbance f and ($f \cong \hat{f}$). As shown in equation (4.21), the control law can be rewritten as:

$$\overline{\tau} = \overline{M}(\tau_0 - \hat{x}_3) \tag{4.22}$$

where $\tau_0 = [\tau_{0_R}, \tau_{0_L}, \tau_{0_1}, \tau_{0_2}, \tau_{0_3}]^T$, and $\hat{x}_3 = [\hat{x}_{3_R}, \hat{x}_{3_L}, \hat{x}_{3_1}, \hat{x}_{3_2}, \hat{x}_{3_3}]^T$. The ADRC tracking performance is presented according to three different scenarios: 1) only partial information of the model is provided; 2) f is completely uncertain; 3) the internal dynamics of the model is completely known.

The nonlinear PD controller τ_0 can be defined as (Gao (2006b):

$$\tau_0 = K_p f_1(e_1) + K_d f_2(e_2) \tag{4.23}$$

with $e_1 = \theta_d - \hat{x}_1$, and $e_2 = \dot{\theta_d} - \hat{x}_2$ are the error and its derivative, respectively; where f_1 and f_2 are appropriate nonlinear functions, such as the one in equations (4.15) and (4.16), and K_p and K_d are the controller gains. The control approach shown to be very effective

because it does not depend on the system model, and it eliminates the total disturbance, hence the notion of robustness and disturbance rejection (Gao *et al.* (2001)).
Combining equations (4.22) and (4.23), the control law equation is described as:

$$\overline{\tau} = \overline{M}\left[(k_p f_1(e_1) + k_d f_2(e_2)) - \hat{x}_3\right] \tag{4.24}$$

4.4 Experiments And Discussion

The MM shown in 4.1 is used to exhibit the effectiveness of the ADRC method in real-time. To verify the satisfactory performance of the proposed control from the perspective of practical implementation, experimental results are performed in this section, by using the MM robot named Mob-ETS. Table 4.1 shows the values of the MM physical parameters.

Table 4.1 Model Parameters

Robot	Parameters	Value	Units
Platform	m_v	2.0	kg
	r	0.05	m
	$2L$	0.27	m
	I_v	$0.0122\ 10^{-4}$	$kg.m^2$
Manipulator	m_1	0.5	kg
	m_2	0.5	kg
	m_3	0.2	kg
	$2L_1$	0.16	m
	$2L_2$	0.2	m
	$2L_3$	0.12	m
	I_1	$2.666\ 10^{-4}$	$kg.m^2$
	I_2	$1.16\ 10^{-4}$	$kg.m^2$
	I_3	$6.01\ 10^{-4}$	$kg.m^2$

In this experiment, the ADRC method is performed on 5-DoF MM by using Simulink with Real Time-Workshop (RTW) of Mathworks. HN-GH12-2217Y DC-motors and Dynamixel motors (MX-64T) are used to actuate all the joints of the robot manipulator and the right and left wheels of the mobile base where the encoder sensors (E4P-100- 079-DH-T-B) are utilized to measure the angular positions. Figure 4.3 illustrates the structure design of the

control and hardware implementation. The communication between the developed program in Matlab/Simulink and the MM is done by Zigbee.

The experimental results that illustrate trajectory tracking in the Cartesian space are shown in Figures 4.4 to 4.6. According to the aforementioned theory analysis of NESO and control law system, all parameters (k_p, k_d, and w_0) are tuned by the empirical trial and error method in the experimental procedure. There are three types of parameters in the NESO, i.e., a linear range δ_1, power terms $\alpha_{1,2}$ and gains β_i. These parameters are selected for the nonlinear functions in equations (4.15) and (4.16) as $\delta_1 = 0.01$, $\alpha_1 = 0.5$, $\alpha_2 = 0.25$ and $w_0 = 0.45$. The controller was implemented with the gains $K_P = diag[225, 225, 225, 225, 225]$ and $K_D = diag[25, 25, 25, 25, 25]$.

During the experimental tests, the end effector is controlled to track the desired trajectory. More specifically, the desired end effector trajectory is a path in the XYZ space. In this trajectory, the starting point is $P_s = [X_s, Y_s, Z_s, \phi_s]^T = [0, 0, 0.48, 0]^T$, and the final point is $P_f = [X_f, Y_f, Z_f, \phi_f]^T = [4, 0, 0.44, 0]^T$. From this presented trajectory of the end effector in the Cartesian space, the desired trajectories in the joint space are obtained using the inverse kinematics. Whereas the tuning of the controller gains K_P and K_d become much simpler and intuitive since the observer gains are tuned by the bandwidth w_0. Thus, changing (reducing or increasing) the bandwidth w_0 affects the estimation characteristics and exhibits a large tracking error, if not well selected.

In the Cartesian trajectory tracking experiment, the real position of the end effector P_e closely and steadily tracks the desired trajectory P_d generated in the Cartesian space as shown in Figures 4.4 to 4.6. A 3-D figure presents the corresponding tracking of the end-effector position in the Cartesian space. The corresponding trajectories are shown in Figure 4.4. Figure 4.5 confirms the results where the desired trajectories of $(X; Y; Z)$ axis and orientation are achieved with excellent tracking. According to Figures 4.4 and 4.5, the ADRC technique provides good experimental results and attains good performances of trajectory tracking.

To clarify and confirm the previous case, the related errors between the desired and the real values are shown in Figure 4.6. As one can see from Figure 4.6, the tracking errors of the end effector position are acceptable and the tracking error amplitude is less than $0.1cm$.

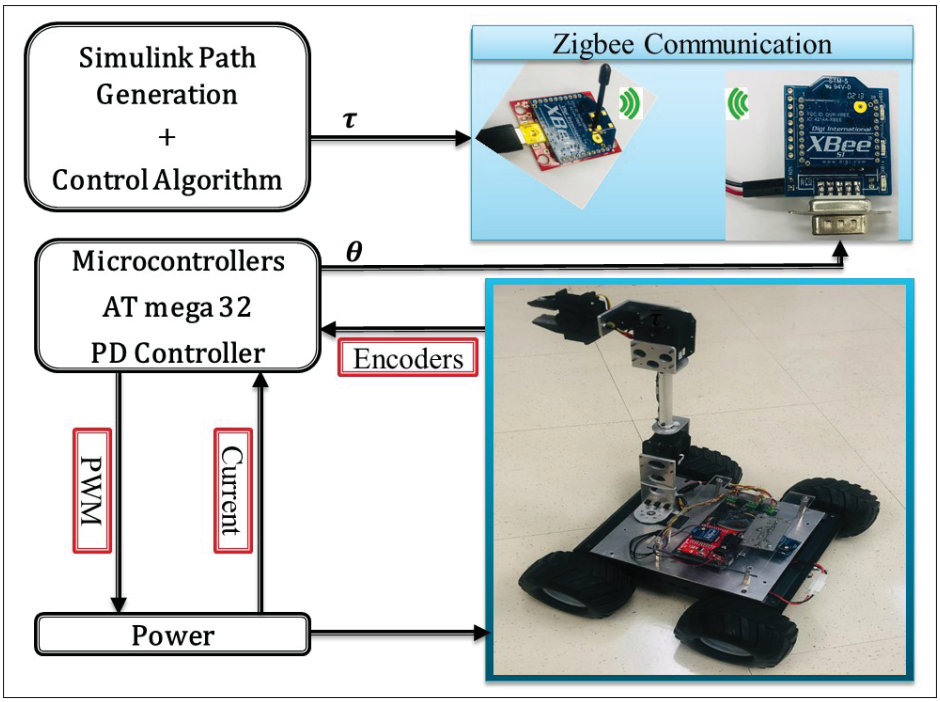

Figure 4.3 Structure design of the controller and hardware implementation

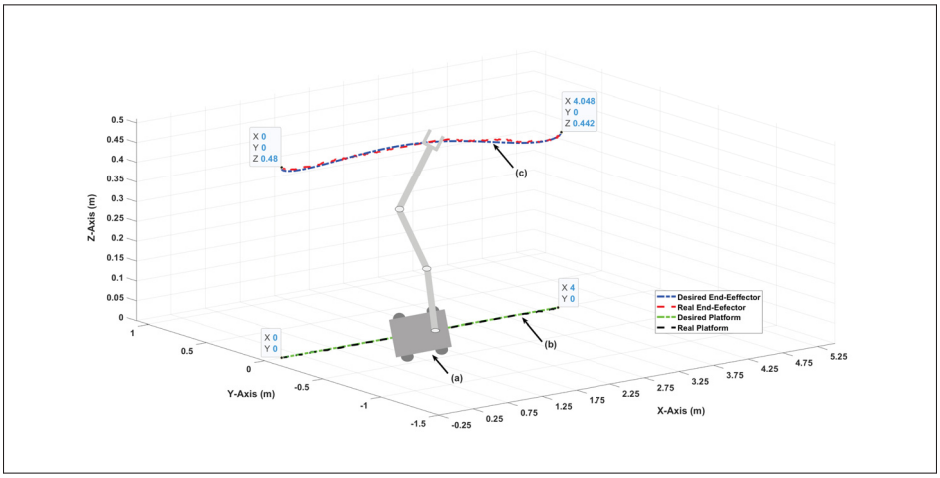

Figure 4.4 ADRC approach: Tracking Performance of the 5-DoF MM in Cartesian Space (a) (X, Y, and Z) End Effector tracking in 3D, (b) (x, y) Mobile Platform tracking in 2D

Furthermore, the tracking mobile platform is illustrated in Figure 4.7, and the tracking errors

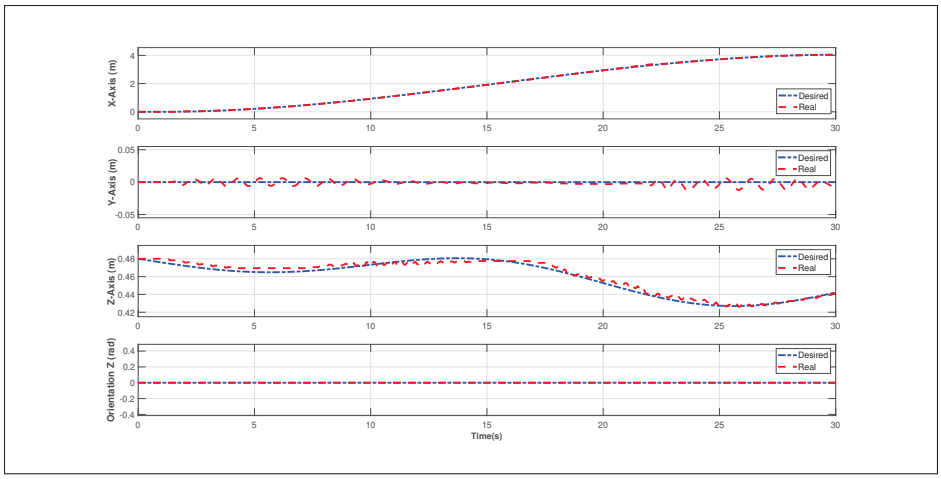

Figure 4.5 ADRC approach: Trajectory tracking of the 5-DoF MM (X, Y, Z axis, and orientation) in Cartesian Space

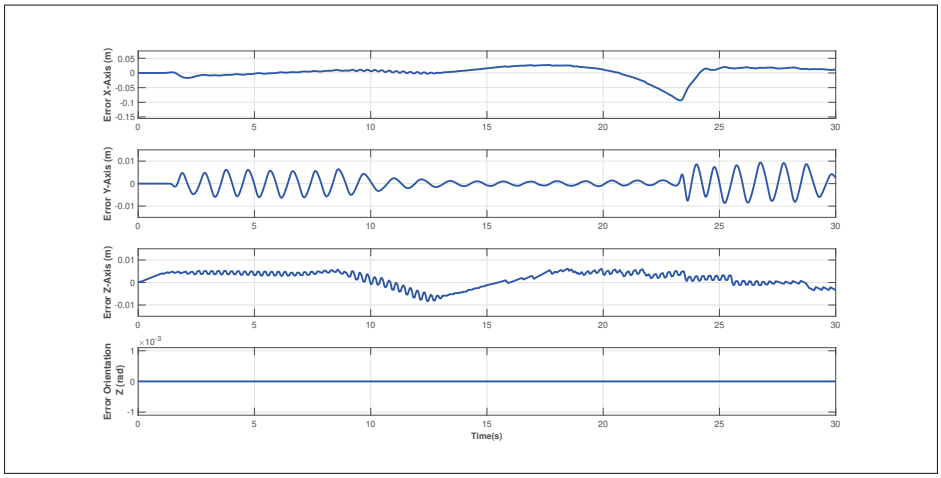

Figure 4.6 ADRC approach: Tracking errors of the 5-DoF MM (X, Y, Z axis, and orientation) in Cartesian Space

are shown in Figure 4.8 where the maximum tracking error amplitude is $0.23cm$ for x; y and ϕ. It is clear from these results that the proposed control presents an acceptable trajectory tracking in the Cartesian space despite the presence of the very small tracking errors of the end effector.

The trajectory tracking experiment performances of the joint positions are presented in Figure 4.9 generated in the joint space. The performed trajectory is very good due to the

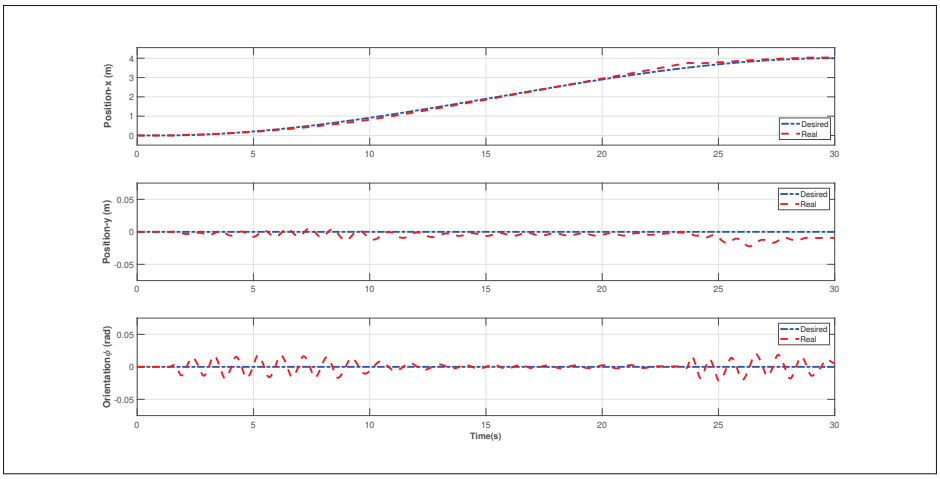

Figure 4.7 ADRC approach: Trajectory tracking of the linear/angular position of the mobile base (x, y, and ϕ)

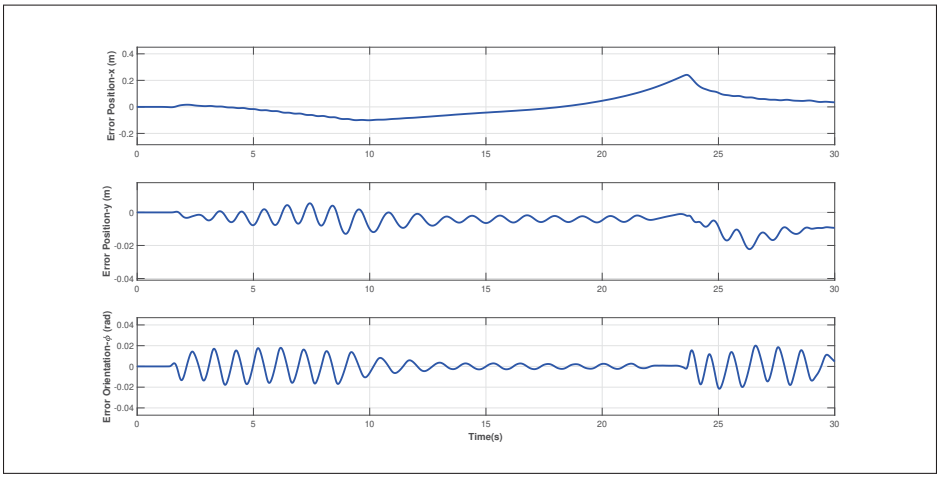

Figure 4.8 ADRC approach: Tracking errors of the linear/angular position of the mobile robot (x, y, and ϕ)

efficiency of the designed controller. Figure 4.10 presents the errors in the joint space where the tracking errors are less than 0.05 rad for $\theta_R, \theta_L, \theta_1, \theta_2$, and θ_3. As can be seen from the obtained results, in the presence of uncertainties and disturbances, the objective of the trajectory tracking control for the MM is successfully achieved. In general, the experimental results present the validity and efficiency of the proposed ADRC controller and the NESO.

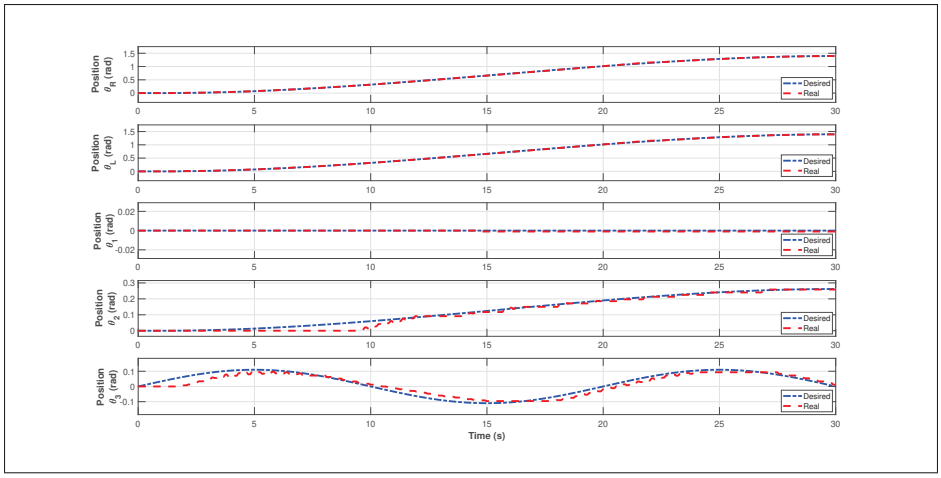

Figure 4.9 ADRC approach: Trajectory tracking of the 5-DoF MM ($\theta_R, \theta_L, \theta_1, \theta_2$, and θ_3) in Joint space

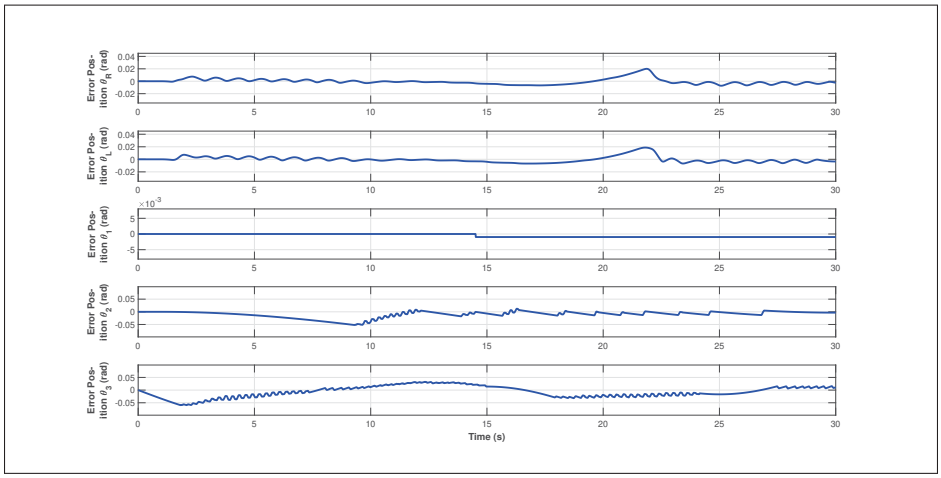

Figure 4.10 ADRC approach: Tracking errors of the 5-DoF MM ($\theta_R, \theta_L, \theta_1, \theta_2$, and θ_3) in Joint space

The applied control torques of the 5-DoF MM ($\tau_R; \tau_L; \tau_1; \tau_2; \tau_3$) are shown in Figure 4.11. The estimated uncertainties ($\hat{x}_3$) of the observer are presented in Figure 4.12. It can be seen that the total disturbances are well estimated by the NESO. The results illustrate the good performance and effectiveness of the ADRC and show that it can react quickly to eliminate disturbances.

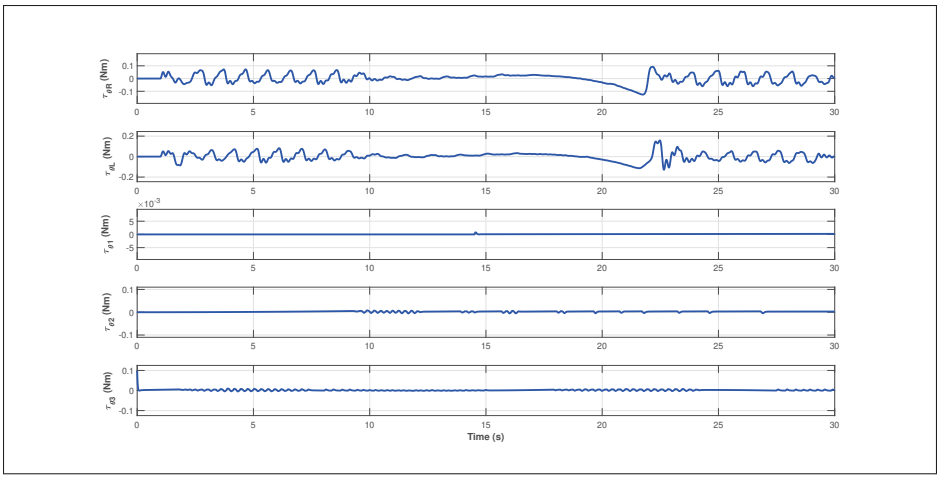

Figure 4.11 ADRC approach: Control input signals for the 5-DoF MM (τ_R, τ_L, τ_1, τ_2, and τ_3)

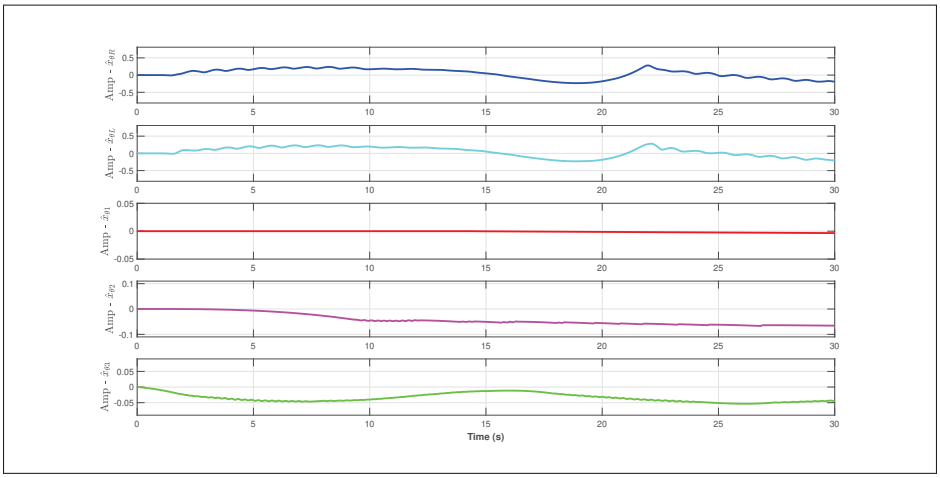

Figure 4.12 ADRC approach: Approximation of unknown nonlinear uncertainties ($\hat{x}$) of the MM using ADRC approach

4.5 CONCLUSIONS

In this paper, the trajectory tracking controller scheme based on a nonlinear ADRC was presented for an MM robotic system in the presence of modeling uncertainties and external disturbances. First, a dynamic model of the MM was given. Then, a nonlinear ADRC scheme was designed for the system, which contained a nonlinear PD controller and an NESO observer. The implementation was done by combining the NESO and a nonlinear

PD controller, in the presence of total disturbances, for the trajectory tracking control for the MM in real-time. The proposed controller effectively estimates the state vector and uncertainties of the MM system. As it can be clearly seen from the experimental results, the ADRC controller accomplished an accurate tracking of the required trajectory, where the tracking errors of the end effector and the joint positions are satisfactory which validates the effectiveness of the proposed approach for the 5-DoF MM. The objective of the trajectory tracking control for the MM is successfully achieved using the proposed control and the results are promising as well. The experimental results have been done in the Cartesian space, as shown in the experiments and discussion section. Future work will focus on designing the ADRC method for MM to handle objects in the end effector. Another possible extension of this work is the integration of ADRC and other robust control methods to improve control performance, which we are implementing in near future.

CHAPTER 5

EXTENDED STATE OBSERVER-BASED IMPROVED NON-SINGULAR FAST TERMINAL SLIDING MODE FOR MOBILE MANIPULATORS

Mhmed Algrnaodi[1],Maarouf Saad[1], Mohamad Saad[2], Raouf Fareh[3], Yassine Kali[1]

[1] Department of Electrical Engineering, École de technologie supérieure, 1100 Notre-Dame Ouest, Montréal, QC, Canada
[2] School of Engineering, Université du Québec en Abitibi-Témiscamingue (UQAT), QC, Canada
[3] Electrical Engineering Department, University of Sharjah, Sharjah, UAE

Article published in the journal "Transactions of the Institute of Measurement and Control" July 2023.

Abstract

The robust non-singular fast terminal sliding mode (NFTSM) controller is adopted in this work to solve the problem of tracking trajectory of a mobile manipulator (MM) suffering from uncertainties. The NFTSM method has the capability to ensure convergence rate, to provide good tracking accuracy and robustness against external perturbations and parameters uncertainties (total disturbances). However, the NFTSM controller needs high discontinuous gain to reject the effect of strong disturbances, which results in vibrations in the steady-state and chattering in the control law. To solve these issues, an extended state observer-based NFTSM technique is proposed for n-DoF coupling MM. The proposed method is designed to approximate and compensate in real-time the uncertainties. It also ensures robustness against total disturbances, good convergence rate, and good tracking accuracy. The stability of the proposed control is also verified based on Lyapunov theory. Experimental works are conducted on a 5-DoF MM where the results obtained demonstrate the effectiveness of the developed technique and prove the stability of the closed-loop system.

Keywords: NFTSM method, mobile manipulators, modeling uncertainty, external disturbances, ESO, composite controller.

5.1 Introduction

Nowadays robots can carry out complex tasks. Modern applications require more advanced functionalities to accomplish the desired tasks. For this reason, robotic systems have an ongoing need to improve and develop their functional systems, to prompt or adapt their reactions to unpredicted circumstances. These missions, which require robots with a significant capability for mobility, adeptness and manipulability of the robotic system, have certain advantages in many applications. Mobile manipulators (MMs) provide enormous opportunities to achieve wide tasks which are not achieved by the fixed-base manipulators or by the mobile base alone. An MM is a robotic system composed of a serial-link robot manipulator (RM) mounted on a wheeled mobile platform (MP). Due to different dynamics, there is a combined interaction between both dynamics of MMs. The trajectory tracking control of the MM is a built-in system including the end-effector of the arm and the mobile base designed to follow their desired trajectories. In addition, to obtain better control performance, it is realistic to take into consideration the trajectory tracking problem with uncertain parameters, nonlinearity, external perturbations, and coupling effects. The control scheme of the MM trajectory tracking is still a challenging control problem and has attracted considerable attention in the control field.

Many researchers have developed various methods for real-time applications in trajectory tracking control. The modeling and compensation of dynamic interactions in effect between both subsystems of the MM have been the focus of several studies (Yamamoto & Yun (1994, 1996)). These authors considered a modular method to calculate the dynamic equations of an MM. The Lagrange-d'Alembert formulation was used to develop the nonholonomic equations of motion of an MM in (Chung & Velinsky (1998)). The tracking control problem utilizing the overall dynamic model was considered in (Walsh *et al.* (1994)), including the redundancy between the RM and the MP.

In recent years, several tracking control approaches have been devoted to tackle the problem of the trajectory tracking for MMs, such as input-output linearization (Chung & Velinsky (1998)), adaptive fuzzy combined with backstepping (Zhong *et al.* (2013)), adaptive sliding mode backstepping (Dong (2002)), adaptive control (Andaluz *et al.* (2012)), robust adaptive

control (Li *et al.* (2008); Peng *et al.* (2014)), robust impedance control (Souzanchi-K, Arab, Akbarzadeh-T & Fateh (2017)), and recurrent neural network (RNN) (Khan *et al.* (2020)). Moreover, decentralized controllers have been developed and applied to MMs (Fareh *et al.* (2017); Savino *et al.* (2020)). However, these techniques heavily depend on the accuracies of the dynamic model and cannot guarantee good performance if the model is not well known. To achieve an excellent performance in trajectory tracking applications, the controller needs complete information on the robot dynamics. In practice, this is a challenging task and the obtained model may be considered with uncertainties, disturbances, and nonlinearities. Thus, an accurate, effective, and robust method for MMs' posture control should be developed with urgent attention.

Sliding mode (SM) control has gained tremendous popularity for its remarkable features such as strong insensitivity to a wide range of perturbations and uncertainties, fast transient response and simplicity (Gu & Wang (2018, 2019); Yang, Li, Su *et al.* (2013)). SMC is based on a reliable and systematic approach to achieving robust control, ensuring system stability and consistent performance, even in the presence of modeling uncertainties and disturbances. Moreover, SMC allows for a design tradeoff between tracking performance and smoothing control discontinuity, making it practical for implementation in most applications (Yang *et al.* (2012)). There are two typical SMC methods: linear SMC and non-linear SMC. Linear SMC is asymptotically stable, while non-linear SMC may result in finite convergence (Wang, Li, Lan *et al.* (2017); Yang *et al.* (2012)). However, the conventional SM with linear sliding manifold cannot ensure finite-time convergence of the system state to the equilibrium point (Jin, Lee, Chang *et al.* (2009)). To ensure this latter, a terminal sliding mode (TSM) (Khawwaf, Zheng, Lu *et al.* (2017); Mobayen & Javadi (2017)) that uses nonlinear sliding manifold was introduced. The TSM, however, has a singularity problem since terms with negative fractional powers may exist (Wu, Yu & Man (1998)). Non-singular TSM (NTSM) was proposed and used to address the problem of singularity (Chen & Lin (2010)). NTSM has good accuracy of tracking, fast convergence, and the property of avoidance of singularity (Madani, Daachi & Djouani (2016a,b)) and continuous nonsingular terminal sliding mode control (SMC) (Rauf, Zhao, Khan *et al.* (2022)). Moreover, a new NFTSM controller for

nonlinear dynamic systems is proposed in (Yang & Yang (2011)). It is designed based on SM theory while overcoming the singularity problem and ensuring the system's convergence in finite-time (Yang & Yang (2011); Boukattaya *et al.* (2018); Feng *et al.* (2002)).

As compared to the developed SM surfaces, the NFTSM avoids singularities, and has a fast finite-time reaching even when the state is far from the equilibrium point (Boukattaya *et al.* (2018)). In view of these promising features, the NFTSM controller has gained popularity for high-accurate tracking control problems in robotic systems such as in RM (Boukattaya *et al.* (2018); Geng, Sheng & Liu (2014); Lu, Ma & Hua (2022)), robotic knee prosthesis (Huang, Ma, He *et al.* (2022)), underactuated quadrotor UAV (Labbadi & Cherkaoui (2020)), and mobile lower limb exoskeleton (Hernandez, Cruz, López-Gutiérrez *et al.* (2020)). Furthermore, NFTSMC techniques have been a few works published recently to solve the problem of tracking trajectory of MM.

In MMs, there is a strong coupling between MP and RM subsystems. It is more meaningful to consider disturbance rejection problem in a complete MM system. However, most of the controllers mentioned above require complete information on the robot dynamics to achieve high performance in trajectory tracking applications.

Because of the uncertainties and complexity, obtaining the upper bound in real-time applications may be difficult. As a result, the SM design introduced the problem associated with the bounded value of unknown uncertainty and dynamic perturbations. Several studies, such as observers-based controllers (Xu, Junejo, Liu *et al.* (2019a)), adaptive methods (Boukattaya *et al.* (2018)), and neural networks (Taghavifar & Rakheja (2019)), have been presented to overcome this dependence.

This paper presents an ESO-based NFTSM scheme for an MM system subject to unmodeled dynamics and disturbances to address the above-mentioned challenging problems. The ESO is used to approximate the system disturbance, improving the control system's robustness and efficiency (Gao *et al.* (2001); Han (2009)). The ESO does not depend on a complete system model information, including external perturbations and dynamic uncertainties, estimated along with the original state variables. Therefore, the used observer is an important part of

the active disturbance rejection control technique (ADRC) (Song *et al.* (2018); Xing *et al.* (2011); Zhang, Chen & Sun (2020); Zhao *et al.* (2018)).

It is worth noting that all the attitude control approaches used the ESO approximation for the total disturbances of the system based on nonlinear SM (Zhang *et al.* (2020)), NTSM (Sun & Liu (2020); Wu, Wang, Zhang *et al.* (2019)), and continuous fast terminal sliding mode CFTSM (Xu *et al.* (2019a); Wang *et al.* (2017)), but neither of them has considered NFTSM. To the best of our knowledge, there are little works that designed and implemented the NFTSM for MM systems in real-time, which motivates us to carry out the current work. In this paper, a technique ESO-based NFTSM is proposed as a composite solution for achieving good trajectory tracking in an MM system subject to external disturbances and parameter uncertainties. To accomplish this, an ESO is used to estimate the total system disturbances, which is then utilized for feed-forward compensation. Unlike previous research, this technique has been successfully applied in real-time for an MM system, resulting in improved suppression of continuous disturbances even under complex nonlinear dynamics. The observer-based controller employed in this approach integrates the benefits of ESO, NFTSM, and robust terms to produce significantly improved experimental outcomes in terms of trajectory tracking, despite the presence of unknown system uncertainties. The main contributions of this paper are given as follows:

(i) This paper provides a composite NFTSM technique with ESO (ESO-based NFTSM) to ensure a good trajectory tracking for an MM system. The ESO can estimate the system total disturbances to be used later as feed-forward compensation.

(ii) Compared with the previous research works, real-time application of the ESO-based NFTSM controller is done for an MM that greatly improves MM's ability to suppress continuous disturbances under a complex nonlinear dynamic model.

(iii) The proposed observer-based controller inherits the benefits of ESO, NFTSM, and the robust term, resulting in significantly improved trajectory tracking experimental results despite the existence of the unknown system uncertainty.

The rest of this paper is organized as follows. Section "Preliminaries and notation" presented the preliminaries and the notation used throughout the paper. A brief description of the

kinematic model and derives the dynamic model of the MM system, and the control objective are shown in section "Description of MM and Control Objective". The control design scheme of the proposed ESO-based NFTSM is presented in the section "ESO-based NFTSM Controller Design", along with the stability analysis of the proposed technique. Section "experiments and discussion" illustrates the validation and effectiveness of the developed controller. Finally, the conclusions of this paper are summarized in section "Conclusion".

5.2 Preliminaries and Notation

Throughout this paper, the following notations are used:

For $x = [x_1, \cdots, x_n]^T \in \mathbb{R}^n$ that is a variable vector , the fractional power of vectors is defined as:

$$|x|^a = [|x_1|^{a_1}, \cdots, |x_n|^{a_n}]^T \in \mathbb{R}^n$$

$$\lfloor x \rfloor^a = diag\,(|x_1|^{a_1}, \cdots, |x_n|^{a_n}) \in \mathbb{R}^{n\times n}$$

while the vector $sign^a(x) \in \mathbb{R}^n$ is defined as:

$$\begin{aligned} sign^a(x) &= diag\left(sign(x)\right).|x|^a \\ &= [\,|x_1|^{a_1} sign(x_1), \cdots, |x_n|^{a_n} sign(x_n)\,]^T \end{aligned}$$

where the $sign(x_i)$ for $i = 1, 2, \cdots, n$ is defined as:

$$sign(x_i) = \begin{cases} 1 & \text{if} \quad x_i > 0 \\ 0 & \text{if} \quad x_i = 0 \\ -1 & \text{if} \quad x_i < 0 \end{cases}$$

Then, if $a_i \geq 1$ for $i = 1, \cdots, n$, it follows that:

$$\begin{aligned} \frac{d}{dt} sign^a(x) &= a\ \lfloor x \rfloor^{a-I_n} \dot{x} \\ &= \left[a_1 \dot{x}_1\, |x_1|^{a_1-1}, \cdots, a_n \dot{x}_n\, |x_n|^{a_n-1}\right]^T \end{aligned} \tag{5.1}$$

where $a = diag\left(a_1, a_2, \cdots, a_n\right)$ and I_n is the n-dimensional unit matrix.

5.3 Description of MM and Control Objective

This section describes the kinematic model and derives the dynamic model of the n-DoF MM in the Cartesian space. The Lagrangian technique is considered for the MM system (Li & Ge (2013)) illustrated in Figure 5.1, where a three-link robotic manipulator is mounted upon the center of a wheeled MP. In the MP, the two front wheels are active, and the two rear wheels are passive. The full MM system has n-DoF, where the RM is subject to a holonomic constraint, and the MP is subject to a nonholonomic constraint.

5.3.1 Kinematics

In most robot applications, the desired trajectory is defined in the Cartesian space. P_e illustrates the position/orientation vector of the MM end-effector as shown in Figure 5.1. The MM can be represented by the generalized coordinates $q = [q_v^T, \theta_a^T]^T$ where $q_v = [X_v, Y_v, \phi_v]^T \in \mathbb{R}^{n_v}$ and $\theta_a = [\theta_1, \cdots, \theta_{n_a}]^T \in \mathbb{R}^{n_a}$ are the state vectors of the MP and the RM, respectively, and $n = n_v + n_a$. The relationship between the generalized coordinates of the MM, its derivative $\dot{q} \in \mathbb{R}^n$, and the end-effector velocity, $V_e \in \mathbb{R}^n$, is described as follows (Brahmi *et al.* (2016); Li & Ge (2013)):

$$V_e = J_e(q)\dot{q} \tag{5.2}$$

where $J_e(q) \in \mathbb{R}^{n \times n}$ is the Jacobian matrix and $\dot{q} = [\dot{q}_v^T, \dot{\theta}_a^T]^T$ with $\dot{q}_v = [\dot{X}_v, \dot{Y}_v, \dot{\phi}_v]^T$ is the linear/angular velocity vector of the MP, and $\dot{\theta}_a = [\dot{\theta}_1, \cdots, \dot{\theta}_{n_a}]^T$ is the joint velocity vector of the RM.

5.3.2 Dynamic Model

Using the Lagrangian technique, mathematical modelling in this paper is based on the coupled dynamics of the MP and the RM is obtained by the following equation (Li *et al.* (2007, 2008)):

$$M(q)\ddot{q} + C(q, \dot{q})\dot{q} + G(q) \ + \tau_d = B(q)\tau - A^T(q)\lambda \tag{5.3}$$

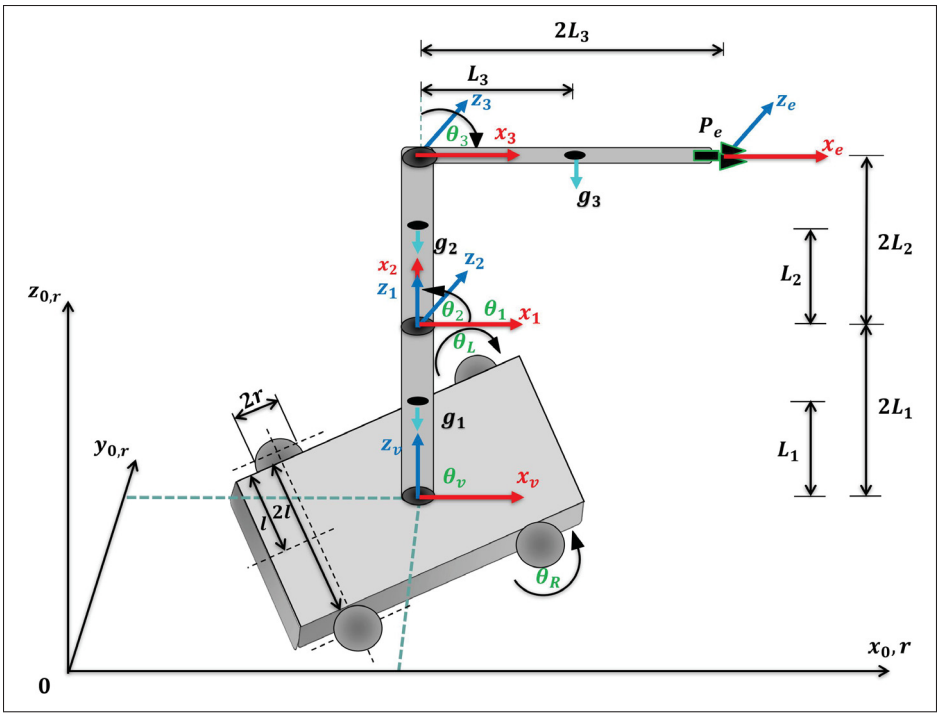

Figure 5.1 The system of n-DoF MM

where $M(q)\in\mathbb{R}^{n\times n}$, $C(q,\dot{q})\dot{q}\in\mathbb{R}^{n}$ and $G(q)\in\mathbb{R}^{n}$ denote the positive-definite and symmetric inertia matrix, the centrifugal and Coriolis forces matrix, and the gravitational vector, respectively, q represents the position vector of the MM system, $\tau_d\in\mathbb{R}^{n}$ denotes the vector of external perturbations, $B(q)\in\mathbb{R}^{n\times k}$ represents the full rank input transformation matrix, $\tau\in\mathbb{R}^{k}$ denotes the input control vector, $A(q)\in\mathbb{R}^{k\times n}$ is a constraint matrix, $\lambda\in\mathbb{R}^{k}$ is the constraint force vector, and are represented as:

$$M(q)=\begin{bmatrix} M_{n_v} & M_{n_v n_a} \\ M_{n_a n_v} & M_{n_a} \end{bmatrix}, C(q)=\begin{bmatrix} C_{n_v} & C_{n_v n_a} \\ C_{n_a n_v} & C_{n_a} \end{bmatrix},$$

$$G(q)=\begin{bmatrix} G_{n_v} \\ G_{n_a} \end{bmatrix}, \tau_d=\begin{bmatrix} \tau_{dn_v} \\ \tau_{dn_a} \end{bmatrix}, B(q)=\begin{bmatrix} B_{n_v} & 0 \\ 0 & B_{n_a} \end{bmatrix},$$

$$\tau=\begin{bmatrix} \tau_{n_v} \\ \tau_{n_a} \end{bmatrix}, A^T(q)=\begin{bmatrix} A_{n_v}^T & 0 \\ 0 & 0 \end{bmatrix}, \lambda=\begin{bmatrix} \lambda_{n_v} \\ \lambda_{n_a} \end{bmatrix}.$$

The mobile platform is subjected to nonholonomic constraints. Therefore, the following equation represents the velocity constraints as given in (Li *et al.* (2007, 2008)).

$$A_{n_v}(q_v)\dot{q}_v = 0 \tag{5.4}$$

where $A_{n_v}(q_v) \in \mathbb{R}^{d \times n_v}$ is the kinematic constraint matrix and d is the number of non-integrable constraints.

Assume $S(q_v) \in \mathbb{R}^{n_v \times (n_v - d)}$ to be the orthocomplement of $A_{n_v}(q_v)$, and (Li & Ge (2013)):

$$S^T(q_v)A_{n_v}^T(q_v) = 0 \tag{5.5}$$

where $S(q_v) = \begin{bmatrix} \cos(\phi_v) & \sin(\phi_v) & 0 \\ 0 & 0 & 1 \end{bmatrix}^T$, and has a set of smooth and linearly independent vector fields that is obtained by spanning the null space of $A_{n_v}(q_v)$. Note that $S^T(q_v)S(q_v)$ is of full rank.

From the constraints (5.4) and (5.5), let the auxiliary vector $\dot{\eta} \in \mathbb{R}^{n_v - d}$, such that:

$$\dot{q}_v = S(q_v)\dot{\eta} \tag{5.6}$$

which is the kinematic model of the nonholonomic MP subsystem. Differentiating (5.6) yields to:

$$\ddot{q}_v = \dot{S}(q_v)\dot{\eta} + S(q_v)\ddot{\eta} \tag{5.7}$$

where $\dot{\eta} = [v_v, w_v]^T$ with v_v as the linear velocity and w_v as the angular velocity of the MP. Let θ_L and θ_R be respectively the left and the right angular positions, and $\dot{\theta}_L$ and $\dot{\theta}_R$ be respectively the left and the right angular velocities of the MP, where the velocity vector of the MP is denoted as $\dot{\theta}_v = [\dot{\theta}_R, \dot{\theta}_L]^T$. Then, the kinematic model of the nonholonomic system can be expressed as follows:

$$\dot{\eta} = R(q_v)\dot{\theta}_v \tag{5.8}$$

where $R(q_v) = \begin{bmatrix} \frac{r}{2} & \frac{r}{2} \\ \frac{r}{2l} & \frac{-r}{2l} \end{bmatrix}$. Thus,

$$H(q_v) = S(q_v)R(q_v) = \begin{bmatrix} \frac{r}{2}cos(\phi_v) & \frac{r}{2}sin(\phi_v) & \frac{r}{2l} \\ \frac{r}{2}cos(\phi_v) & \frac{r}{2}sin(\phi_v) & \frac{-r}{2l} \end{bmatrix}^T \tag{5.9}$$

where r is the wheel radius and $2l$ is the platform width as shown in Figure 5.1.
Considering equations (5.5), (5.6), and (5.7), the term of the nonholonomic constraint $A^T(q)\lambda$ can be eliminated from (5.3). Then, the dynamics in (5.3) can be reformulated as:

$$\overline{M}(\theta)\ddot{\theta} + \overline{C}(\theta, \dot{\theta})\dot{\theta} + \overline{G}(\theta) = \overline{\tau} - \overline{\tau}_d \tag{5.10}$$

where $\theta = [\theta_v^T, \theta_a^T]^T$ are the generalized coordinates with $\theta_v = [\theta_R, \theta_L]^T$ being the angular position of the MP, $\dot{\theta} = [\dot{\theta}_R, \dot{\theta}_L, \dot{\theta}_1, \cdots, \dot{\theta}_{n_a}]^T$, and

$$\overline{M}(\theta) = \begin{bmatrix} H^T M_{n_v} H & H^T M_{n_v n_a} \\ M_{n_a n_v} H & M_{n_a} \end{bmatrix} \in \mathbb{R}^{\overline{n}\times\overline{n}}, \overline{G}(\theta) = \begin{bmatrix} H^T G_{n_v} \\ G_{n_a} \end{bmatrix} \in \mathbb{R}^{\overline{n}},$$
$$\overline{C}(\theta, \dot{\theta}) = \begin{bmatrix} H^T M_{n_v}\dot{H} + H^T C_{n_v} H & H^T C_{n_v n_a} \\ M_{n_a n_v}\dot{H} + C_{n_a n_v} H^T & C_{n_{n_a}} \end{bmatrix} \in \mathbb{R}^{\overline{n}\times\overline{n}},$$
$$\overline{\tau}_d = \begin{bmatrix} H^T \tau_{dn_v} \\ \tau_{dn_a} \end{bmatrix} \in \mathbb{R}^{\overline{n}}, \overline{\tau} = \overline{B}\,\tau \in \mathbb{R}^{\overline{n}}, \quad \overline{B} = \begin{bmatrix} H^T B_{n_v} & 0 \\ 0 & B_{n_a} \end{bmatrix}.$$

where $\overline{n} = n_a + n_v - d$. The mathematical model in (5.10) verifies (Li *et al.* (2008)):
Property 1: $\overline{M}$ is a positive definite and symmetric matrix.
Property 2: $S = \dot{\overline{M}} - 2\overline{C}$ is a skew symmetric matrix, i.e. $\forall z \in \mathbb{R}^{\overline{n}}$, we have $z^T(\dot{\overline{M}} - 2\overline{C})z = 0$.
Remark 1: In this paper, the MM robot is considered as a fully actuated arm mounted on the holonomic mobile platform. There is a dimension reduction of the state in (5.11) compared with (5.3) due to the kinematic constraints.

The uncertainties and the external perturbations acting on the MM system are unknown. For this reason, they should be estimated during the control design in order to avoid any undesired behavior.

5.3.3 Control Objective

According to the properties 1 and 2, and considering that $\overline{M}(\theta) = \overline{M}_k(\theta) + \overline{M}_u(\theta)$ with $\overline{M}_k(\theta)$ and $\overline{M}_u(\theta)$ denote respectively the known and the unknown parts of the matrix $\overline{M}(\theta)$, a dynamic model of MM system containing the uncertain dynamic and external perturbations, which is defined in (5.10), can be rewritten as:

$$\ddot{\theta} = f(\theta, \dot{\theta}) + D(\theta)\,\overline{\tau} \tag{5.11}$$

where $f(\theta, \dot{\theta}) = -D(\theta)(\overline{\tau}_d + \overline{M}_u(\theta)\ddot{\theta} + \overline{C}(\theta, \dot{\theta})\dot{\theta} + \overline{G}(\theta))$ is considered as the "total disturbance" of the five joints MM, including the dynamic coupling effects between the RM and the MP, the perturbations and the uncertain dynamics, and $D(\theta) = \overline{M}_k^{-1}(\theta)$.
Define $x_1 = \theta$ and $x_2 = \dot{\theta}$, respectively. The model dynamics (4.11) can be written as:

$$\begin{cases} \dot{x}_1 = x_2 \\ \dot{x}_2 = f(x_1, x_2) + D(x_1)\,\overline{\tau} \end{cases} \tag{5.12}$$

Suppose that the reference signal is described by θ_d and its derivative $\dot{\theta}_d$. According to the dynamic system of MM in (5.12), the tracking error can be expressed as:

$$\begin{cases} e_1 = x_1 - x_d \\ e_2 = \dot{x}_1 - \dot{x}_d = x_2 - \dot{x}_d \end{cases} \tag{5.13}$$

where e_1 and $e_2 \in \mathbb{R}^{\overline{n}}$ are respectively the measured position and the measured velocity of the tracking errors for the system, and $x_d = \theta_d$ is the known desired position trajectory generated in the workspace while $\dot{x}_d$ represents its first time derivative.

Substituting (5.12) into the time derivative of (5.13), the error system dynamics can be written as

$$\begin{cases} \dot{e}_1 = e_2 \\ \dot{e}_2 = f(x_1, x_2) + D(x_1)\,\overline{\tau} - \ddot{x}_d \end{cases} \tag{5.14}$$

The control objective here is to construct a convenient ESO-based NFTSM for the considered nonlinear system that ensures the system position vector θ follows its reference vector θ_d in the presence of external perturbations and uncertainties. The inverse kinematics is used to obtain the joint space desired trajectory θ_d from the Cartesian position/orientation trajectory P_d. The following assumption is required to achieve this goal.

Assumption 1: The total perturbations $f(x_1, x_2)$ are generally unknown. Assume that they are bounded and differentiable, such as there exists a positive constant $\mu > 0$ verifying (Van, Ge & Ren (2016)):

$$\|f(x_1, x_2)\| \leq \mu \tag{5.15}$$

with $\|f(x_1, x_2)\|$ represents the Euclidean norm of $f(x_1, x_2)$.

5.4 ESO-based NFTSM Controller Design

A ESO-based NFTSM scheme is proposed to handle the perturbations and the uncertainties due to its robustness. An ESO is used to estimate the total disturbances of the MM system in order to reduce the interferences of uncertainties from dynamic system. When the NFTSM and ESO are combined, the closed-loop control system becomes more effective in dealing with process disturbances and uncertainties.

5.4.1 NFTSM Controller Design

SM design typically consists of 3 steps: (1) the selection of the sliding manifold; (2) the design of the equivalent control part; and (3) the design of the discontinuous control part. The following NFTSM surface is introduced in the first step (Yang & Yang (2011)):

$$s = e_1 + k_1\, sign^{\sigma_1}(e_1) + k_2\, sign^{\sigma_2}(e_2) \tag{5.16}$$

where $k_1 = diag(k_{11}, \cdots, k_{1\overline{n}})$, $k_2 = diag(k_{21}, \cdots, k_{2\overline{n}})$, $\sigma_1 = diag(\sigma_{11}, \cdots, \sigma_{1\overline{n}})$ and $\sigma_2 = diag(\sigma_{21}, \cdots, \sigma_{2\overline{n}})$ with $k_{1i} > 0$, $k_{2i} > 0$, $\sigma_{1i} > \sigma_{2i}$, and $1 < \sigma_{2i} < 2$, respectively, for every $i = 1, 2, \cdots, \overline{n}$. The NFTSM surface (5.16) can ensure singularity avoidance and fast finite time convergence for any given initial condition.

When $\dot{s} = 0$ is achieved, the system dynamics are equivalent to the nonlinear differential equation shown below:

$$e_2 + k_1 \sigma_1 \lfloor e_1 \rfloor^{\sigma_1 - I_{\overline{n}}} . e_2 + k_2 \sigma_2 \lfloor e_2 \rfloor^{\sigma_2 - I_{\overline{n}}} . \dot{e}_2 = 0 \tag{5.17}$$

The following is a definition of the overall control law:

$$\overline{\tau} = D^{-1}(x_1) (\overline{\tau}_{eq} + \overline{\tau}_b) \tag{5.18}$$

$$\begin{aligned} \overline{\tau}_{eq} = & - \left(\lfloor e_2 \rfloor^{\sigma_2 - I_{\overline{n}}} \right)^{-1} \sigma_2^{-1} k_2^{-1} \left(I_{\overline{n}} + k_1 \sigma_1 \lfloor e_1 \rfloor^{\sigma_1 - I_{\overline{n}}} \right) e_2 \\ & - f(x_1, x_2) + \ddot{x}_d \end{aligned} \tag{5.19}$$

To satisfy the sliding mode reaching conditions, a robust control law $\overline{\tau}_b$ is designed by taking into account the total disturbances as:

$$\overline{\tau}_b = - k_3 \, s - k_4 \, sign(s) \tag{5.20}$$

where $k_3 = diag(k_{31}, \cdots, k_{3\overline{n}})$, and $k_4 = diag(k_{41}, \cdots, k_{4\overline{n}})$ are positive definite matrices, respectively, and satisfy $k_{3i}, k_{4i} > 0$ for $i = 1, 2, \cdots, \overline{n}$.

The expression of the overall control can be obtained using the above formulas as follows:

$$\begin{aligned} \overline{\tau} = & D^{-1}(x_1) \Bigg(- \left(\lfloor e_2 \rfloor^{\sigma_2 - I_{\overline{n}}} \right)^{-1} \sigma_2^{-1} \, k_2^{-1} \, \Big(I_{\overline{n}} + k_1 \, \sigma_1 \\ & \lfloor e_1 \rfloor^{\sigma_1 - I_{\overline{n}}} \Big) e_2 - f(x_1, x_2) + \ddot{x}_d - k_3 \, s - k_4 \, sign(s) \Bigg) \end{aligned} \tag{5.21}$$

Remark 2: In practice the function $f(x_1, x_2)$ in relation (5.21) is unknown. Only an estimation of $f(x_1, x_2)$ can be obtained. This issue will be considered later in the paper.

Theorem 1. If the NFTSM surface for the system (5.12) is selected as (5.16), and $\overline{\tau}$ is designed as (5.21) to control it, then the system trajectory will converge asymptotically to zero within a finite time. Furthermore, no singularity will occur during the entire process.

Proof: The time derivative of (5.16) is calculated as:

$$\dot{s} = e_2 + k_1\,\sigma_1\,\lfloor e_1 \rfloor^{\sigma_1 - I_{\overline{n}}}.\,e_2 + k_2\,\sigma_2\,\lfloor e_2 \rfloor^{\sigma_2 - I_{\overline{n}}}.\,\dot{e}_2 \tag{5.22}$$

Thus, substituting the expression (5.14) into (5.22) we have:

$$\begin{aligned} \dot{s} = {} & e_2 + k_1\,\sigma_1\,\lfloor e_1 \rfloor^{\sigma_1 - I_{\overline{n}}}.\,e_2 \\ & + k_2\,\sigma_2\,\lfloor e_2 \rfloor^{\sigma_2 - I_{\overline{n}}}.\,\left(f(x_1, x_2) + D(x_1)\,\overline{\tau} - \ddot{x}_d\right) \end{aligned} \tag{5.23}$$

After substituting the control law (5.21) into (5.23), the $\dot{s}$ becomes as follows:

$$\dot{s} = -\,k_2\,\sigma_2\,\lfloor e_2 \rfloor^{\sigma_2 - I_{\overline{n}}}.\left(k_3\,s + k_4\,sign(s)\right) \tag{5.24}$$

For the stability analysis, the Lyapunov function $V_1 = 0.5\,s^T s$ will be considered and then its derivative is computed as:

$$\begin{aligned} \dot{V}_1 = {} & -\,s^T\,k_2\,\sigma_2\,\lfloor e_2 \rfloor^{\sigma_2 - I_{\overline{n}}}.\left(k_3\,s + k_4\,sign(s)\right) \\ & \leq -\,\eta_1 V_1 - \eta_2 V_1^{1/2} \leq 0 \end{aligned} \tag{5.25}$$

where $\eta_1 = \lambda_{min}\left(k_2\,\sigma_2\,\lfloor e_2 \rfloor^{\sigma_2 - I_{\overline{n}}}\,k_3\right) > 0$, and $\eta_2 = \lambda_{min}\left(k_2\,\sigma_2\,\lfloor e_2 \rfloor^{\sigma_2 - I_{\overline{n}}}\,k_4\right)\sqrt{2} > 0$. According to the theory of Lyapunov, the closed-loop system dynamics is asymptotically stable (the selected sliding manifold converges to zero $s = 0$).

The above equation can be rewritten as:

$$dt \leq \frac{-dV_1}{\eta_1 V_1 + \eta_2 V_1^{1/2}} = \frac{-V_1^{-1/2} dV_1}{\eta_1 V_1^{1/2} + \eta_2} = -2\frac{dV_1^{1/2}}{\eta_1 V_1^{1/2} + \eta_2} \tag{5.26}$$

Assume that t_r is the required time to reach $s = 0$ (i.e., $V_1(t_r) = 0$) starting from an initial surface $s(0) \neq 0$. Then, by taking the integration of both sides of (5.26), yields:

$$\int_0^{t_r} dt \leq \int_{V_1(0)}^{V_1(t_r)} -2\frac{dV_1^{1/2}}{\eta_1 V_1^{1/2} + \eta_2} \tag{5.27}$$

After a simple calculation, we have

$$t_r \leq \frac{2}{\eta_1} ln\left(\frac{\eta_1 V_1^{1/2}(0) + \eta_2}{\eta_2}\right) \tag{5.28}$$

According to the theory of Lyapunov, the NFTSM surface s expressed in (5.16) converges to zero at a finite time t_r. Therefore, despite the existence of total disturbance, the tracking error will achieve convergence to zero in finite time if $s = 0$. This completes the proof.

5.4.2 Extended State Observer (ESO)

Here, an ESO is developed to cope with the total disturbances of the $\overline{n}$-DoF MM system (5.12). Its merit is that it is simpler to implement, and independent of the dynamic model of the plant (Gao *et al.* (2001)). That is, the fundamental mechanism of ESO is to estimate the total disturbance via its observer (Huang & Xue (2014)). From the idea of ESO theory, the total disturbances are expanded as an extended state for the system in equation (5.11) which are estimated and compensated by the observer and a controller, respectively (Algrnaodi, Saad, Saad, Fareh & Brahmi (2021); Fareh, Khadraoui, Abdallah, Baziyad & Bettayeb (2021); Zhao, Liu & Wang (2019)).

In the present context, by defining $x_3 = f(x_1, x_2)$ as the extra state variable of the system, x_3 is the extended state vector.

The robot dynamic system in equation (5.12) can be rewritten in state-space form as:

$$\begin{cases} \dot{x}_1 = x_2 \\ \dot{x}_2 = x_3 + D(x_1)\,\overline{\overline{\tau}} \\ \dot{x}_3 = h(t) \end{cases} \tag{5.29}$$

where $h(t)$ is the derivative of x_3 and is the unknown part required for the implementation of the control law $\overline{\overline{\tau}}$. Note that $h(t)$ is bounded in practice.

Defining $\hat{x}_3$ as the estimation of x_3, the simplest way to estimate x_3 is using equation (5.11) as:

$$\hat{x}_3(t) = -(D(x_1)\,\overline{\overline{\tau}} - \dot{x}_2) \tag{5.30}$$

which needs the measurement of the acceleration $\dot{x}_2$. However, the acceleration is not available for measurement. For this reason, the ESO will be utilized.

The ESO proposed in (Han (2009)) is a nonlinear observer employed to estimate x_3. From equation (5.29), we construct an ESO in the form of:

$$\begin{cases} \varepsilon_1 = \hat{x}_1 - x_1 \\ \dot{\hat{x}}_1 = \hat{x}_2 - \beta_1\,\varepsilon_1 \\ \dot{\hat{x}}_2 = \hat{x}_3 - \beta_2\,f_1(\varepsilon_1) + D(x_1)\,\overline{\overline{\tau}} \\ \dot{\hat{x}}_3 = -\beta_3\,f_2(\varepsilon_1) \end{cases} \tag{5.31}$$

where $\varepsilon_1 \in \mathbb{R}^{\overline{n}}$ is the observer's error for the state $x_1 \in \mathbb{R}^{\overline{n}}$, $\hat{x}_i \in \mathbb{R}^{\overline{n}}$ are the observer's output and are the estimation of state variables $x_i \in \mathbb{R}^{\overline{n}}$; $\beta_i \in \mathbb{R}^{\overline{n}\times\overline{n}}$ are the observer's gains with $i = 1, 2, 3$; $f_\chi(\varepsilon_1) \in \mathbb{R}^{\overline{n}}$ for $\chi = 1, 2$ are two different nonlinear functions applied to increase the convergence speed of the observer's signals with:

$$f_\chi(\varepsilon_1) = \left[fal_{\chi 1}(\varepsilon_{11}, \alpha_\chi, \delta), \cdots, fal_{\chi\overline{n}}(\varepsilon_{1\overline{n}}, \alpha_\chi, \delta)\right]^T$$

and the fal functions are selected for $\chi = 1, 2$ as (Gao *et al.* (2001)):

$$fal_{\chi j}(\varepsilon_{1j}, \alpha_\chi, \delta) = \begin{cases} |\varepsilon_{1j}|^{\alpha_\chi} \, sign(\varepsilon_{1j}), & |\varepsilon_{1j}| > \delta \\ \varepsilon_{1j}/\delta^{1-\alpha_\chi}, & |\varepsilon_{1j}| \leq \delta \end{cases} \tag{5.32}$$

In this case: $j = 1, \cdots, \overline{n}$, α_1, α_2, and δ are positive parameters to be determined, and:

$$\begin{cases} \beta_1 = diag(3w_0, 3w_0, 3w_0, 3w_0, 3w_0) \\ \beta_2 = diag(3w_0^2, 3w_0^2, 3w_0^2, 3w_0^2, 3w_0^2) \\ \beta_3 = diag(w_0^3, w_0^3, w_0^3, w_0^3, w_0^3) \end{cases} \tag{5.33}$$

Here, β_i is obtained by the observer bandwidth w_0 where $w_0 = 3w_c$ and w_c is a design parameter that needs to be determined through tuning (Gao *et al.* (2001)). In practical engineering situations, the parameter w_0 is the only parameter involved, which makes it easy to determine through trial and error. The function (fal) is important for the ESO system because of its characteristics of "big error, small gain; small error, big gain" when α_1 and $\alpha_2 < 1$. When α_1 and $\alpha_2 = 1$, this nonlinear function turns into a linear one (Pu *et al.* (2015)). The appropriate setting of the parameters β_1, β_2 and β_3 is crucial for achieving a dynamic response in ESO. By selecting suitable values of these parameters, the states $\hat{x}_1$ and $\hat{x}_2$ can track the output signal and its differential in the plant process, respectively. Additionally, the extended state $\hat{x}_3$ is able to estimate the combined effect of uncertain models and system disturbances.

Considering the $\overline{n}$-DoF MM system (5.29) and the ESO (5.31), the estimated error system can be given as follows:

$$\begin{cases} \dot{\varepsilon}_1 = \varepsilon_2 - \beta_1 \, \varepsilon_1 \\ \dot{\varepsilon}_2 = \varepsilon_3 - \beta_2 \, f_1(\varepsilon_1) \\ \dot{\varepsilon}_3 = -h(t) - \beta_3 \, f_2(\varepsilon_1) \end{cases} \tag{5.34}$$

where $\varepsilon_2 \in \mathbb{R}^{\overline{n}}$ and $\varepsilon_3 \in \mathbb{R}^{\overline{n}}$ are the observer's error for the states $x_2 \in \mathbb{R}^{\overline{n}}$ and $x_3 \in \mathbb{R}^{\overline{n}}$. According to analysis in (Zhao, Yang, Xia & Liu (2015)), the convergence of the error system (5.34) is obtained by using a self-stable region technique. Therefore, the observed states $\hat{x}_1$, $\hat{x}_2$, and $\hat{x}_3$ converge to x_1, x_2, and x_3, respectively.

5.4.3 Design of the ESO-based NFTSM

In this section, a composite NFTSM algorithm with ESO is introduced to control the MM system. The operating principle of the ESO is to estimate the system uncertainty and disturbance. The ESO requires the control input of the NFTSM and the system output. Then, it estimates state variables θ of the system, which includes the equivalent total disturbance observed. The output variable will be used by the NFTSM to modify the robust control law in real-time in order to reduce the effect of the disturbances.

According to Theorem 1, a robust control law based on ESO can be designed for tracking positions as:

$$\begin{aligned} \overline{\overline{\tau}} &= D^{-1}(x_1)\,(\overline{\overline{\tau}}_{eq} + \overline{\overline{\tau}}_b) \\ \overline{\overline{\tau}}_{eq} &= -\left(\lfloor e_2 \rfloor^{\sigma_2 - I_{\overline{n}}}\right)^{-1} \sigma_2^{-1} k_2^{-1}\left(I_{\overline{n}} + k_1 \sigma_1 \lfloor e_1 \rfloor^{\sigma_1 - I_{\overline{n}}}\right) e_2 \\ &\quad - \hat{x}_3 + \ddot{x}_d \\ \overline{\overline{\tau}}_b &= -k_3\, s - k_4\, sign(s) \end{aligned} \tag{5.35}$$

The composite robust ESO-based NFTSM can be expressed as:

$$\begin{aligned} \overline{\overline{\tau}} = D^{-1}(x_1)\Big(&-\left(\lfloor e_2 \rfloor^{\sigma_2 - I_{\overline{n}}}\right)^{-1} \sigma_2^{-1} k_2^{-1}\left(I_{\overline{n}} + k_1 \sigma_1\right. \\ &\left.\lfloor e_1 \rfloor^{\sigma_1 - I_{\overline{n}}}\right).\, e_2 - \hat{x}_3 + \ddot{x}_d - k_3\, s - k_4\, sign(s)\Big) \end{aligned} \tag{5.36}$$

Assumption 2. Assuming that the derivative of $\tilde{x}_3$ is bounded, and there exists a constant $\tilde{\mu} > 0$, such as:

$$\|\dot{\tilde{x}}_3(t)\| \leq \tilde{\mu} \qquad \forall t \geq 0 \tag{5.37}$$

where $\tilde{x}_3 = x_3 - \hat{x}_3$ is the estimation error.

Theorem 2. Let the system (5.29) satisfies Assumption 2, applying the control law (5.36) the system state can converge to zero in finite time, if the gain satisfies $\|k_4\| > \tilde{\mu}$.

Proof: According to (5.16), we can rewrite (5.22) as follows:

$$\begin{aligned} \dot{s} =& e_2 + k_1\, \sigma_1\, \lfloor e_1 \rfloor^{\sigma_1 - I_{\overline{n}}}.\, e_2 \\ &+ k_2\, \sigma_2\, \lfloor e_2 \rfloor^{\sigma_2 - I_{\overline{n}}}.\, \left(x_3 + D(x_1)\, \overline{\overline{\tau}} - \ddot{x}_d \right) \end{aligned} \tag{5.38}$$

The time derivative of s becomes after substituting the control law (4.36):

$$\dot{s} = -\, k_2\, \sigma_2\, \lfloor e_2 \rfloor^{\sigma_2 - I_{\overline{n}}}.\, \Big(-\, \tilde{x}_3 + k_3\, s + k_4\, sign(s) \Big) \tag{5.39}$$

Performing the stability analysis based on the Lyapunov function $V_2 = 0.5\, s^T\, s$, its time derivative leads to:

$$\dot{V}_2 = -\, s^T\, k_2\, \sigma_2\, \lfloor e_2 \rfloor^{\sigma_2 - I_{\overline{n}}}.\, \left(k_3\, s + k_4\, sign(s) - \tilde{x}_3 \right) \tag{5.40}$$

According to Assumption 2, (5.40) can be rewritten as

$$\begin{aligned} \dot{V}_2 \leq& -\, s^T k_2\, \sigma_2\, \lfloor e_2 \rfloor^{\sigma_2 - I_{\overline{n}}}.\, k_3\, s \\ &-\, s^T k_2\, \sigma_2\, \lfloor e_2 \rfloor^{\sigma_2 - I_{\overline{n}}}\, sign(s)\, \left(\overline{k}_4 - \tilde{\mu} \right) \leq 0 \end{aligned} \tag{5.41}$$

where $\overline{k}_4 = \lambda_{min}(k_4)$ that represents the minimum eigenvalue of k_4.

According to (5.41), it is verified from the above inequality with $\lambda_{min}(k_4) > \tilde{\mu}$ that the system states converge to the $s = 0$ asymptotically. Therefore, the tracking errors can reach zero in finite time. The architecture of the ESO-based NFTSM controller for the 5-DoF MM is shown in Figure 5.2.

Remark 3: The estimated disturbance was obtained by the ESO and fed to the controller. However, estimation errors between the total disturbance value $f(x_1, x_2)$ and the estimated value $\hat{x}_3$ exist in the system. The proposed ESO-based NFTSM in this article has the capability of rejecting the total disturbance. Besides, the MM closed-loop control system is

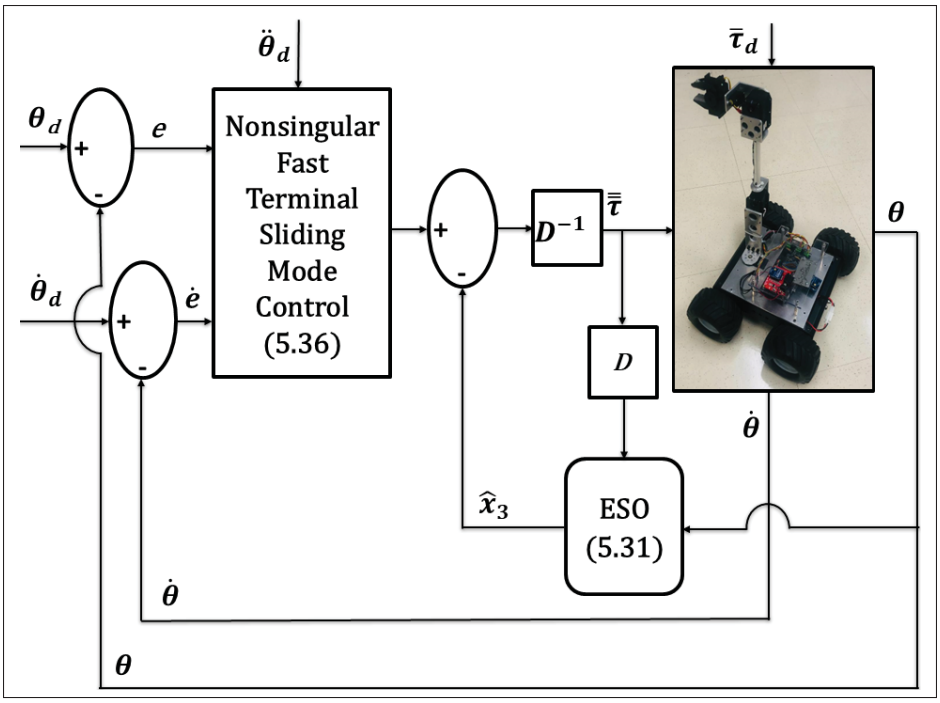

Figure 5.2 Structure of the ESO-based NFTSM controller for 5-DoF MM

converged to be stable if the parameter k_4 in the controller is tuned sufficiently large, which is derived from the Lyapunov principle. The following experimental results will validate this.

5.5 Experiments And Discussion

Figure 5.3 shows the controller and hardware implementation structure as developed in the laboratory. A home-made MM robot called Mob-ETS is used in real-time practical implementation to verify the proposed control's satisfactory performance. The values of the RM physical parameters are given as $m_v = 2\,kg, r = 0.05\,m, 2L = 0.27\,m$, and $I_v = 0.0122 \times 10^{-4}\,kg.m^2$ and of the MP are given as $m_1 = 0.5\,kg, m_2 = 0.5\,kg, m_3 = 0.2\,kg, 2L_1 = 0.16\,2L_2 = 0.2\,2L_3 = 0.12\,I_1 = 2.666\times10^{-4}\,kg.m^2, I_2 = 1.16\times10^{-4}\,kg.m^2$, and $I_3 = 6.01 \times 10^{-4}\,kg.m^2$.

Simulink with Mathworks' Real-Time Workshop (RTW) is used to perform the ESO-based NFTSM on a 5-DoF MM in this experiment. The three joints of the RM, as well as the right and left wheels of the MP, are actuated by HN-GH12-2217Y DC-motors and Dynamixel

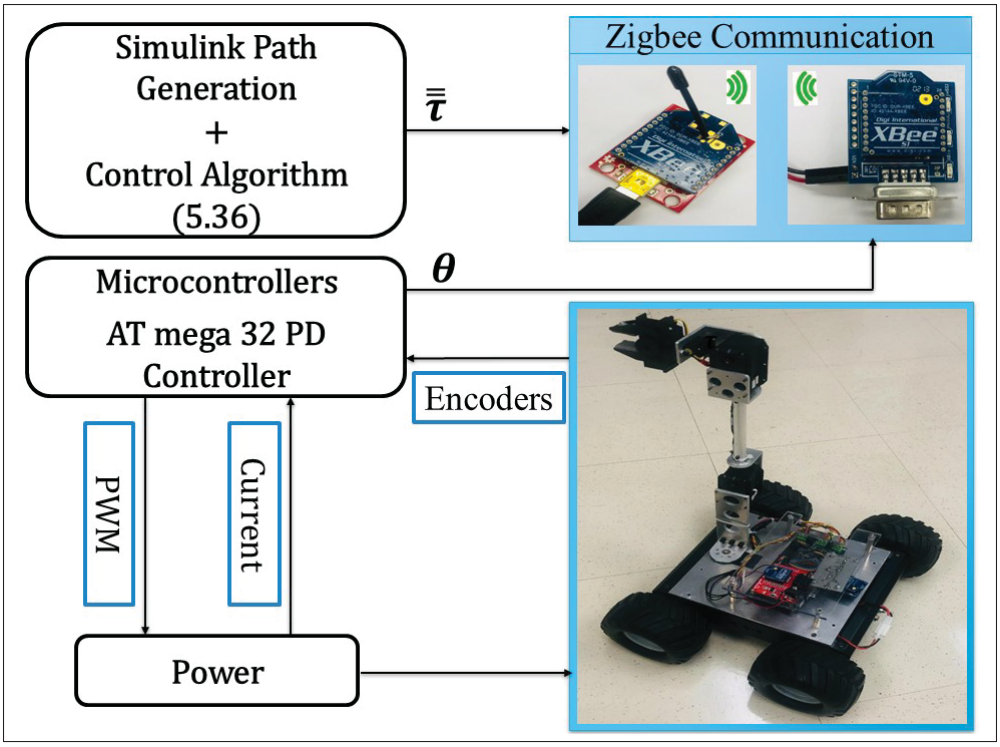

Figure 5.3 The structure of the experimental setup

motors (MX-64T), with encoder sensors (E4P-100- 079-DH-T-B) utilized to calculate angular positions. Zigbee is used to communicate between the Matlab/Simulink developed program and the MM.

For comparison purposes, the robust NFTSM described in Theorem 1 is applied to compare with the robustness of the proposed control approach in Theorem 2. The two control schemes, NFTSM and the proposed ESO-based NFTSM method have been compared experimentally, for the end-effector being controlled to track the desired trajectory. The parameters of the NFTSM controller and the proposed controller are chosen with the same values as $\sigma_1 = 2$, $\sigma_2 = 5/3$, $k_1 = diag(0.001, \cdots, 0.001) \in \mathbb{R}^{\bar{n}}$, $k_2 = diag(0.0018, \cdots, 0.0018) \in \mathbb{R}^{\bar{n}}$, $k_3 = diag(36, \cdots, 36) \in \mathbb{R}^{\bar{n}}$ and $k_4 = diag(215, \cdots, 215) \in \mathbb{R}^{\bar{n}}$.

The empirical trial and error method is adopted in the experimental procedure to tune the control scheme parameters. Firstly, the robust NFTSM is applied to control the MM, which assumes that the knowledge of the system uncertainty is known. Then, in the presence of the system uncertainty, the proposed ESO-based NFTSM's performance is validated for

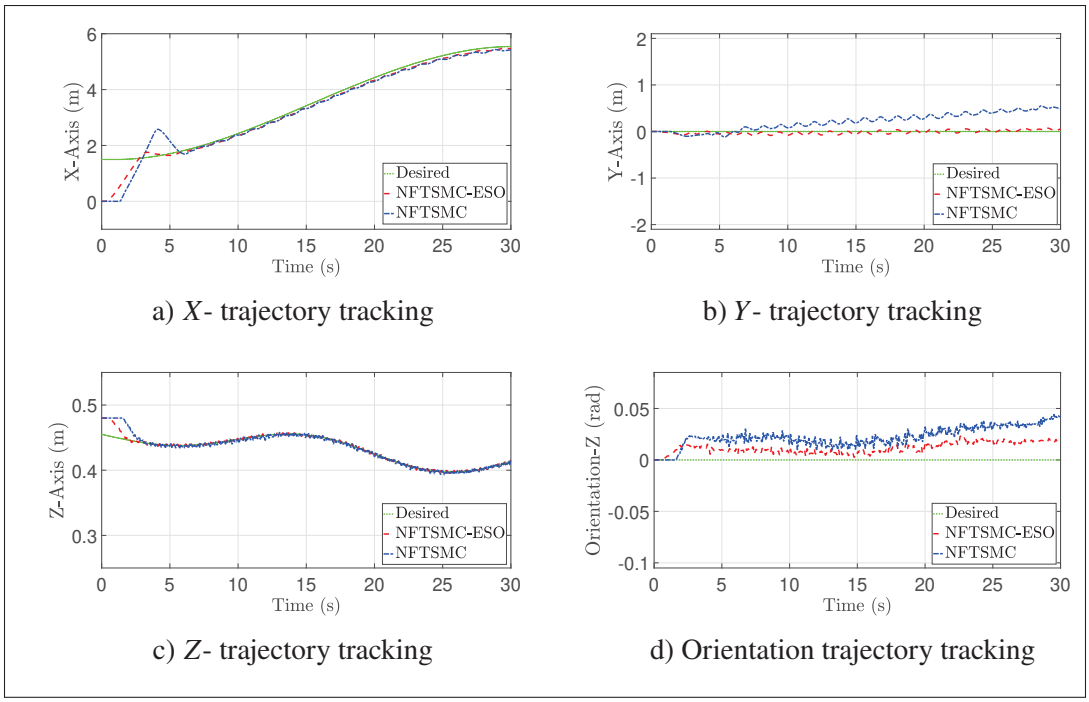

Figure 5.4 Trajectory Tracking of the 5-DoF MM (X, Y, Z axis, and orientation) in Cartesian Space

control system applications. The ESO has three types of parameters, based on the previously developed theory analysis of ESO, i.e., a linear range δ, power terms $\alpha_{1,2}$ and gains β_i. The parameters of ESO are also tuned by the empirical trial and error method in the experimental part as $w_0 = 5$, $\delta = 0.01$, $\alpha_1 = 0.5$, and $\alpha_2 = 0.25$, where the bandwidth w_0 is used to tune the observer gains.

As a comparative result, the tracking performances of both controllers are represented in Figures 5.4 - 5.10. The trajectory tracking for the end-effector MM in the Cartesian space is shown in Figures. 5.4 - 5.5.. In both cases, the desired trajectory of the end-effector is a path in the XYZ space, which is selected with the starting point $P_s = [X_s, Y_s, Z_s, \phi_s]^T = [1.5, 0, 0.455, 0]^T$, and the final point is $P_f = [X_f, Y_f, Z_f, \phi_f]^T = [5.5, 0, 0.42, 0]^T$. The inverse kinematics is used to obtain the desired trajectories in the joint space from the presented trajectory in Cartesian space of the end-effector.

Figure 5.4 shows the desired trajectory P_d of the end-effector P_e in Cartesian space as well as the actual position for the NFTSM with and without the ESO observer. Compared to

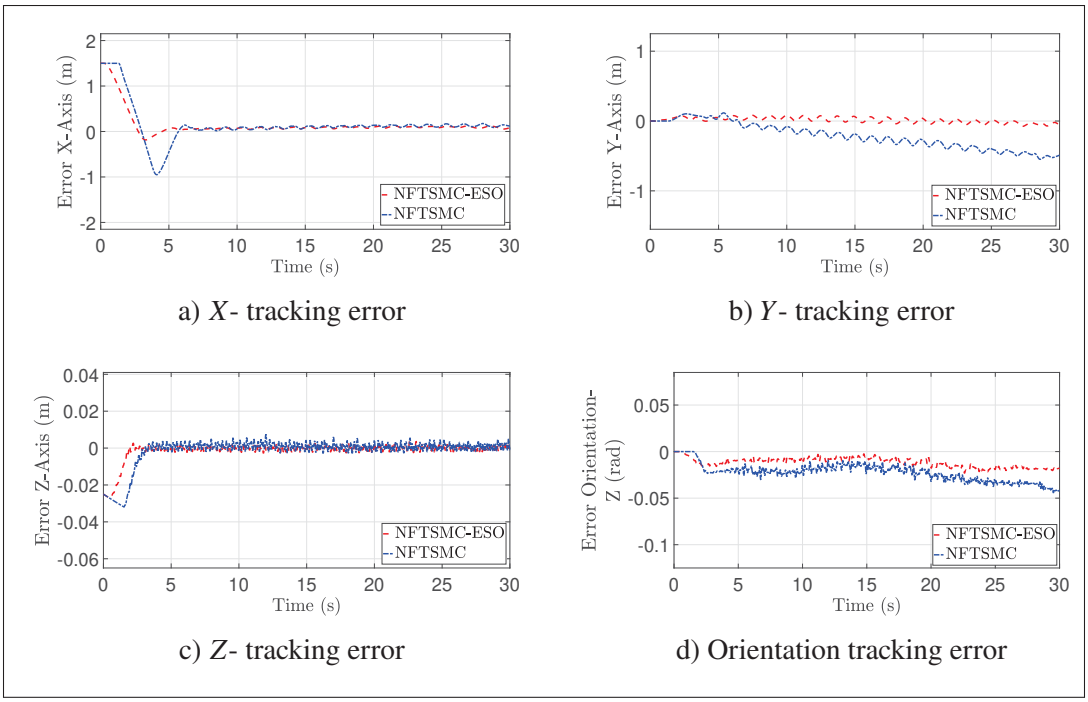

Figure 5.5 Tracking errors of the 5-DoF MM (X, Y, Z axis, and orientation) in Cartesian Space

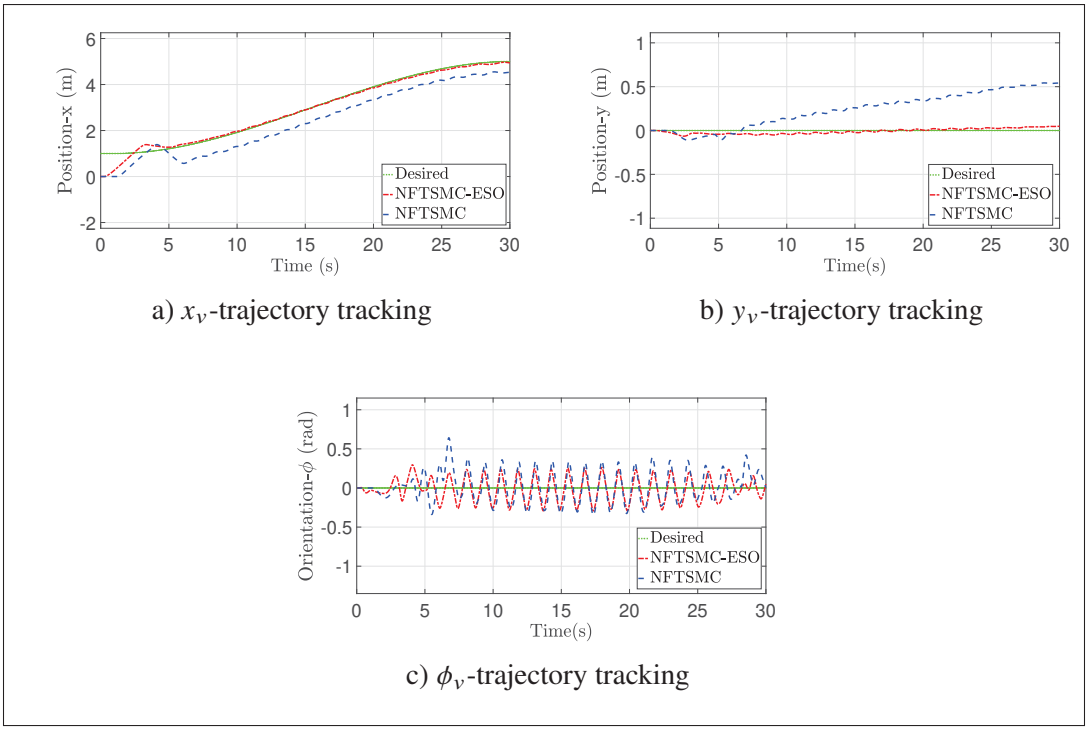

Figure 5.6 Trajectory Tracking of the 5-DoF MM (X, Y, Z axis, and orientation) in Cartesian Space

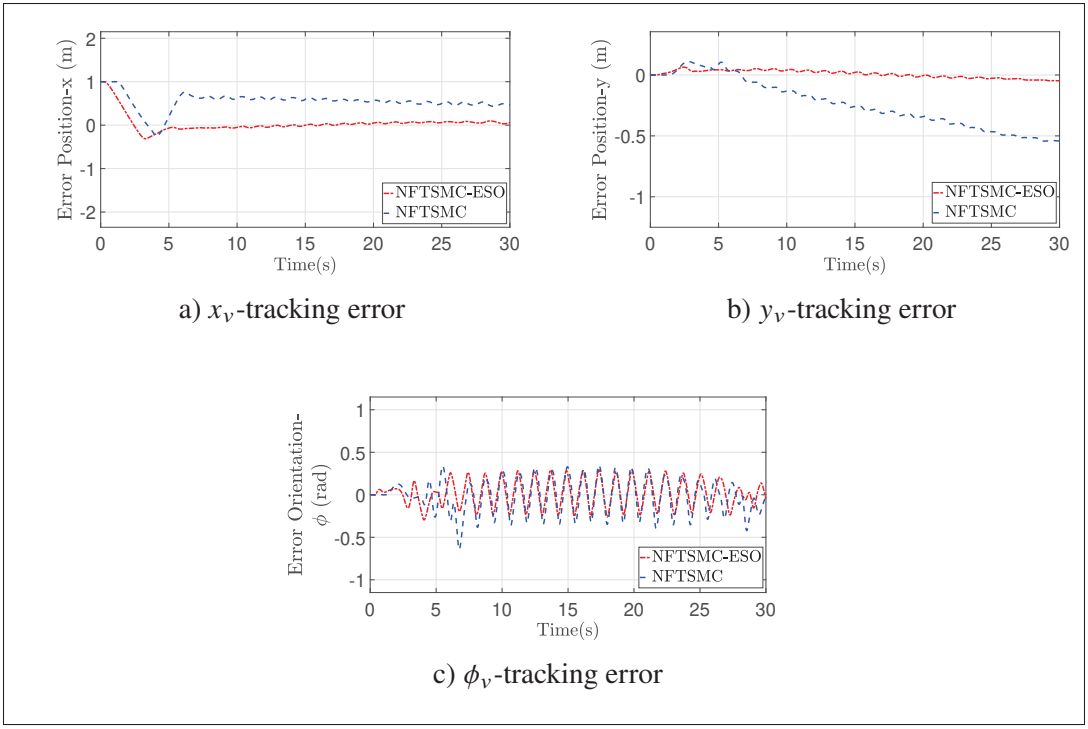

a) x_v-tracking error

b) y_v-tracking error

c) ϕ_v-tracking error

Figure 5.7 Tracking errors of the linear/angular position of the MP (x_v, y_v, and ϕ_v)

NFTSM, the end-effector closely and consistently follows the desired trajectory when adding the observer. In addition, the convergence time with the NFTSM and ESO is less than 2.5 s, whereas it is more than 5 s with the NFTSM alone. Figure 5.5 shows the tracking errors for both methods. The tracking error amplitude is less than 0.1 cm which clearly reveals that the proposed ESO-based NFTSM scheme has better disturbance rejection and estimation with quick convergence of the system.

To present the robustness of the proposed ESO-based NFTSM scheme compared with the NFTSM, Figure 5.6 and Figure 5.7 show the tracking position and tracking errors of the MP, respectively, with the maximum tracking error amplitude of $0.3cm$ for x_v, y_v and ϕ_v. As shown in these results, the responses of the ESO-based NFTSM scheme achieve superior robust performance compared with NFTSM. It can be verified that although the system uncertainties are unknown, the proposed control provides excellent experimental results and achieves good performances of trajectory tracking.

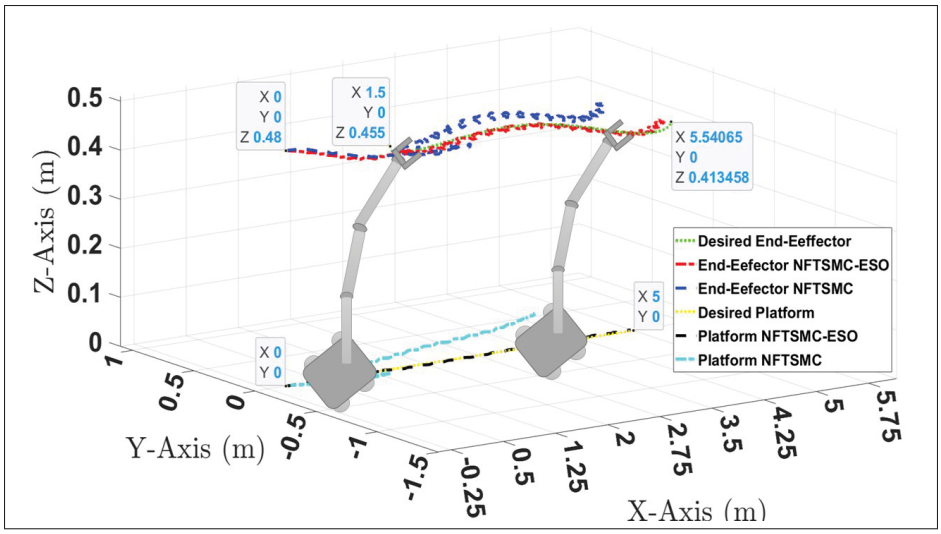

Figure 5.8 Tracking Performance of the 5-DoF MM in Cartesian Space (a) (X, Y, and Z) End-Effector tracking in 3D, (b) (x_v, y_v) MP tracking in 2D

In Figure 5.8, the corresponding tracking of the 3-D Figure end-effector and the 2-D Figure MP positions are illustrated in Cartesian space. Figure 5.8 shows the comparison results of the $(X; Y; Z)$ axis and end-effector orientation and the $(X; Y)$ MP applying the NFTSM and ESO-based NFTSM controllers. The results indicate that the ESO-based NFTSM controller gives better results than the NFTSM controller.

In the joint-position trajectory tracking, Figure 5.9 shows the trajectory tracking of the MM in the joint space. Due to the obvious efficiency of the designed controller, the performed trajectory is very good. Figure 5.10 shows the tracking errors in the joint space for $\theta_R, \theta_L, \theta_1, \theta_2$, and θ_3 where the tracking errors are less than 0.5 rad. Thus, it is concluded that the ESO-based NFTSM has high performance, such as fast convergence, high tracking accuracy, singularity avoidance and strong robustness against the total disturbances. The experimental results illustrate that the objective of the trajectory tracking control for the MM is successfully achieved with the composite ESO-based NFTSM controller in the presence of the system disturbances.

Figure 5.11 shows the applied control torques of the 5-DoF MM ($\tau_R; \tau_L; \tau_1; \tau_2; \tau_3$). The experimental results depict the validity and efficiency of the proposed control and its ability to

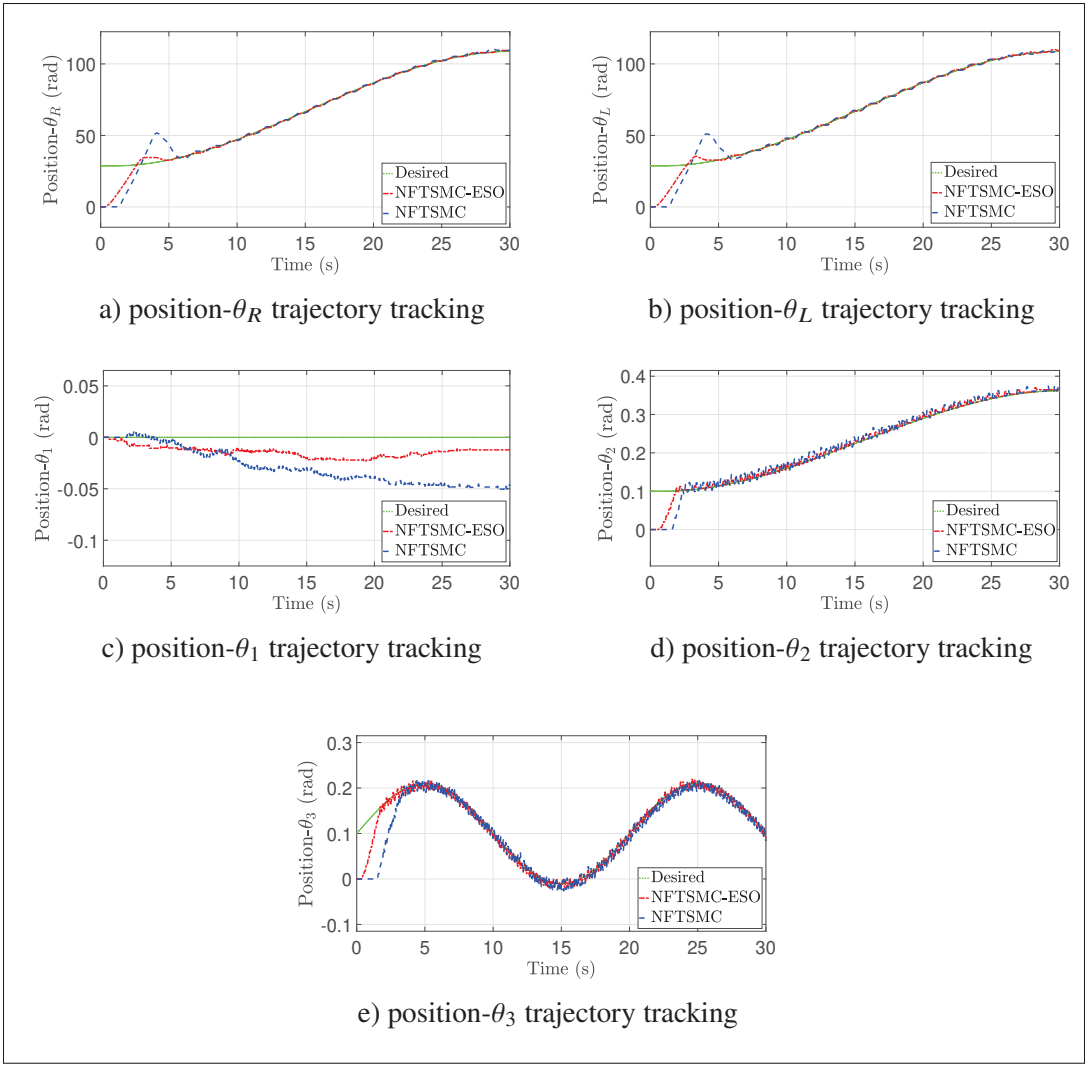

Figure 5.9 Trajectory tracking of the 5-DoF MM ($\theta_R, \theta_L, \theta_1, \theta_2$, and θ_3) in Joint space

respond quickly to disturbances. Experimental tests were done by varying the controller gains by 30%. The obtained results are not depicted since a similar trajectory tracking performance and similar control efforts were obtained due to the accuracy of the ESO estimation.

Remark 4: In theorem 1, the control law (5.21) is utilized to develop an NFTSM type of reaching law with term τ_{eq} (5.19) which can ensure the system's convergence in a fast-finite time. Whereas, the term τ_b (5.20) is adopted to enhance robustness against total disturbances. The stability of the closed-loop MM system was demonstrated in Theorem 2 using composite

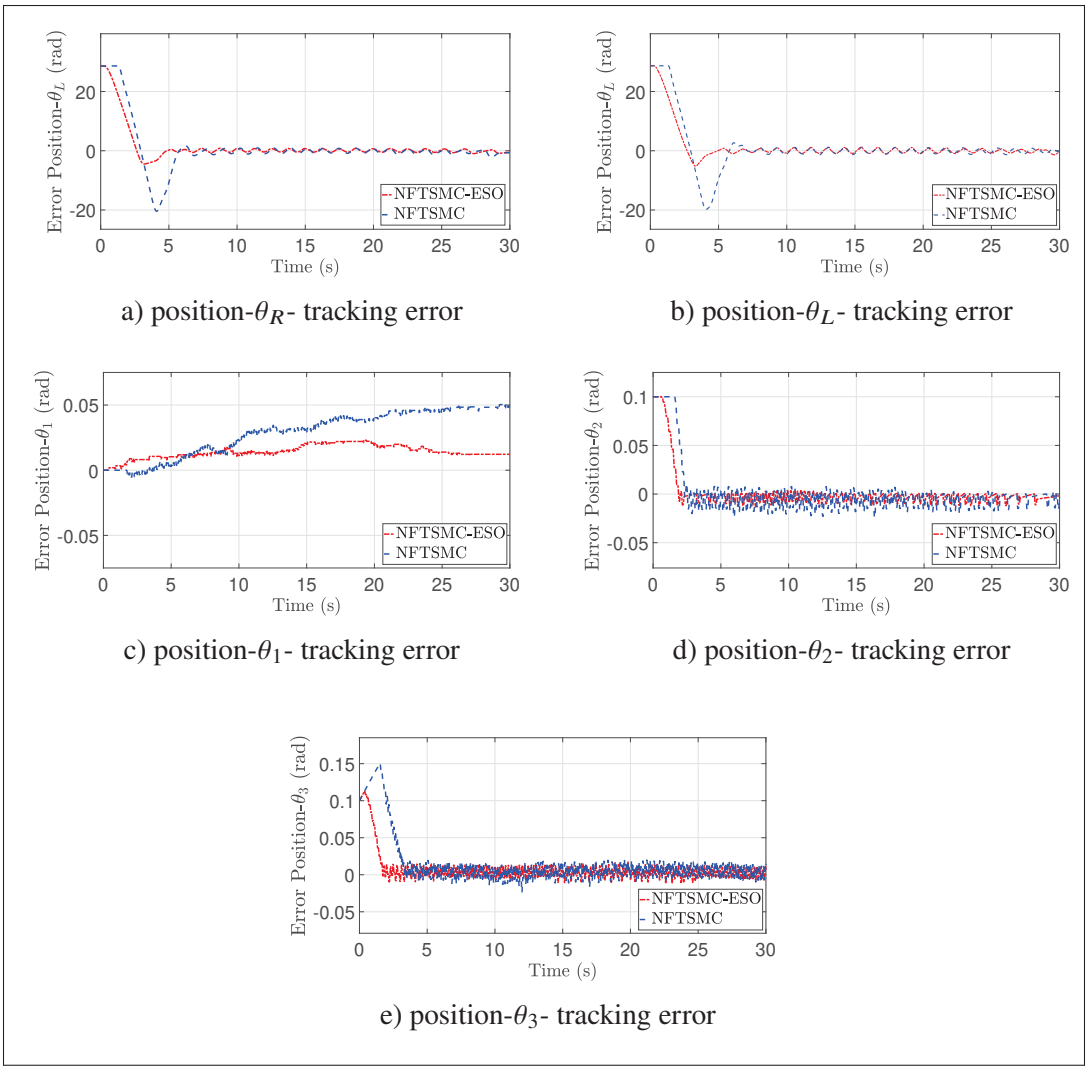

Figure 5.10 Tracking error of the 5-DoF MM ($\theta_R, \theta_L, \theta_1, \theta_2$, and θ_3) in Joint space

ESO-based NFTSM controller (5.40), based on the assumption (2) and assumes the upper bound of system uncertainty. It is obvious that the proposed controller does not need exact knowledge of the system dynamics. The experimental findings have also demonstrated the excellent performance of the proposed method. Consequently, the contribution of this paper is confirmed.

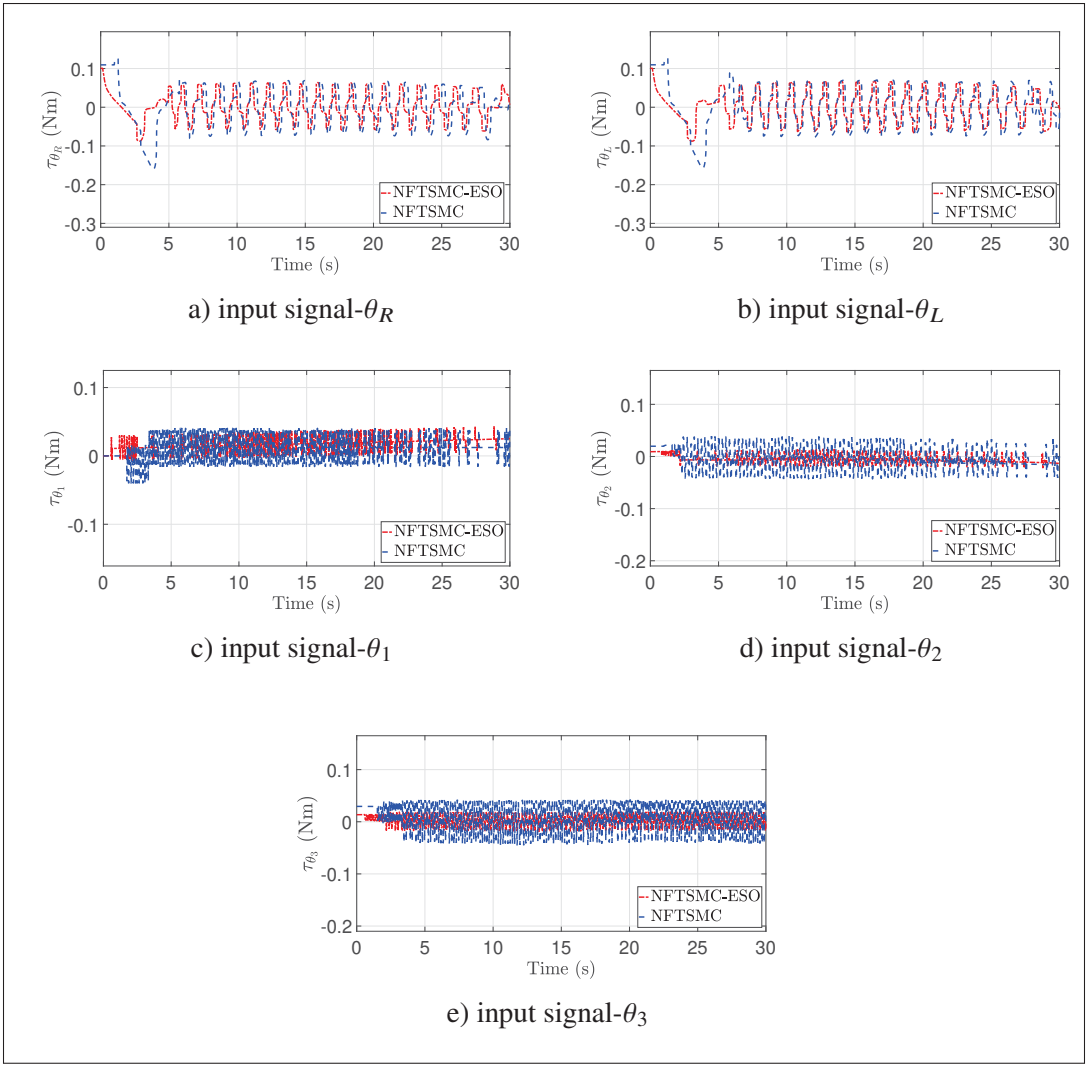

Figure 5.11 Control input signals for the 5-DoF MM (τ_R, τ_L, τ_1, τ_2, and τ_3)

5.6 Conclusion

In this paper, a robust ESO-based NFTSM control scheme was proposed for the MM system to overcome the problem of trajectory tracking. First, a dynamic model of the MM was given. The developed control law was then improved based on the significant characteristics of the NFTSM principle, which can direct the system state to the origin within a prescribed finite time. However, with the NFTSM method, the complexity of the disturbances and uncertainties can be encountered, which often occurs in real-time applications. Finally, the composite ESO-based NFTSM for uncertainties and disturbances estimation has been

introduced for more precise tracking. Moreover, it provides a faster convergence rate and good robustness compared to the NFTSM. Therefore, the ESO effectively estimates the total disturbances of the MM system. Based on NFTSM, the feedback control was designed to guarantee the closed-loop stability, and the proposed control was used to compensate for system uncertainties. The stability of the proposed control has been verified by the Lyapunov stability function. The experimental results clearly show that the ESO-based NFTSM controller achieved accurate tracking of the appropriate trajectory, with adequate tracking errors of the end-effector and joint positions, validating the effectiveness of the proposed approach for the 5-DoF MM in Cartesian space.

CHAPTER 6

FIXED-TIME ESO-BASED DECOUPLED TERMINAL SLIDING MODE FOR MOBILE MANIPULATOR

Mhmed Algrnaodi[1], Yassine Kali[2], Maarouf Saad[1], Mohamad Saad[2], Raouf Fareh[3]

[1] Electrical Engineering Department, École de technologie supérieure,
1100 Notre-Dame Ouest, Montréal, QC, Canada
[2] DIFIA Laboratory, School of Engineering, Université du Québec en
Abitibi-Témiscamingue, Rouyn-Noranda, QC, Canada
[3] Department of Electrical Engineering, University of Sharjah, Sharjah, UAE

Article submitted for publication to "IEEE Access", October 2025

Abstract

Mobile manipulators are highly nonlinear and strongly coupled systems that are affected by modeling uncertainties and external disturbances, making accurate and predictable trajectory tracking a challenging task. Conventional and terminal sliding mode control methods provide robustness, but they often suffer from chattering amplification in robotic systems and convergence times that depend on the initial conditions. This paper proposes a decoupled fixed-time terminal sliding mode control strategy integrated with a fixed-time extended state observer to address these limitations. A novel sliding surface that incorporates the inertia matrix is designed to structurally decouple the control inputs and mitigate cross coupling nonlinearities, thereby reducing chattering effects. The fixed time extended state observer estimates and compensates for lumped uncertainties and disturbances in real-time. The resulting observer and controller framework guarantees convergence within a prescribed fixed-time independent of initial conditions. Stability is established using Lyapunov analysis. Experimental validation on a physical five degrees of freedom mobile manipulator under external disturbance conditions demonstrates fast convergence within the derived fixed-time bounds, high tracking accuracy in Cartesian and joint spaces, and strong robustness. The proposed approach provides a predictable and practically implementable control solution for safety critical and real-time robotic applications.

Keywords: Decoupled controller, Extended state observer, Fixed-time stability, Mobile manipulator, nonlinear Sliding mode.

6.1 Introduction

In recent years, Mobile Manipulators (MMs) have made substantial progress in intelligence and autonomy, necessitating the development of increasingly sophisticated control strategies to ensure reliable task execution. A fundamental challenge in this context is to achieve precise trajectory tracking in real-world environments, where system performance can be significantly affected by uncertainties and external disturbances. These factors not only degrade operational efficiency, but may also pose risks to system integrity and safety. Consequently, the design of, robust real-time control approaches for accurate trajectory tracking is critical (Li & Ge (2013) to enable reliable and efficient deployment of MMs in complex and dynamic settings.

In this context, Sliding Mode (SM) approach has emerged as a powerful method for controlling nonlinear systems due to its inherent robustness, fast response, and ease of design (Drakunov & Utkin (1992); Choi *et al.* (2020); Kali, Saad & Benjelloun (2025); Liang (2025)). It offers the capability to maintain stability and satisfactory performance even in the presence of modeling errors and external disturbances. The SM technique has been widely applied to a variety of robotic and mechatronic systems (Xian *et al.* (2022); Zhang, Zhao, Miao, Li & Zhou (2025); Fallaha, Saad, Ghommam & Kali (2021); Liu *et al.* (2025a,b)). A well-known drawback of SMC that is limiting its real-life use is the chattering phenomenon (Liang, Yu & Li (2025)) which is a high-frequency oscillations caused by the discontinuous control action. This phenomenon can lead to excessive wear on actuators and degrade control precision. In the context of MMs, this effect is particularly harmful as it may compromise both the mechanical integrity of the system and the smooth coordination between the mobile base and the manipulator arm, ultimately impacting overall task performance. The chattering problem has been extensively addressed, and several solutions have been proposed in the literature (Levant (2010); Dorel & Levant (2008); Lala (2025)). Moreover, performance also strongly depends on the design of the sliding surface. An inappropriate one can lead to slow convergence or instability (Önen (2023)). Additionally, in coupled nonlinear

systems as MMs, designing a suitable multi-dimensional sliding manifold is complex and may fail to ensure global stability.

Among the various approaches proposed to address the aforementioned issue, the Non-singular Terminal SM (NTSM) control has attracted significant attention due to its capability to ensure finite-time convergence during both the reaching and sliding phases (Bhat & Bernstein (2000); Vo & Kang (2019); Kim *et al.* (2023)). Although NTSM ensures finite-time convergence in theory, its convergence rate tends to deteriorate near the equilibrium point, as the control law's nonlinear components diminish, resulting in slower error reduction and extended settling time. The reduced convergence rate is mitigated through the proposition of a Non-singular Fast Terminal SM (Chen, Tao & Tang (2024); Liu *et al.* (2019); Alnufaie (2023)). Complementary power terms are integrated into the surface, ensuring that the control action is maintained both far from and near the equilibrium. Nonetheless, the finite-time convergence depends on the initial system state, which can lead to slow reaching when the initial trajectories are far. In addition, it is hard to analyze the convergence speed when the initial value is unknown.

Unlike finite-time control, fixed-time control theory ensures convergence within a maximal time that is independent of initial conditions (Basin, Ramírez & Guerra-Avellaneda (2018); Wang, Su & Zhang (2020b)). This property provides predictable and consistent convergence which is very advantageous for safety-critical and real-time applications, particularly in systems subject to large initial errors or variable operating conditions. One of the earliest results that embedded fixed-time convergence within SM theory proposes a new fixed-time surface and a fixed-time reaching law (Zuo (2015)). Therefore, the approach has found extensive application in several areas (Zhang *et al.* (2019); Wang, Du, Zhang, Wu & Zhu (2020a); Hu *et al.* (2025)), where it contributes to improving control system effectiveness.The design of fixed-time SM generally involves selecting large control gains capable of dominating uncertainties and nonlinearities for all possible initial conditions.

To address this limitation, recent research considers neural networks-based fixed-time SM Sun *et al.* (2022); Liu *et al.* (2023); Abdallah, Kali, Saad, Fareh & Bettayeb (2025). Neural networks offer a powerful tool for approximating unknown dynamics, which enables effective control of systems exhibiting strong nonlinearities or time-varying parameters. By learning

and compensating for uncertainties, the neural network enhances robustness and reduces the reliance on high control gains compared to purely model-based fixed-time SM which decreases the overall control effort. Despite their advantages, these solutions present some practical challenges. Indeed, the real-time adaptation can impose a significant computational burden.

Additionally, the performance is also highly sensitive to the selection of learning parameters; inappropriate choices can result in slow adaptation or even instability. Furthermore, although neural networks are capable of approximating unknown nonlinearities, residual approximation errors may persist, potentially degrading steady-state performance under rapid or abrupt changes in system dynamics. Another promising solution is the observers-based fixed-time SM (Duong, Pham, Giap & Vu (2023); Farhat, Kali, Saad, Rahman & Lopez-Herrejon (2025); Zhang, Hu, Cheng, Wu & Yan (2024)). The proposed observers enhance robustness by compensating for matched uncertainties, thereby improving system resilience and steady-state accuracy through real-time estimation and compensation of unknown dynamics.

Despite the improvements offered by advanced fixed-time SM strategies, they remain susceptible to chattering. This phenomenon becomes particularly pronounced in highly coupled multi-input multi-output (MIMO) nonlinear systems which is the case of MMs, where the interactions between multiple Degrees of Freedom (DoF) amplify discontinuities in the control signal, potentially affecting performance and actuator longevity. To address all the mentioned challenges, this paper proposes a novel fixed-time terminal SM control strategy that integrates a fixed-time Extended State Observer (Cui *et al.* (2022)) (ESO) and a new coupled fixed-time nonlinear sliding surface, aiming to decouple the control law, reduce chattering, improve robustness, and ensure predictable convergence. The new controller also aims to improve trajectory tracking in MMs operating in real-time conditions. The main contributions of this work are threefold:

1. Novel coupled fixed-time nonlinear sliding surface: A new sliding surface is proposed that explicitly incorporates the MM inertia matrix, enabling the resulting control law to be completely decoupled, and thereby significantly reducing the chattering effect. By carefully designing the nonlinear surface dynamics, the controller ensures fast and

convergence of the sliding variable in fixed-time, enhancing transient performance and stability during the sliding phase.

2. Composite fixed-time SM–ESO framework with experimental validation: A novel composite control architecture is developed by integrating the proposed coupled fixed-time sliding surface with a fixed-time ESO for real-time disturbance and nonlinear dynamics compensation. This framework aims to achieve high-precision trajectory tracking, increased robustness, and guaranteed fixed-time convergence. Its effectiveness is experimentally demonstrated on a 5-DoF MM, where superior tracking performance is observed in both Cartesian and joint spaces, highlighting the practical applicability and significance of the proposed approach.

The remainder of this paper is structured as follows. Section II provides a comprehensive overview of the MM, including its kinematic and dynamic models, and formally states the control objectives. Section III details the design of the proposed fixed-time SM controller integrated with fixed-time ESO, accompanied by a rigorous Lyapunov stability analysis. Section IV describes the experimental setup, implementation procedures, and presents an in-depth discussion of the results, demonstrating the effectiveness and robustness of the proposed control strategy. Finally, Section V concludes the paper by summarizing the key contributions and highlighting potential directions for future research.

6.2 Overview of the Mobile Manipulator and Control Objectives

This section provides a detailed description of the kinematic and dynamic models of the n-DoF MM operating within Cartesian space. The system's dynamics are derived using the Lagrangian formulation, as illustrated in Figure 6.1. The MM system consists of a three-link robotic manipulator (RM) mounted on a wheeled mobile platform (MP), featuring actively driven front wheels and passive rear wheels. The MM has n-DoF, where the RM is subject to holonomic constraints, while the MP is subject to nonholonomic constraints.

6.2.1 Kinematics

In most robotic applications, desired trajectories are defined in Cartesian space and then mapped to joint space. Figure 6.1 illustrates P_e, the position and orientation vector of the

manipulator's end-effector. The configuration of the MM is represented by the generalized coordinate vector $q = \left[q_v^T,\ \theta_a^T\right]^T \in \mathbb{R}^n$, where $q_v = \left[X_v,\ Y_v,\ \phi_v\right]^T \in \mathbb{R}^{n_v}$ denotes the motion platform's state, and $\theta_a = \left[\theta_1,\ \cdots,\ \theta_{n_a}\right]^T \in \mathbb{R}^{n_a}$ represents the robotic manipulator's state. These combine to give $n = n_v + n_a$, with n_v corresponding to the actuated DoF of the MP, and n_a to those of the RM. The relationship between the joint states and the end-effector velocity is given by (Algrnaodi, Saad, Saad, Fareh & Kali (2024)):

$$V_e = J_e(q)\dot{q} \tag{6.1}$$

where $J_e(q) \in \mathbb{R}^{n\times n}$ represents the Jacobian matrix, and $\dot{q} = [\dot{q}_v^T, \dot{\theta}_a^T]^T$, includes the velocities $\dot{q}_v = [\dot{X}_v, \dot{Y}_v, \dot{\phi}_v]^T$ for the MP and $\dot{\theta}_a = [\dot{\theta}_1, \cdots, \dot{\theta}_{n_a}]^T$ for the RM.

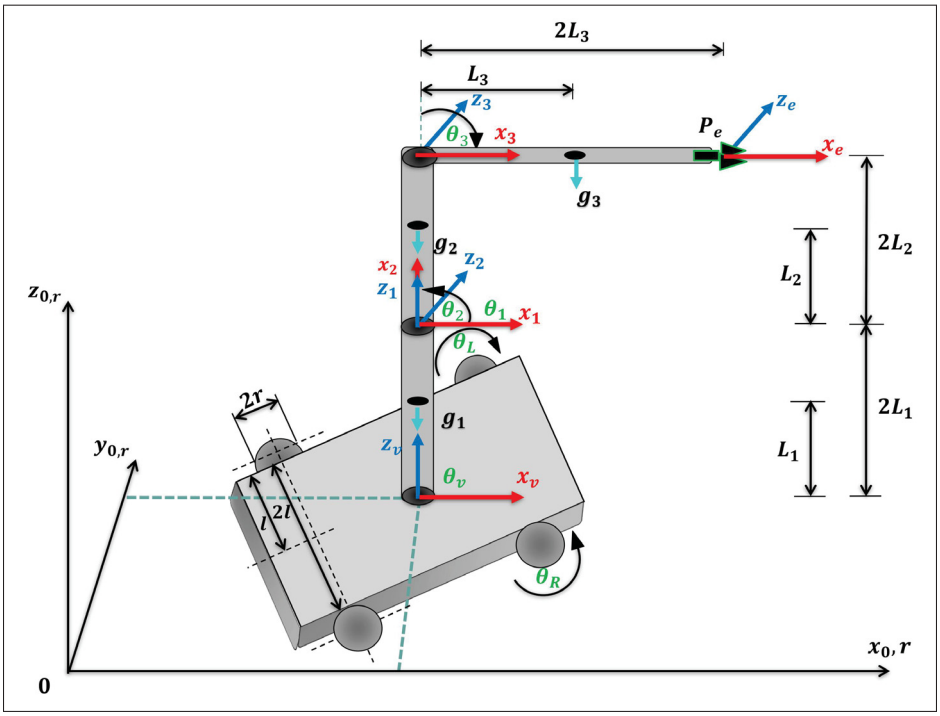

Figure 6.1 The system of n-DoF MM

6.2.2 Dynamic Model

The dynamic behavior of the MM system is described using the Lagrangian technique, capturing the coupled dynamics between the MP and the MR. The overall dynamic model of

the MM (Algrnaodi *et al.* (2024); Li *et al.* (2007)) is expressed as:

$$M(\theta)\ddot{\theta} + C(\theta, \dot{\theta})\dot{\theta} + G(\theta) = \tau - \tau_d \tag{6.2}$$

In this model, the matrices $M(\theta)$, $C(\theta, \dot{\theta})$, and $G(\theta)$ denote the positive-definite inertia matrix, the Coriolis and centrifugal matrix, and the gravitational torque vector, respectively. The vector $\theta = \begin{bmatrix} \theta_v^{\mathrm{T}} & \theta_a^{\mathrm{T}} \end{bmatrix}^{\mathrm{T}}$ includes all generalized coordinates, where θ_v corresponds to the angular positions of the MP, and $\dot{\theta}$ comprises their time derivatives. The control input vector is denoted by $\tau \in \mathbb{R}^k$, and $\tau_d \in \mathbb{R}^n$ represents unknown disturbances acting on the system.

Remark 1: In this study, the MM system is modeled as a holonomic platform equipped with a fully actuated manipulator arm. Due to the imposed kinematic constraints, the overall system states are reduced, allowing for a simplified but effective dynamic representation (6.3).

6.2.3 Control Objective

To handle modeling uncertainties and unknown disturbances, the dynamic model is rewritten by incorporating total disturbances. This reformulated model is given by:

$$M(\theta)\ddot{\theta} = f(\theta, \dot{\theta}) + \tau \tag{6.3}$$

Here, the function $f(\theta, \dot{\theta}) = -\tau_d - C(\theta, \dot{\theta})\dot{\theta} - G(\theta)$ is treated as the "total disturbance" affecting the system, encapsulating the dynamic coupling effects between the RM and the MP, as well as the perturbations and uncertain dynamics. By defining the state variables $x_1 = \theta$, $x_2 = \dot{\theta}$, and introducing an augmented state variable $x_3 = M^{-1}(x_1)f(x_1, x_2)$ with $f(x_1, x_2) = f(\theta, \dot{\theta})$, the dynamics of the MM can be rewritten as:

$$\begin{cases} \dot{x}_1 = x_2 \\ \dot{x}_2 = x_3 + M^{-1}(x_1)\,\tau \\ \dot{x}_3 = \chi \end{cases} \tag{6.4}$$

where χ is the derivative of $M^{-1}(x_1)f(x_1, x_2)$ and assume that this term is differentiable. It should be emphasized that the reformulated dynamics in (6.3) and (6.4) do not represent a linear system. The configuration preserves the intrinsic nonlinear and coupled nature of the mobile manipulator dynamics since it depends on the inertia matrix, the Coriolis terms and the gravity effects. The studied system verifies the following property:

Property: The inertia matrix $M(x_1)$ is symmetric positive-definite such as:

$$0 < \underline{m} \leq \|M(x_1)\| \leq \overline{m} < \infty \tag{6.5}$$

where $\underline{m}$ and $\overline{m}$ are known positive constants.

In addition, the following assumptions are made for the design procedure:

Assumption 1: It is considered that the total perturbations, denoted as $f(x_1, x_2)$, are typically not known a priori. However, it is assumed that these perturbations are both bounded and differentiable. To quantify this, a positive constant $\mu > 0$ is introduced, which represents the maximum value of the total disturbance while ensuring that the norm of the perturbations satisfies the following condition:

$$\|f(x_1, x_2)\| \leq \mu \tag{6.6}$$

Assumption 2: (Zhang, Wei, Wu & Cui (2018)) The first derivative of x_3 with respect to time, represented as χ, is bounded constant such that $\|\chi\| \leq \overline{\mu}$. Here, $\overline{\mu}$ represents a known upper limit on the magnitude of the disturbance's derivative, χ.

Suppose the reference signals are defined as $x_{1d} = \theta_d$ and $x_{2d} = \dot{\theta}_d$. The tracking error and its first time derivative can then be expressed as:

$$\begin{cases} e = x_1 - x_{1d} \\ \dot{e} = \dot{x}_1 - \dot{x}_{1d} = x_2 - x_{2d} \end{cases} \tag{6.7}$$

For mobile manipulators operating in dynamic and uncertain environments, initial tracking errors may vary significantly due to navigation inaccuracies, payload changes, and external

disturbances. In such conditions, finite-time controllers typically exhibit convergence times that depend on the initial state, leading to unpredictable task completion. In contrast, the fixed-time property guarantees a uniform upper bound on the convergence time, which is particularly advantageous for coordinated motion, scheduling, and safety-critical operations. Motivated by these practical considerations, the primary objective of this paper is to develop a novel decoupled fixed-time control strategy, supported by a fixed-time extended state observer, to handle the nonlinear dynamics of the considered system. The proposed scheme ensures accurate tracking of the position vector x_1 toward its reference trajectory x_{1d}, despite external disturbances and uncertainties, where the desired Cartesian trajectory P_d is converted into the corresponding joint-space trajectory x_{1d} via inverse kinematics.

6.3 Fixed-Time Controller Design

This section introduces a novel decoupled fixed-time SM approach augmented by a fixed-time ESO designed to enhance robustness against disturbances and uncertainties in the system. The fixed-time ESO is utilized to estimate the "total disturbance" affecting the system, effectively mitigating the adverse effects of dynamic uncertainties and external perturbations. *lemma 1*: (Chen *et al.* (2020)) Consider the system $\dot{x} = f(x, u)$, suppose there is a continuous function $V(x)$ that is definite positive such as:

$$\dot{V}(x) \leq -A_1 V^{\nu_1}(x) - A_2 V^{\nu_2}(x) - A_3 V(x) \tag{6.8}$$

where $A_i > 0$ for $i = 1, 2, 3$, $\nu_1 \in (0, 1)$ and $\nu_2 > 1$. Then, the origin is practical fixed-time stable and the maximal required time to reach $V(x) \equiv 0$ is defined as follows:

$$T_{max} = \frac{1}{A_3(1-\nu_1)} \ln\left(1 + \frac{A_3}{A_1}\right) + \frac{1}{A_3(\nu_2 - 1)} \ln\left(1 + \frac{A_3}{A_2}\right) \tag{6.9}$$

6.3.1 Fixed-Time Extended State Observer

The fixed-time ESO used here estimates the exact state of the total disturbances, denoted as x_3. The observer's design is based on the following augmented system dynamics:

$$\begin{cases} \dot{\hat{x}}_1 = & \hat{x}_2 + \zeta_1 \operatorname{sig}^{\varepsilon_1 I}(\tilde{x}_1) + \xi_1 \operatorname{sig}^{\vartheta_1 I}(\tilde{x}_1) \\ \dot{\hat{x}}_2 = & \hat{x}_3 + \zeta_2 \operatorname{sig}^{\varepsilon_2 I}(\tilde{x}_1) + \xi_2 \operatorname{sig}^{\vartheta_2 I}(\tilde{x}_1) + M^{-1}(x_1)\tau \\ \dot{\hat{x}}_3 = & \zeta_3 \operatorname{sig}^{\varepsilon_3 I}(\tilde{x}_1) + \xi_3 \operatorname{sig}^{\vartheta_3 I}(\tilde{x}_1) + K\operatorname{sign}(\tilde{x}_1) \end{cases} \tag{6.10}$$

where $\hat{x}_i$ are the estimates of the states x_i for $i = 1, 2, 3$ and $\tilde{x}_1 = x_1 - \hat{x}_1$ represents the estimation error vector, $\operatorname{sig}^{\varepsilon_i I}(\tilde{x}_1) = [|\tilde{x}_{11}|^{\varepsilon_{i1}}\operatorname{sign}(\tilde{x}_{11}), \cdots, |\tilde{x}_{1n}|^{\varepsilon_{in}}\operatorname{sign}(\tilde{x}_{1n})]^T$ with: $0 < \varepsilon_{ij} = 1 + i(\varepsilon_j^\star - 1) < 1$ and $0.8 < \varepsilon_j^\star < 1$ for $j = 1, \cdots, n$ and $\operatorname{sig}^{\vartheta_i I}(\tilde{x}_1) = \left[|\tilde{x}_{11}|^{\vartheta_{i1}}\operatorname{sign}(\tilde{x}_{11}), \cdots, |\tilde{x}_{1n}|^{\vartheta_{in}}\operatorname{sign}(\tilde{x}_{1n})\right]^T$ with: $\vartheta_{ij} = 1 + i(\vartheta_j^\star - 1) > 1$ and $1 < \vartheta_j^\star < 1.2$, $K = \operatorname{diag}(k_1, \cdots, k_n)$ verifies $\underline{\lambda}(K) > \overline{\mu}$ such as $\underline{\lambda}\{\bullet\}$ is the minimum eigenvalue of the matrix $\bullet$.

Finally, ζ_i and ξ_i are $(n \times n)$ diagonal matrices selected such that for each state, the following matrices p_{1j} and p_{2j} are Hurwitz for $j = 1, \cdots, n$:

$$p_{1j} = \begin{bmatrix} \zeta_{1j} & 1 & 0 \\ \zeta_{2j} & 0 & 1 \\ \zeta_{3j} & 0 & 0 \end{bmatrix}, \quad p_{2j} = \begin{bmatrix} \xi_{1j} & 1 & 0 \\ \xi_{2j} & 0 & 1 \\ \xi_{3j} & 0 & 0 \end{bmatrix}$$

Based on *Assumption 2*, the proposed fixed-time ESO ensures accurate estimation of the state variables x_1, x_2, and x_3. The estimation error of the total disturbance, denoted as $\tilde{x}_3 = x_3 - \hat{x}_3$, is proven to converge to zero within a fixed-time, bounded by:

$$T_{0j} \leq \frac{\overline{\lambda}^{(1-\varepsilon_j^\star)}(\Phi_{1j})}{(1-\varepsilon_j^\star)\varphi_{1j}} + \frac{1}{(\vartheta_j^\star - 1)\varphi_{2j}\omega_j^{(1-\varepsilon_j^\star)}} \tag{6.11}$$

where $\overline{\lambda}\{\bullet\}$ is the maximum eigenvalue of the matrix $\bullet$, $\varphi_{1j} = \underline{\lambda}(\Psi_{1j})/\overline{\lambda}(\Phi_{1j})$, $\varphi_{2j} = \underline{\lambda}(\Psi_{2j})/\overline{\lambda}(\Phi_{2j})$, $\omega_j \leq \underline{\lambda}(\Phi_{2j})$. $\Phi_{1j}, \Phi_{2j}, \Psi_{1j}$ and Ψ_{2j} are matrices designed to be symmetric

positive-definite verifying:

$$\Phi_{1j} p_{1j} + p_{1j}^T \Phi_{1j} = -\Psi_{1j}, \quad \Phi_{2j} p_{2j} + p_{2j}^T \Phi_{2j} = -\Psi_{2j} \tag{6.12}$$

The fixed-time ESO errors are defined as follows:

$$\begin{cases} \tilde{x}_1 = & x_1 - \hat{x}_1 \\ \tilde{x}_2 = & x_2 - \hat{x}_2 \\ \tilde{x}_3 = & x_3 - \hat{x}_3 \end{cases} \tag{6.13}$$

Using the above equation as well as (6.10), one can obtain:

$$\begin{cases} \dot{\tilde{x}}_1 = & \tilde{x}_2 \, \zeta_1 \, \mathrm{sig}^{\varepsilon_1 I}(\tilde{x}_1) - \xi_1 \, \mathrm{sig}^{\vartheta_1 I}(\tilde{x}_1) \\ \dot{\tilde{x}}_2 = & \tilde{x}_3 - \zeta_2 \, \mathrm{sig}^{\varepsilon_2 I}(\tilde{x}_1) - \xi_2 \, \mathrm{sig}^{\vartheta_2 I}(\tilde{x}_1) \\ \dot{\tilde{x}}_3 = & \dot{x}_3 - \zeta_3 \, \mathrm{sig}^{\varepsilon_3 I}(\tilde{x}_1) - \xi_3 \, \mathrm{sig}^{\vartheta_3 I}(\tilde{x}_1) - K \, \mathrm{sign}(\tilde{x}_1) \end{cases} \tag{6.14}$$

According to the results in Theorem 2 in Zhang *et al.* (2018) and Theorem 1 in Basin *et al.* (2017), the convergence of the error system (6.13) is obtained in a fixed-time. If $t \leq T_0$, $\tilde{x} = [\tilde{x}_1, \, \tilde{x}_2, \, \tilde{x}_3]^T$ will converge to zero, i.e., $\tilde{x} = 0$. Therefore, x_3 can be considered as an extended state.

Remark 2: Designing an effective observer in real-time applications poses significant challenges; however, the used fixed-time ESO structure simplifies the selection of observer gains ($\zeta_1 = \xi_1$, $\zeta_2 = \xi_2$, $\zeta_3 = \xi_3$, K), allowing for precise estimation of the state and disturbances within a fixed time frame, thereby enhancing the system's overall performance.

6.3.2 Fixed-time ESO-based fixed-time SM Design

The novel coupled fixed-time nonlinear sliding surface is defined as follows:

$$s = M(x_1)\dot{e} + \Gamma(e) \tag{6.15}$$

where $\Gamma(e)$ is given by:

$$\Gamma(e) = \gamma_1 \, \mathrm{sig}^{\alpha_1 I}(e) + \gamma_2 \, \mathrm{sig}^{\alpha_2 I}(e) + \gamma_3 \, e \tag{6.16}$$

The matrices $\gamma_1, \gamma_2, \gamma_3$ are $(n \times n)$ positive-definite matrices, $\mathrm{sig}^{\alpha_1 I}(e) = [|e_1|^{\alpha_1}\mathrm{sign}(e_1), \cdots, |e_n|^{\alpha_1}\mathrm{sign}(e_n)^T$ and $\mathrm{sig}^{\alpha_2 I}(e) = [|e_1|^{\alpha_2}\mathrm{sign}(e_1), \cdots, |e_n|^{\alpha_2}\mathrm{sign}(e_n)]^T$ with $0.5 < \alpha_1 < 1$ and $\alpha_2 > 1$. The selection of the exponents has a direct impact on the convergence time.

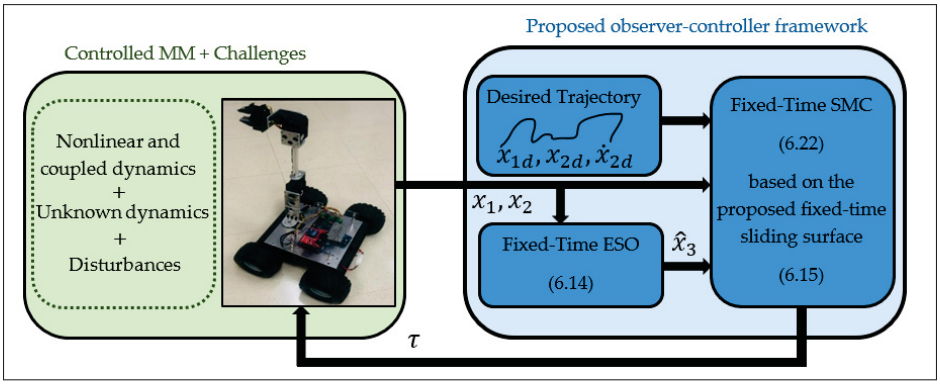

Figure 6.2 Block diagram of the proposed Fixed-time ESO-based decoupled terminal SM for 5-DoF MM

Remark 3: Unlike linear sliding surfaces or terminal ones defined solely as nonlinear combinations of tracking errors, the proposed surface in (6.15) explicitly incorporates the inertia matrix. This design exploits the physical structure of the mobile manipulator dynamics, allowing complete decoupling of the n-DoF interactions at the level of the computed control inputs. As a result, cross-coupling nonlinearities are not amplified, leading to reduced chattering.

The dynamics when $\dot{s} = 0$ are represented by the nonlinear differential equation:

$$M(x_1)\ddot{e} + \frac{dM(x_1)}{dt}\dot{e} + \frac{d\Gamma(e)}{dt} = 0 \tag{6.17}$$

This can be rewritten, incorporating the system dynamics and the control input τ, as:

$$f(x_1, x_2) + \tau - M(x_1)\dot{x}_{2d} + \frac{dM(x_1)}{dt}\dot{e} + \frac{d\Gamma(e)}{dt} = 0 \tag{6.18}$$

where the derivative of $\Gamma(e)$ is computed as:

$$\frac{d\Gamma(e)}{dt} = \gamma_1 \alpha_1 I \lfloor e \rfloor^{(\alpha_1-1)I} \dot{e} + \gamma_2 \alpha_2 I \lfloor e \rfloor^{(\alpha_2-1)I} \dot{e} + \gamma_3 \dot{e} \tag{6.19}$$

where $\lfloor e \rfloor^{(\alpha_1-1)I} = \text{diag}\left(|e_1|^{\alpha_1-1}, \cdots, |e_n|^{\alpha_1-1}\right)$ and $\lfloor e \rfloor^{(\alpha_2-1)I} = \text{diag}\left(|e_1|^{\alpha_2-1}, \cdots, |e_n|^{\alpha_2-1}\right)$. By choosing a Lyapunov definite-positive function $V_1 = 0.5e^T e$, such as its derivative is computed when $s = 0$ as follows:

$$\begin{aligned}
\dot{V}_1 =& e^T \dot{e} = -e^T M^{-1} \Gamma(e) \\
=& - e^T M^{-1} \left(\gamma_1 \text{sig}^{\alpha_1 I}(e) + \gamma_2 \, \text{sig}^{\alpha_2 I}(e) + \gamma_3 \, e \right) \\
\leq& - \underline{\lambda}\{\gamma_1\} \|M^{-1}\| (2V_1)^{\frac{\alpha_1+1}{2}} - \underline{\lambda}\{\gamma_2\} \|M^{-1}\| (2V_1)^{\frac{\alpha_2+1}{2}} \\
& - \underline{\lambda}\{\gamma_3\} \|M^{-1}\| (2V_1) \\
\leq& - \frac{\underline{\lambda}\{\gamma_1\}}{\underline{m}} 2^{\frac{\alpha_1+1}{2}} V_1^{\frac{\alpha_1+1}{2}} - \frac{\underline{\lambda}\{\gamma_2\}}{\underline{m}} 2^{\frac{\alpha_2+1}{2}} V_1^{\frac{\alpha_2+1}{2}} - \frac{2\underline{\lambda}\{\gamma_3\}}{\underline{m}} V_1 \leq 0
\end{aligned} \tag{6.20}$$

Hence, according to *Lemma 1*, the tracking error converges to zero in a fixed-time. Its maximum is given by:

$$\begin{aligned}
T_{s,max} =& T_{r,max} + \frac{\underline{m}}{\underline{\lambda}\{\gamma_3\}(1-\alpha_1)} \ln\left(1 + 2^{\frac{1-\alpha_1}{2}} \frac{\underline{\lambda}\{\gamma_3\}}{\underline{\lambda}\{\gamma_1\}}\right) \\
& + \frac{\underline{m}}{\underline{\lambda}\{\gamma_3\}(\alpha_2-1)} \ln\left(1 + 2^{\frac{1-\alpha_2}{2}} \frac{\underline{\lambda}\{\gamma_3\}}{\underline{\lambda}\{\gamma_2\}}\right)
\end{aligned} \tag{6.21}$$

where $T_{r,max}$ is the reaching time.

Subsequently, the overall control law, designed to satisfy fixed-time stability and to ensure robustness, is defined as:

$$\tau = \tau_0 + \tau_1 \tag{6.22}$$

$$\tau_0 = M(x_1)(\dot{x}_{2d} - \hat{x}_3) - \frac{dM(x_1)}{dt}\dot{e} - \frac{d\Gamma(e)}{dt} \tag{6.23}$$

$$\tau_1 = -K_1 \text{sig}^{\eta_1 I}(s) - K_2 \text{sig}^{\eta_2 I}(s) - K_3 s - K_4 \text{sign}(s) \tag{6.24}$$

where K_1, K_2, K_3, and K_4 are diagonal positive-definite matrices, $\text{sig}^{\eta_1 I}(s) = [|s_1|^{\eta_1}\text{sign}(s_1), \cdots, |s_n|^{\eta_1}\text{sign}(s_n)^T$ and $\text{sig}^{\eta_2 I}(s) = [|s_1|^{\eta_2}\text{sign}(s_1), \cdots, |s_n|^{\eta_2}\text{sign}(s_n)]^T$ with $0 < \eta_1 < 1$ and $\eta_2 > 1$.

For the stability analysis, let us first substitute the computed controller (6.22) into (6.17) to obtain the closed-loop system dynamics:

$$\dot{s} = M(x_1)\tilde{x}_3 - K_1\text{sig}^{\eta_1 I}(s) - K_2\text{sig}^{\eta_2 I}(s) - K_3 s - K_4\text{sign}(s) \tag{6.25}$$

Then, let us consider the following second Lyapunov function candidate and its first time derivative:

$$\begin{aligned} V_2 =& \frac{1}{2}s^T s \\ \dot{V}_2 =& s^T \dot{s} \end{aligned} \tag{6.26}$$

Using the obtained closed-loop system dynamics, $\dot{V}_2$ becomes:

$$\begin{aligned} \dot{V}_2 =& s^T \left(M\tilde{x}_3 - K_1\text{sig}^{\eta_1 I}(s) - K_2\text{sig}^{\eta_2 I}(s) - K_3 s - K_4\text{sign}(s) \right) \\ \leq& -\underline{\lambda}\{K_1\}(2V_2)^{\frac{\eta_1+1}{2}} - \underline{\lambda}\{K_2\}(2V_2)^{\frac{\eta_2+1}{2}} - 2\underline{\lambda}\{K_3\}V_2 \\ & - \left(\underline{\lambda}\{K_4\} - \|M(x_1)\|\|\tilde{x}_3\|\right)\|s\| \end{aligned} \tag{6.27}$$

According to the above inequality, it is verified that $\dot{V}_2$ is negative-definite if:

$$\underline{\lambda}\{K_4\} > \|M(x_1)\|\|\tilde{x}_3\| \geq \overline{m}\|\tilde{x}_3\| \tag{6.28}$$

Therefore, the following inequality is true while (6.28) is met:

$$\dot{V}_2 \leq -\underline{\lambda}\{K_1\}(2V_2)^{\frac{\eta_1+1}{2}} - \underline{\lambda}\{K_2\}(2V_2)^{\frac{\eta_2+1}{2}} - 2\underline{\lambda}\{K_3\}V_2 \tag{6.29}$$

Finally, using the result of *Lemma 1*, the proposed sliding surface (6.15) converges to zero in a fixed-time where its maximum is given by:

$$T_{r,max} = \frac{1}{\underline{\lambda}\{K_3\}(1-\eta_1)} \ln\left(1 + 2^{\frac{1-\eta_1}{2}} \frac{\underline{\lambda}\{K_3\}}{\underline{\lambda}\{K_1\}}\right) + \frac{1}{\underline{\lambda}\{K_3\}(\eta_2-1)} \ln\left(1 + 2^{\frac{1-\eta_2}{2}} \frac{\underline{\lambda}\{K_3\}}{\underline{\lambda}\{K_2\}}\right) \tag{6.30}$$

The architecture of the developed controller for the 5-DoF MM is shown in Figure 6.2.

6.4 EXPERIMENTS AND DISCUSSION

To validate the proposed technique, an experimental validation is conducted on custom-built 5-DoF MM named Mob-ETS. The real-time setup of the Mob-ETS consists of a control architecture integrating MATLAB/Simulink, wireless communication, and embedded control. The proposed control scheme was implemented in MATLAB/Simulink using MathWorks Real-Time Workshop (RTW), where the high-level trajectory generation and control algorithm were executed. The trajectories are transmitted from the host computer to the MM via a ZigBee wireless link. An ATmega32 microcontroller performed the low-level PD control using encoder feedback to generate PWM signals driving the motors. The manipulator's joints and wheels were actuated by HN-GH12-2217Y and Dynamixel MX-64T DC motors, respectively, with angular positions measured by E4P-100-079-DH-T-B encoders. The system includes current monitoring and power management to ensure stable operation, enabling real-time trajectory tracking and experimental validation of the proposed control algorithm. The considered MM integrates a mobile platform equipped with a 3-DoF serial manipulator. The physical parameters of the mobile platform and manipulator links are summarized in Tables 6.1 and 6.2, respectively.

Table 6.1 Mobile Platform Parameters

Parameter	**Symbol**	**Value**
Mass	m_v	2 kg
Wheel radius	r	0.05 m
Wheelbase	$2L$	0.27 m
Moment of inertia	I_v	1.22×10^{-5} kg $\cdot$ m^2

Table 6.2 Manipulator Link Parameters

Link	**Mass (kg)**	**Length (m)**	**Inertia** ($\mathrm{kg} \cdot \mathrm{m}^2$)
1	0.5	0.16	2.666×10^{-4}
2	0.5	0.20	1.16×10^{-4}
3	0.2	0.12	6.01×10^{-4}

Table 6.3 Control and Observer Parameters

Controller Gains	$\gamma_1 = 0.2, \gamma_2 = 0.4, \gamma_3 = 0.6,$ $\alpha_1 = 0.75, \alpha_2 = 1.55, \sigma_1 = 0.2,$ $\eta_1 = 0.55, \eta_2 = 1.75,$ $k_1 = \mathrm{diag}(5.5, 5.5, 5.5, 5.5, 5.5),$ $k_2 = \mathrm{diag}(0.55, 0.55, 0.55, 0.55, 0.55),$ $k_3 = \mathrm{diag}(25, 25, 25, 25, 25),$ $k_4 = \mathrm{diag}(5, 5, 5, 5, 5)$
Observer Parameters	$\zeta_1 = \xi_1 = 5, \zeta_2 = \xi_2 = 10, \zeta_3 = \xi_3 = 20,$ $\varepsilon_1 = 0.95, \varepsilon_2 = 0.9, \varepsilon_3 = 0.85,$ $\vartheta_1 = 1.05, \vartheta_2 = 1.1, \vartheta_3 = 1.15, K = 5$

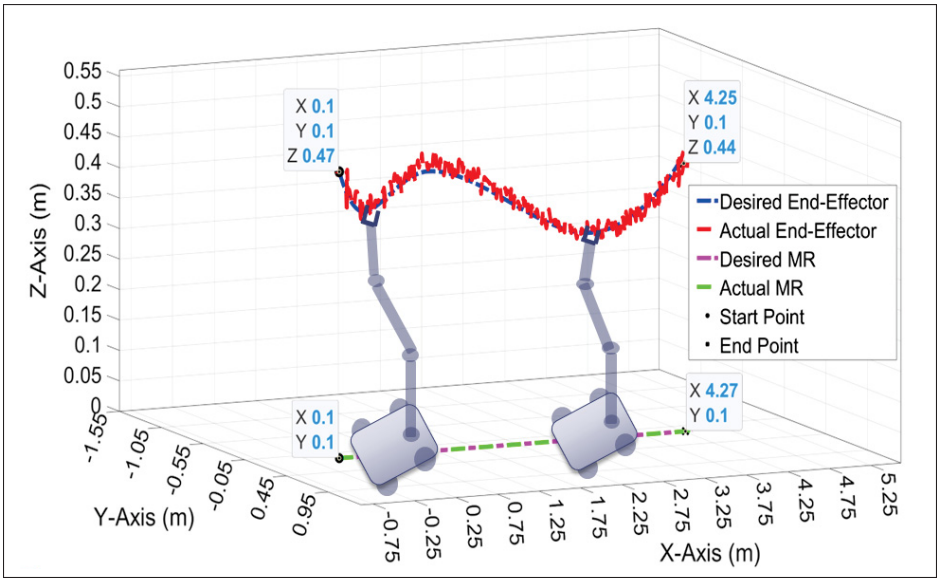

Figure 6.3 3D Desired Trajectory

The observer-controller gains were empirically tuned to achieve a trade-off between robustness, tracking accuracy, and convergence speed. The selected parameters are listed in Table 6.3.

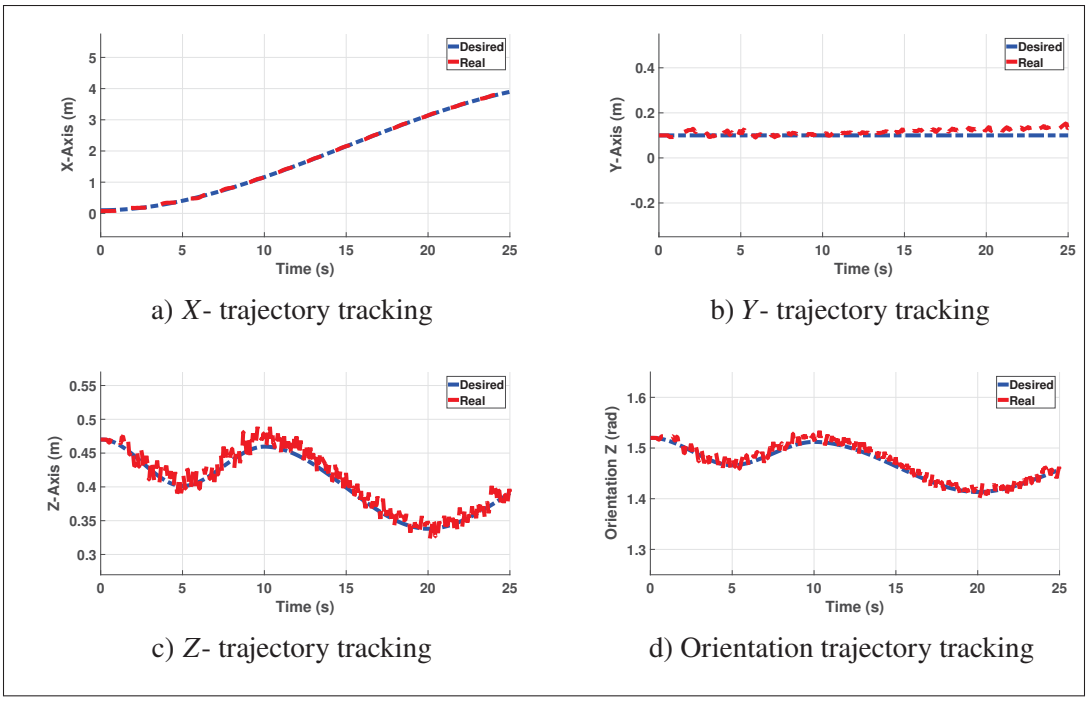

a) X- trajectory tracking

b) Y- trajectory tracking

c) Z- trajectory tracking

d) Orientation trajectory tracking

Figure 6.4 Trajectory tracking of the 5-DoF MM (X, Y, Z axis, and orientation) in Cartesian Space

The desired Cartesian trajectory was defined from the initial position $\mathbf{P}_s = [X_s, Y_s, Z_s] = [0.1, 0.1, 0.47]$ m to the final position $\mathbf{P}_f = [X_f, Y_f, Z_f] = [4.25, 0.1, 0.44]$ m, with the corresponding joint-space trajectories obtained via inverse kinematics.

Figure 6.3 depicts the three-dimensional evolution of the end effector together with the planar motion of the mobile platform. The close coincidence between desired and measured trajectories indicates that the proposed control law enforces coordinated motion of the coupled system despite the complete uncertainty in the nonlinear dynamics. This observation is further quantified in Figure 6.4, where the Cartesian position and orientation signals exhibit negligible steady state deviation and rapid transient decay, consistent with the analytically derived fixed-time convergence bounds.

The Cartesian tracking errors shown in Fig. 6.5 demonstrate uniform boundedness and fast attenuation without residual drift. From a systems perspective, this behavior reflects two key structural properties of the proposed design: first, the coupled sliding surface reshapes the closed-loop dynamics by embedding the configuration dependent mass matrix, thereby

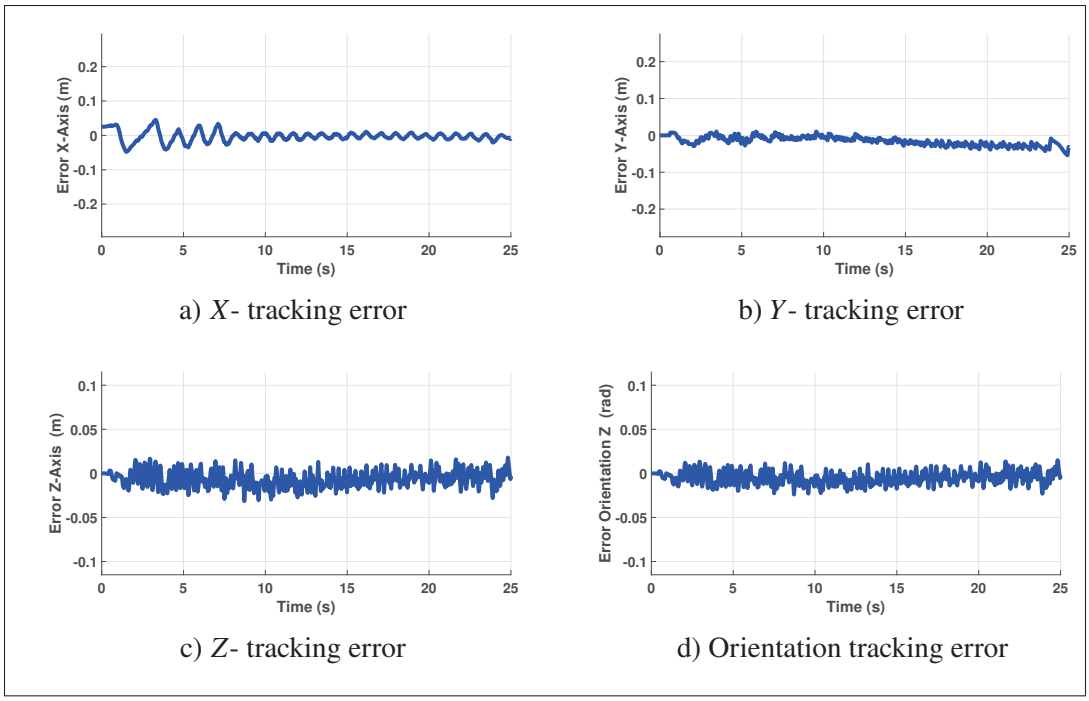

a) X- tracking error

b) Y- tracking error

c) Z- tracking error

d) Orientation tracking error

Figure 6.5 Tracking error of the 5-DoF MM (X, Y, Z axis, and orientation) in Cartesian Space

aligning the surface dynamics with the natural energy structure of the system; second, the fixed-time ESO compensates the nonlinear dynamics and disturbances in real-time, ensuring that the error dynamics satisfy the fixed-time stability conditions.

Figures 6.6 and 6.7 provide joint space validation across all five actuated degrees of freedom. Although transient errors may reach up to 1.2 rad during initial motion, all states converge within the theoretically predicted upper bound $T_{s,max} \cong 2.78$ sec seconds, with dominant joints settling significantly faster. The agreement between theoretical convergence guarantees and experimental settling times confirms that the fixed-time analysis accurately characterizes the practical closed-loop behavior. Importantly, the absence of amplified oscillations across coupled joints indicates that the structural decoupling mechanism effectively mitigates cross coupling propagation in the MM. The mobile platform tracking performance in Figs. 6.8 and 6.9 further demonstrates sub-centimeter translational accuracy and tightly bounded angular errors. Such precision under unknown nonlinear dynamics confirms that the proposed

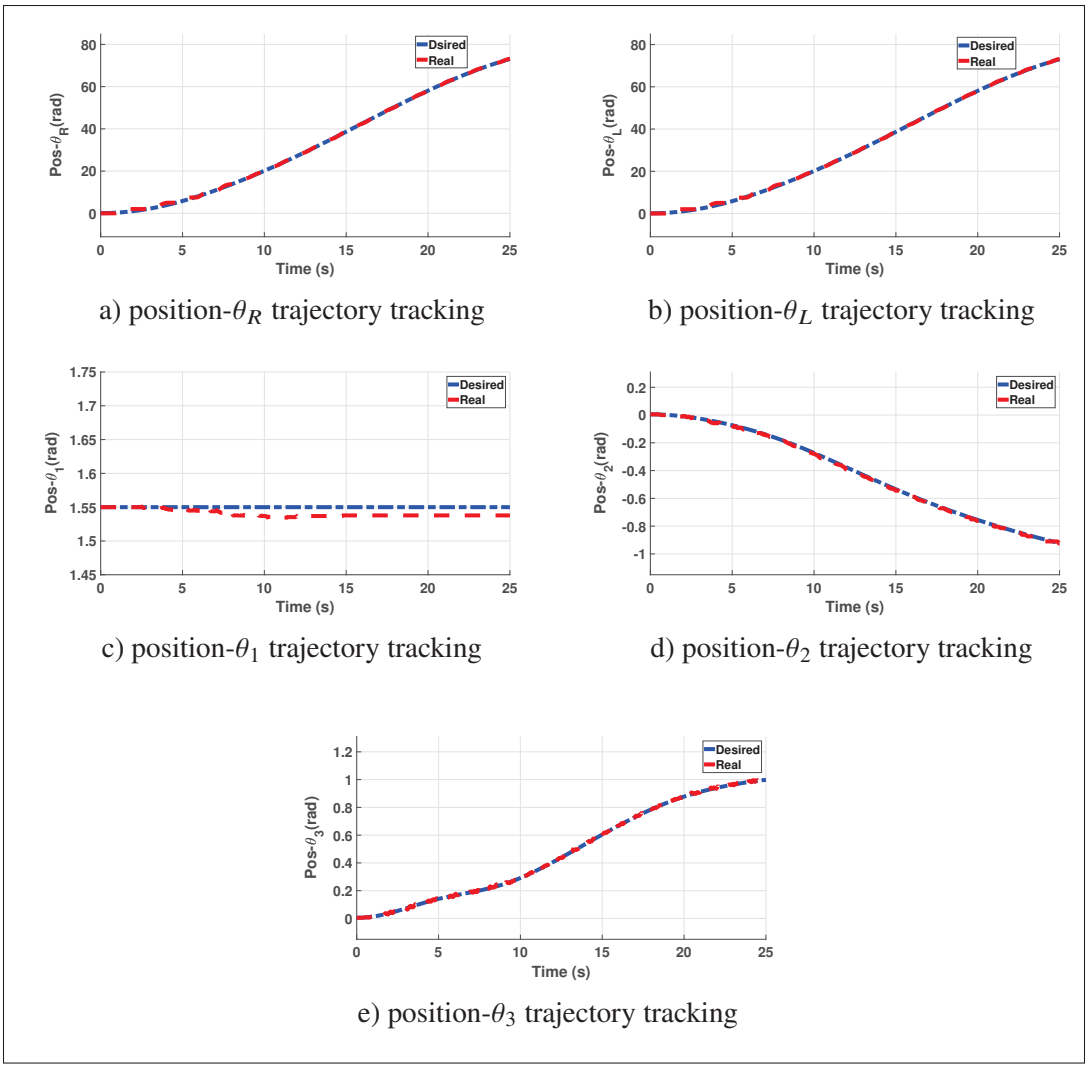

Figure 6.6 Trajectory tracking of the 5-DoF MM (θ_R, θ_L, θ_1, θ_2, and θ_3) in joint space

framework achieves disturbance rejection and stability without relying on explicit model knowledge.

Overall, the experimental results validate that incorporating the inertia matrix into the sliding surface modifies the geometric structure of the error dynamics, enabling fixed-time convergence independent of initial conditions while preserving robustness in strongly coupled nonlinear systems. The combination of structural decoupling and observer based disturbance estimation yields a closed-loop system that exhibits predictable transient performance,

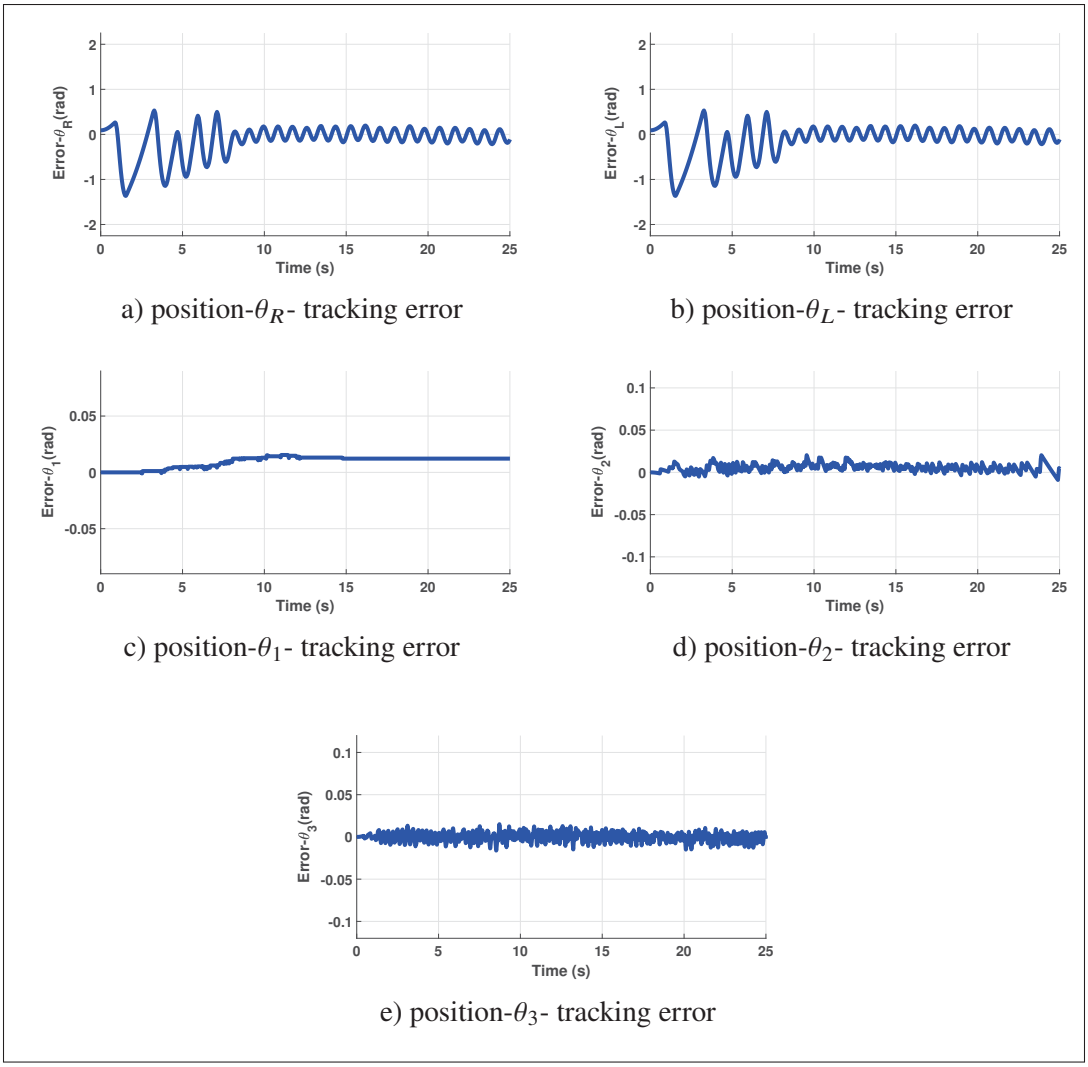

Figure 6.7 Tracking error of the 5-DoF MM (θ_R, θ_L, θ_1, θ_2, and θ_3) in joint space

bounded control effort, and high tracking accuracy, thereby providing a theoretically grounded and practically viable solution for nonlinear mobile manipulator control.

6.5 CONCLUSION

This work addressed the trajectory tracking problem of MMs operating under completely unknown nonlinear dynamics and external disturbances. The central takeaway is that a fixed-time convergence can be achieved in multi-DoF robotic systems without requiring an exact dynamic model. By embedding the inertia matrix into the sliding surface and

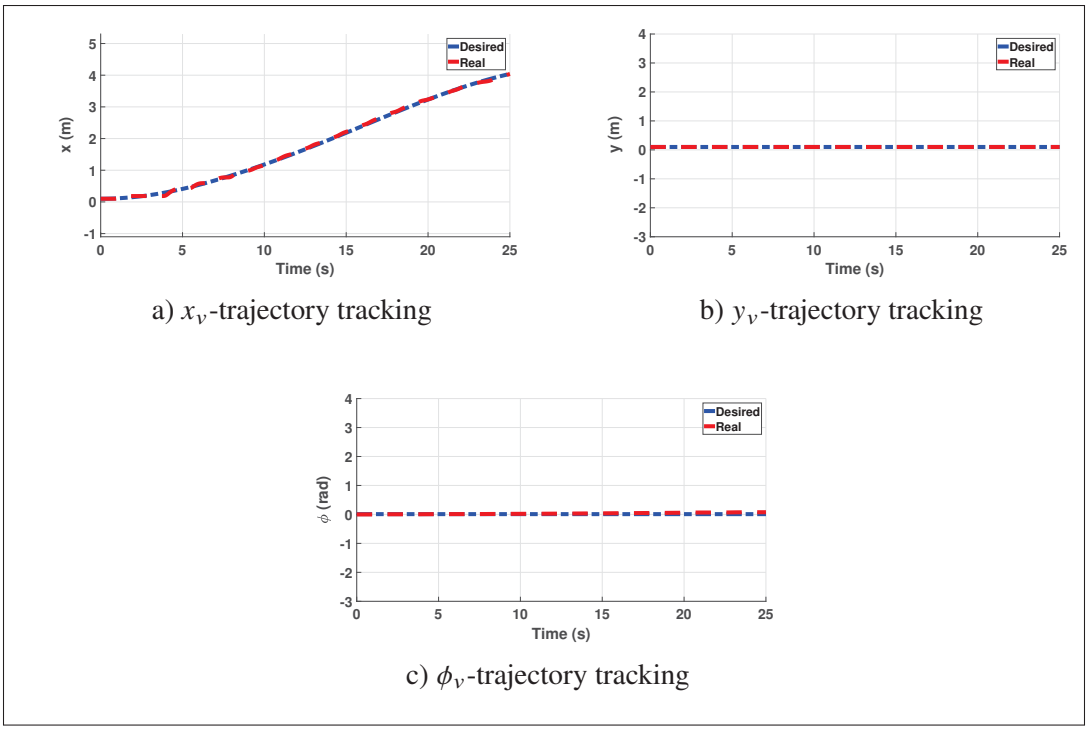

a) x_v-trajectory tracking

b) y_v-trajectory tracking

c) ϕ_v-trajectory tracking

Figure 6.8 Trajectory tracking of the linear/angular position of the MP in Joint space

integrating a fixed-time ESO, the proposed framework ensures control decoupling, dynamics and disturbance compensation, and convergence within a time bound independent of initial conditions. The experimental validation on a 5-DoF MM substantiated these theoretical claims. Convergence properties were ascertained by measuring Cartesian and joint space tracking errors and comparing their convergence times with the analytical ones. The results showed rapid error attenuation, bounded transients. High tracking accuracy was quantified through the small steady-state errors observed in both Cartesian coordinates and joint variables, while robustness was demonstrated by maintaining stability and precision despite treating the entire nonlinear dynamics as unknown and subject to disturbances. The key results collectively reveal an important relationship between surface design and convergence guarantees: incorporating the inertia matrix reshapes the closed-loop dynamics to mitigate cross coupling amplification, while the observer-based disturbance estimation enforces fixed-time stability conditions in practice. The consequence is a control architecture that

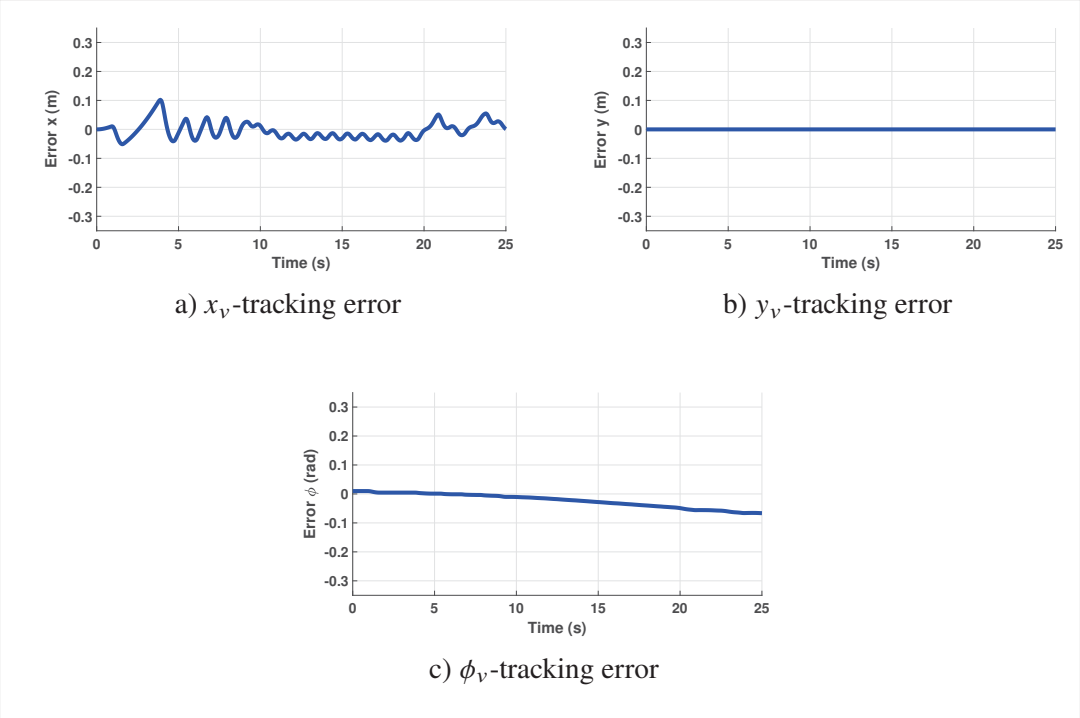

a) x_v-tracking error

b) y_v-tracking error

c) ϕ_v-tracking error

Figure 6.9 Tracking error of the linear/angular position of the MP in Joint space

combines predictable transient behavior, strong disturbance rejection, and high precision tracking in a nonlinear robotic system. The main message of this research is that fixed-time observer-based decoupled fixed-time sliding mode control can be made both theoretically rigorous and experimentally viable for real robotic platforms. This contribution advances the deployment of MMs in time critical and safety-critical applications where robustness, convergence predictability, and real-time implementation are essential. Future work will focus on reducing conservatism in fixed-time bounds and extending the framework to broader classes of nonlinear robotic systems.

CONCLUSION AND RECOMMENDATIONS

This doctoral thesis delivers a unified and robust observer–controller framework that provides a comprehensive solution to the challenging problem of high-precision trajectory tracking for mobile manipulators. The proposed framework successfully operates under conditions of significant model uncertainty, strong dynamic coupling, nonholonomic constraints, and external disturbances. The core philosophy of this work is to treat all sources of uncertainty as a single, lumped total disturbance, which is then estimated and actively compensated for in real-time.

The research culminated in a progressive series of three nonlinear control architectures, each building upon the last to achieve higher performance, robustness, and predictability. The investigation began with a Nonlinear Active Disturbance Rejection Controller (NADRC), advanced to a finite-time convergent Extended State Observer–based Non-Singular Fast Terminal Sliding Mode Controller (ESO-INF-TSMC), and concluded with the principal contribution: a Fixed-Time Terminal Sliding Mode Controller integrated with a Fixed-Time Extended State Observer (FTSMC-FESO). This final architecture represents a significant advancement by guaranteeing trajectory convergence within a predefined time, irrespective of initial conditions a key requirement for time-sensitive and predictable robotic applications. Rigorous experimental validation on the 5-DoF Mob-ÉTS mobile manipulator platform confirmed the superior tracking accuracy, enhanced disturbance rejection, and practical applicability of the proposed methods, thereby successfully achieving the research objectives.

Summary of Contributions

The primary contributions of this dissertation, corresponding to its manuscript-based chapters, are:

1. Nonlinear Active Disturbance Rejection Control (NADRC) for Mobile Manipulators: Development and experimental implementation of a NADRC scheme utilizing a Nonlinear Extended State Observer (NESO). This controller effectively estimates and compensates

for lumped disturbances. Its experimental validation confirmed superior performance compared to classical linear controllers, establishing a robust baseline for the subsequent advanced frameworks.

2. Finite-Time Convergent Control with Chattering Reduction: Advancement of the framework by integrating an Extended State Observer (ESO) with an Improved Non-Singular Fast Terminal Sliding Mode Controller (ESO-INF-TSMC). This synergistic design leverages the ESO's disturbance estimate to significantly reduce the reliance on high-gain discontinuous control, thereby mitigating the chattering phenomenon inherent to traditional SMC. The controller successfully achieved finite-time convergence, demonstrating faster transient response and higher steady-state accuracy than the baseline NADRC.
3. Fixed-Time Decoupled Control for Predictable Performance: The thesis's principal contribution: the development of the FTSMC-FESO framework. This architecture provides a formal guarantee of fixed-time stability, ensuring tracking errors converge to zero within a predefined time bound that is independent of initial conditions. A key innovation was a novel decoupled sliding surface incorporating the inertia matrix, which simplified the control law. The experimental validation of this fixed-time observer–controller pair on a real-world platform is a significant step toward highly reliable, predictable, and safety-critical robotic systems.
4. Rigorous Experimental Validation: An overarching contribution is the comprehensive experimental verification of these advanced nonlinear control theories on the 5-DoF Mob-ÉTS mobile manipulator. By successfully translating complex theoretical constructs into deployable, real-world software, this research demonstrates the practical viability of these advanced theoretical constructs in a real-world setting, bridging a critical gap between nonlinear control theory and applied robotics.

Recommendations for Future Work

The research presented in this thesis establishes a robust foundation for the control of mobile manipulators and opens several promising avenues for future investigation. The following recommendations are proposed to extend and build upon this work:

- Adaptive Observer and Control Design: The fixed-gain observers developed herein performed exceptionally well but required manual tuning. A significant avenue for future work is the development of an adaptive fixed-time extended state observer (A-FESO). Such a system, where observer gains are tuned online via an adaptive law, would enhance the system's autonomy and resilience to unforeseen or rapidly changing disturbance characteristics without manual intervention.
- Multi-Robot Cooperative Control: This work focused on a single mobile manipulator. A natural and challenging extension is to apply these fixed-time control concepts to multi-robot systems for cooperative manipulation and transportation. This would necessitate designing distributed fixed-time controllers and observers that enable a team of robots to cooperatively transport a common object, guaranteeing the entire multi-agent system achieves predictable, fixed-time convergence.
- Integration of Vision-Based Guidance: This research assumed a predefined desired trajectory. A crucial next step for practical autonomy is the integration of the proposed robust controllers with a vision-based perception and guidance system. This would empower the mobile manipulator to operate autonomously in unstructured environments by generating its own trajectories in real-time, for example, to interact with dynamic objects or navigate obstacles. The FTSMC-FESO framework would then serve as the robust execution layer, ensuring these dynamically generated paths are followed with high fidelity.
- Robustness to Imperfect Information: The current framework assumes reliable state information and, in the context of possible multi-robot extensions, communication links.

Future work could investigate the framework's resilience to more realistic conditions, such as communication delays and packet loss in the multi-robot scenario, or noisy and intermittent data from vision sensors. Developing event-triggered or predictive control mechanisms based on the FTSMC-FESO core could be a powerful approach to maintain stability and performance under such imperfect information.

LIST OF REFERENCES

Abdallah, M., Kali, Y., Saad, M., Fareh, R. & Bettayeb, M. (2025). Wearable exoskeleton robot control using radial basis function-based fixed-time terminal sliding mode with prescribed performance. *Asian Journal of Control*, 1–17.

Aguilar-Ibañez, C., Sira-Ramirez, H. & Suarez-Castanon, M. S. (2017). Stability of active disturbance rejection control for uncertain systems: A Lyapunov perspective. *International Journal of Robust and Nonlinear Control*, 27(18), 4541–4553. doi: 10.1002/rnc.3812.

Ahi, B. & Haeri, M. (2018). Linear active disturbance rejection control from the practical aspects. *IEEE/ASME Transactions on Mechatronics*, 23(6), 2907–2917.

Algrnaodi, M., Saad, M., Saad, M., Fareh, R. & Brahmi, A. (2021). Trajectory tracking for mobile manipulator based on nonlinear active disturbance rejection control. *International Journal of Modelling, Identification and Control*, 37(2), 95–105.

Algrnaodi, M., Saad, M., Saad, M., Fareh, R. & Kali, Y. (2024). Extended state observer-based improved non-singular fast terminal sliding mode for mobile manipulators. *Transactions of the Institute of Measurement and Control*, 46(4), 785–798.

Alnufaie, L. (2023). Nonsingular fast terminal sliding mode controller for a robotic system: A fuzzy approach. *IEEE Access*, 11, 75522–75527.

Andaluz, V., Roberti, F., Toibero, J. M. & Carelli, R. (2012). Adaptive unified motion control of mobile manipulators. *Control Engineering Practice*, 20(12), 1337–1352.

Åström, K. J. & Hägglund, T. (1995). *PID Controllers: Theory, Design, and Tuning*. Instrument Society of America.

Basin, M., Yu, P. & Shtessel, Y. (2017). Finite-and fixed-time differentiators utilising HOSM techniques. *IET Control Theory & Applications*, 11(8), 1144–1152.

Basin, M. V., Ramírez, P. C. R. & Guerra-Avellaneda, F. (2018). Continuous fixed-time controller design for mechatronic systems with incomplete measurements. *IEEE/ASME Transactions on Mechatronics*, 23(1), 57–67.

Bhat, S. P. & Bernstein, D. S. (2000). Finite-time stability of continuous autonomous systems. *SIAM Journal on Control and Optimization*, 38(3), 751–766.

Boukattaya, M., Mezghani, N. & Damak, T. (2018). Adaptive nonsingular fast terminal sliding-mode control for the tracking problem of uncertain dynamical systems. *ISA Transactions*, 77, 1–19.

Brahmi, A., Saad, M., Gauthier, G., Brahmi, B., Zhu, W.-H. & Ghommam, J. (2016). Adaptive backstepping control of mobile manipulator robot based on virtual decomposition approach. *2016 8th International Conference on Modelling, Identification and Control (ICMIC)*, pp. 707–712. doi: 10.1109/ICMIC.2016.7804203.

Brahmi, A., Saad, M., Gauthier, G., Zhu, W.-H. & Ghommam, J. (2019). Adaptive backstepping control of multi-mobile manipulators handling a rigid object in coordination. *International Journal of Modelling, Identification and Control*, 31(2), 169–181.

Castañeda, L. A., Luviano-Juárez, A. & Chairez, I. (2014). Robust trajectory tracking of a delta robot through adaptive active disturbance rejection control. *IEEE Transactions on Control Systems Technology*, 23(4), 1387–1398.

Chen, C., Li, L., Peng, H., Yang, Y., Mi, L. & Zhao, H. (2020). A new fixed-time stability theorem and its application to the fixed-time synchronization of neural networks. *Neural Networks*, 123, 412–419.

Chen, N., Song, F., Li, G., Sun, X. & Ai, C. (2013). An adaptive sliding mode backstepping control for the mobile manipulator with nonholonomic constraints. *Communications in Nonlinear Science and Numerical Simulation*, 18(10), 2885–2899.

Chen, S. Y. & Lin, F. J. (2010). Robust nonsingular terminal sliding-mode control for nonlinear magnetic bearing system. *IEEE Transactions on Control Systems Technology*, 19(3), 636–643.

Chen, W., Tao, D. & Tang, B. (2024). A new reaching law based nonsingular terminal sliding mode control scheme for the servo system with periodic uncertainties. *IEEE Access*, 12, 64461–64472.

Choi, J., Baek, J., Lee, W., Lee, Y. S. & Han, S. (2020). Adaptive model-free control with nonsingular terminal sliding-mode for application to robot manipulators. *IEEE Access*, 8, 159177–159189.

Chung, J.-H. & Velinsky, S. A. (1998). Modeling and control of a mobile manipulator. *Robotica*, 16(6), 607–613.

Cui, L., Jin, N., Chang, S., Zuo, Z. & Zhao, Z. (2022). Fixed-time eso based fixed-time integral terminal sliding mode controller design for a missile. *ISA Transactions*, 125, 237–251.

Dong, W. (2002). On trajectory and force tracking control of constrained mobile manipulators with parameter uncertainty. *Automatica*, 38(9), 1475–1484.

Dorel, L. & Levant, A. (2008). On chattering-free sliding-mode control. *2008 47th IEEE Conference on Decision and Control*, pp. 2196–2201.

Drakunov, S. V. & Utkin, V. I. (1992). Sliding mode control in dynamic systems. *International Journal of Control*, 55(4), 1029–1037.

Duong, A. T., Pham, T. L., Giap, V. N. & Vu, P. (2023). Disturbance observer based on fixed time sliding mode control and optimal state observer for three-phase three-level t-type inverters. *IEEE Access*, 11, 62091–62108.

Fallaha, C., Saad, M., Ghommam, J. & Kali, Y. (2021). Sliding mode control with model-based switching functions applied on a 7-dof exoskeleton arm. *IEEE/ASME Transactions on Mechatronics*, 26(1), 539–550.

Fareh, R., Brahmi, A., Saad, M., Saad, M. & Bettayeb, M. (2017). Tracking control for non-holonomic mobile manipulator using decentralised control strategy. *International Journal of Modelling, Identification and Control*, 28(1), 58–69.

Fareh, R., Al-Shabi, M., Bettayeb, M. & Ghommam, J. (2019). Robust active disturbance rejection control for flexible link manipulator. *Robotica*, 1–18.

Fareh, R., Khadraoui, S., Abdallah, M. Y., Baziyad, M. & Bettayeb, M. (2021). Active disturbance rejection control for robotic systems: A review. *Mechatronics*, 80, 102671. doi: 10.1016/j.mechatronics.2021.102671.

Farhat, M., Kali, Y., Saad, M., Rahman, M. H. & Lopez-Herrejon, R. E. (2025). New fixed-time observer-based model-free fixed-time sliding mode of joint angle commanded NAO humanoid robot. *IEEE Transactions on Control Systems Technology*, 33(1), 304–315.

Feng, Y., Yu, X. & Man, Z. (2002). Non-singular terminal sliding mode control of rigid manipulators. *Automatica*, 38(12), 2159–2167.

Fu, H., Li, Y., Wang, Y. & Zhang, Z. (2018). Omnidirectional mobile robot active disturbance rejection control. *2018 IEEE International Conference on Mechatronics and Automation (ICMA)*, pp. 227–232.

Gao, Z. (2006a). Active disturbance rejection control: a paradigm shift in feedback control system design. *2006 American Control Conference*, pp. 7–pp.

Gao, Z. (2006b). Scaling and bandwidth-parameterization based controller tuning. *Proceedings of the 2006 American Control Conference*, pp. 4989–4996.

Gao, Z., Hu, S. & Jiang, F. (2001). A novel motion control design approach based on active disturbance rejection. *Proceedings of the 40th IEEE Conference on Decision and Control*, 5, 4877–4882.

Geng, J., Sheng, Y. & Liu, X. (2014). Time-varying nonsingular terminal sliding mode control for robot manipulators. *Journal of Intelligent & Robotic Systems*, 74(3-4), 863–877.

Gu, J.-J. & Wang, J.-M. (2018). Sliding mode control of the Orr-Sommerfeld equation cascaded by both the Squire equation and ODE in the presence of boundary disturbances. *Journal of the Franklin Institute*, 355(17), 8791–8816.

Gu, J.-J. & Wang, J.-M. (2019). Sliding mode control for N-coupled reaction-diffusion PDEs with boundary input disturbances. *IEEE Transactions on Automatic Control*, 64(12), 5154–5161.

Guo, B.-Z. & Zhao, Z.-L. (2016). *Active Disturbance Rejection Control for Nonlinear Systems: An Introduction*. John Wiley & Sons.

Han, J. (2009). From PID to active disturbance rejection control. *IEEE Transactions on Industrial Electronics*, 56(3), 900–906.

Henein, M., Aboul-Seoud, A. & El-Metwally, S. (2022). A Holistic Approach to Reactive Mobile Manipulator Control for Non-Holonomic Constraints. *IEEE Access*, 10, 12345–12356.

Hernandez, J. H., Cruz, S. S., López-Gutiérrez, R. et al. (2020). Robust non-singular fast terminal sliding-mode control for sit-to-stand task using a mobile lower limb exoskeleton. *IEEE Access*, 8, 213630–213643.

Hu, G., Xu, D., Hua, W., Jiang, B., Shi, P. & Rudas, I. J. (2025). Fixed-time cooperative sliding mode control for synchronization of multilinear motor systems. *IEEE/ASME Transactions on Mechatronics*, 1–12. Early Access.

Huang, Y., Ma, H., He, Q. et al. (2022). Robust and compliance control for robotic knee prosthesis using admittance model and sliding-mode controller. *IEEE Transactions on Industrial Electronics*, 69(12), 13225–13236.

Huang, Y. (1999). A new synthesis method for uncertain systems the self-stable region approach. *International Journal of Systems Science*, 30(1), 33–38.

Huang, Y. & Han, J. (2000). Analysis and design for the second order nonlinear continuous extended states observer. *Chinese Science Bulletin*, 45(21), 1938.

Huang, Y. & Xue, W. (2014). Active disturbance rejection control: methodology and theoretical analysis. *ISA Transactions*, 53(4), 963–976.

Jin, M., Lee, J., Chang, P. H. et al. (2009). Practical nonsingular terminal sliding-mode control of robot manipulators for high-accuracy tracking control. *IEEE Transactions on Industrial Electronics*, 56(9), 3485–3492.

Jiuhong, R., Xuewen, R. & Sanyou, W. (2007). Study on ADRC controller design and simulation of rock drill robot joint hydraulic drive system. *2007 Chinese Control Conference*, pp. 133–136.

Kali, Y., Saad, M. & Benjelloun, K. (2025). Chattering reduction via prescribed performance controller-based sliding mode for robotic systems. *2025 33rd Mediterranean Conference on Control and Automation (MED)*, pp. 619–623.

Khan, A. H., Li, S. & Chen, D. (2020). Tracking control of redundant mobile manipulator: An RNN based metaheuristic approach. *Neurocomputing*, 400, 272–284.

Khawwaf, J., Zheng, J., Lu, R. et al. (2017). Robust tracking control of an IPMC actuator using nonsingular terminal sliding mode. *IEEE Transactions on Control Systems Technology*, 25(5), 1875–1882.

Kim, Y.-G., Ahn, H.-S., Hu, M.-H. & You, K.-H. (2023). Improved non-singular fast terminal sliding mode control for SPMSM speed regulation. *IEEE Access*, 11, 65924–65933.

Klancar, G., Zdesar, A., Blazic, S. & Skrjanc, I. (2025). *Wheeled Mobile Robots: Control and Implementation*. Elsevier.

Labbadi, M. & Cherkaoui, M. (2020). Robust adaptive nonsingular fast terminal sliding-mode tracking control for an uncertain quadrotor UAV subjected to disturbances. *ISA Transactions*, 99, 290–304.

Lala, T. (2025). Safe switching model-free value iteration for general nonlinear systems. *IEEE Access*, 13, 132170–132193.

Levant, A. (2010). Chattering analysis. *IEEE Transactions on Automatic Control*, 55(6), 1380–1389.

Li, B., Yang, H. & Su, Y. (2016). Trajectory-Tracking Control of Mobile Robot Systems Incorporating Neural-Dynamic Optimized Model Predictive Approach. *IEEE Transactions on Industrial Electronics*, 63(11), 6913–6923.

Li, J., Xia, Y., Qi, X. & Wan, H. (2018). On convergence of the discrete-time nonlinear extended state observer. *Journal of the Franklin Institute*, 355(1), 501–519.

Li, Z. & Ge, S. S. (2013). *Fundamentals in modeling and control of mobile manipulators*. crc press.

Li, Z., Ge, S. S. & Ming, A. (2007). Adaptive robust motion/force control of holonomic-constrained nonholonomic mobile manipulators. *IEEE Transactions on Systems, Man, and Cybernetics, Part B (Cybernetics)*, 37(3), 607–616.

Li, Z., Ge, S. S. & Wang, Z. (2008). Robust adaptive control of coordinated multiple mobile manipulators. *Mechatronics*, 18(5-6), 239–250.

Liang, H., Yu, J. & Li, H. (2025). Singularity-free practical fixed-time fault-tolerant control of underwater unmanned vehicles with input and output constraints. *IEEE Transactions on Vehicular Technology*, 1–14. Early Access.

Liang, Y. (2025). Robot trajectory tracking control based on neural networks and sliding mode control. *IEEE Access*, 13, 96740–96757.

Liu, J., Sun, Y., Liu, Z., Gao, Y., Wu, L., Leon, J. I. & Franquelo, L. G. (2025a). Predefined-time reliable control for robotic systems with prescribed performance. *IEEE Transactions on Industrial Electronics*, 1–9. Early Access.

Liu, W., Chen, S. & Huang, H.-x. (2019). Adaptive nonsingular fast terminal sliding mode control for permanent magnet synchronous motor based on disturbance observer. *IEEE Access*, 7, 153791–153798.

Liu, Y., Hu, T., Guan, X., Wang, Y., Zhang, B., Wang, Y. & Li, G. (2025b). Adaptive mpc-based multi-terrain trajectory tracking framework for mobile spherical robots. *IEEE/ASME Transactions on Mechatronics*, 1–13. Early Access.

Liu, Z., Zhang, O., Gao, Y., Zhao, Y., Sun, Y. & Liu, J. (2023). Adaptive neural network-based fixed-time control for trajectory tracking of robotic systems. *IEEE Transactions on Circuits and Systems II: Express Briefs*, 70(1), 241–245.

Lu, N., Ma, L. & Hua, X. (2022). Nonsingular fast terminal sliding mode control based on neural network with adaptive robust term for robotic manipulators with actuators. *IET Control Theory & Applications*, 16(5), 567–578.

Madani, T., Daachi, B. & Djouani, K. (2016a). Non-singular terminal sliding mode controller: Application to an actuated exoskeleton. *Mechatronics*, 33, 136–145.

Madani, T., Daachi, B. & Djouani, K. (2016b). Modular-controller-design-based fast terminal sliding mode for articulated exoskeleton systems. *IEEE Transactions on Control Systems Technology*, 25(3), 1133–1140.

Mobayen, S. & Javadi, S. (2017). Disturbance observer and finite-time tracker design of disturbed third-order nonholonomic systems using terminal sliding mode. *IEEE Transactions on Industrial Electronics*, 64(3), 2408–2415.

Önen, A. (2023). Model-free controller design for nonlinear underactuated systems with uncertainties and disturbances by using extended state observer based chattering-free sliding mode control. *IEEE Access*, 11, 2875–2885.

Peng, J., Yu, J. & Wang, J. (2014). Robust adaptive tracking control for nonholonomic mobile manipulator with uncertainties. *ISA Transactions*, 53(4), 1035–1043.

Polyakov, A. (2011). Nonlinear feedback design for fixed-time stabilization of linear control systems. *IEEE transactions on Automatic Control*, 57(8), 2106–2110.

Pu, Z., Yuan, R., Yi, J. & Tan, X. (2015). A class of adaptive extended state observers for nonlinear disturbed systems. *IEEE Transactions on Industrial Electronics*, 62(9), 5858–5869.

Qi, X., Li, J., Xia, Y. & Gao, Z. (2017). On the robust stability of active disturbance rejection control for SISO systems. *Circuits, Systems, and Signal Processing*, 36(1), 65–81.

Radke, A. & Gao, Z. (2006). A survey of state and disturbance observers for practitioners. *2006 American Control Conference*, pp. 5183–5188.

Rauf, A., Zhao, Z., Khan, A. et al. (2022). Finite-time robust control of robotic manipulator with input deadzone and time-varying disturbance compensation. *IEEE Access*, 10, 13727–13738.

Ren, C., Zhang, M., Ma, S. & Wei, D. (2018). Trajectory tracking control of an omnidirectional mobile manipulator based on active disturbance rejection control. *2018 13th World Congress on Intelligent Control and Automation (WCICA)*, pp. 1537–1542.

Savino, H. J., Pimenta, L. C., Shah, J. A. & Adorno, B. V. (2020). Pose consensus based on dual quaternion algebra with application to decentralized formation control of mobile manipulators. *Journal of the Franklin Institute*, 357(1), 142–178.

Sebastian, B. & Ben-Tzvi, P. (2019). Active disturbance rejection control for handling slip in tracked vehicle locomotion. *Journal of Mechanisms and Robotics*, 11(2).

Shtessel, Y. B., Edwards, C., Fridman, L. M. & Levant, A. (2014). *Sliding Mode Control and Observation*. Springer.

Slotine, J.-J. E. & Li, W. (1991). *Applied Nonlinear Control*. Prentice Hall.

Song, R., Li, Y., Yu, W., Wang, F. & Ruan, J. (2008). Study on adre based lateral control for tracked mobile robots on stairs. *2008 IEEE International Conference on Automation and Logistics*, pp. 2048–2052.

Song, S., Tang, C., Wang, Z. & Yan, G. (2018). Active disturbance rejection controller design for stable walking of a compass-like biped. *Transactions of the Institute of Measurement and Control*, 40(14), 4063–4077.

Souzanchi-K, M., Arab, A., Akbarzadeh-T, M. R. & Fateh, M. M. (2017). Robust impedance control of uncertain mobile manipulators using time-delay compensation. *IEEE Transactions on Control Systems Technology*, 26(6), 1942–1953. Published online 2017, print version 2018.

Su, Y., Li, B. & Yang, H. (2025). Finite Time Model Predictive Control for Mobile Manipulators With Flating-Base. *IEEE Transactions on Industrial Informatics*.

Su, Y.-X., Sun, D., Ren, L. & Mills, J. K. (2006). Integration of saturated PI synchronous control and PD feedback for control of parallel manipulators. *IEEE Transactions on Robotics*, 22(1), 202–207.

Sun, L. & Liu, Y. (2020). Extended state observer augmented finite-time trajectory tracking control of uncertain mechanical systems. *Mechanical Systems and Signal Processing*, 135, 106370.

Sun, Y., Gao, Y., Zhao, Y., Liu, Z., Wang, J., Kuang, J., Yan, F. & Liu, J. (2022). Neural network-based tracking control of uncertain robotic systems: Predefined-time nonsingular terminal sliding-mode approach. *IEEE Transactions on Industrial Electronics*, 69(10), 10510–10520.

Taghavifar, H. & Rakheja, S. (2019). A novel terramechanics-based path-tracking control of terrain-based wheeled robot vehicle with matched-mismatched uncertainties. *IEEE Transactions on Control Systems Technology*, 28(4), 1421–1430.

Talole, S. E., Kolhe, J. P. & Phadke, S. B. (2009). Extended-state-observer-based control of flexible-joint system with experimental validation. *IEEE Transactions on Industrial Electronics*, 57(4), 1411–1419.

Utkin, V. I. (1977). Variable structure systems with sliding modes. *IEEE Transactions on Automatic Control*, 22(2), 212–222.

Van, M., Ge, S. S. & Ren, H. (2016). Finite time fault tolerant control for robot manipulators using time delay estimation and continuous nonsingular fast terminal sliding mode control. *IEEE Transactions on Cybernetics*, 47(7), 1681–1693.

Vo, A. T. & Kang, H.-J. (2019). An adaptive terminal sliding mode control for robot manipulators with non-singular terminal sliding surface variables. *IEEE Access*, 7, 8701–8712.

Walsh, G. C., Tilbury, D. M., Sastry, S. S., Murray, R. M. & Laumond, J.-P. (1994). Stabilization of trajectories for systems with nonholonomic constraints. *IEEE Transactions on Automatic Control*, 39(1), 216–222.

Wang, H., Li, S., Lan, Q. et al. (2017). Continuous terminal sliding mode control with extended state observer for PMSM speed regulation system. *IEEE Transactions on Industrial Electronics*, 64(4), 3128–3136.

Wang, L., Du, H., Zhang, W., Wu, D. & Zhu, W. (2020a). Implementation of integral fixed-time sliding mode controller for speed regulation of PMSM servo system. *Nonlinear Dynamics*, 102(1), 185–196.

Wang, Z., Su, Y. & Zhang, L. (2020b). Fixed-time fault-tolerant attitude tracking control for rigid spacecraft. *ISA Transactions*, 98, 186–196.

Wei, D., Ren, C., Zhang, M., Li, X., Ma, S. & Mu, C. (2017). Position/force control of a holonomic-constrained mobile manipulator based on active disturbance rejection control. *IECON 2017-43rd Annual Conference of the IEEE Industrial Electronics Society*, pp. 6751–6756.

Wu, D. & Chen, K. (2012). Frequency-domain analysis of nonlinear active disturbance rejection control via the describing function method. *IEEE Transactions on Industrial Electronics*, 60(9), 3906–3914.

Wu, D. & Chen, K. (2014). Limit cycle analysis of active disturbance rejection control system with two nonlinearities. *ISA Transactions*, 53(4), 947–954.

Wu, Y., Yu, X. & Man, Z. (1998). Terminal sliding mode control design for uncertain dynamic systems. *Systems & Control Letters*, 34(5), 281–286.

Wu, Y., Wang, L., Zhang, J. et al. (2019). Path following control of autonomous ground vehicle based on nonsingular terminal sliding mode and active disturbance rejection control. *IEEE Transactions on Vehicular Technology*, 68(7), 6379–6390.

Xian, J., Shen, L., Chen, J. & Feng, W. (2022). Continuous sliding mode control of robotic manipulators based on time-varying disturbance estimation and compensation. *IEEE Access*, 10, 43473–43480.

Xing, H. L., Jeon, J. H., Park, K. C. & Oh, I. K. (2011). Active disturbance rejection control for precise position tracking of ionic polymer-metal composite actuators. *IEEE/ASME Transactions on Mechatronics*, 18(1), 86–95.

Xing, L., Li, B. & Yang, H. (2025). Trajectory Tracking Control of Wheeled Mobile Manipulators With Joint Flexibility via Virtual Decomposition Approach. *IEEE Transactions on Systems, Man, and Cybernetics: Systems*.

Xu, W., Junejo, A. K., Liu, Y. et al. (2019a). Improved continuous fast terminal sliding mode control with extended state observer for speed regulation of PMSM drive system. *IEEE Transactions on Industrial Electronics*, 66(11), 8849–8859.

Xu, X., Zhang, C. & Hu, H. (2019b). Research on reconfigurable control for a hovering PVTOL aircraft. *International Journal of Modelling, Identification and Control*, 32(3-4), 232–237.

Xue, W., Madonski, R., Lakomy, K., Gao, Z. & Huang, Y. (2017). Add-on module of active disturbance rejection for set-point tracking of motion control systems. *IEEE Transactions on Industry Applications*, 53(4), 4028–4040.

Yamamoto, Y. & Yun, X. (1994). Modeling and compensation of the dynamic interaction of a mobile manipulator. *Proceedings of the 1994 IEEE International Conference on Robotics and Automation*, pp. 2187–2192.

Yamamoto, Y. & Yun, X. (1996). Effect of the dynamic interaction on coordinated control of mobile manipulators. *IEEE Transactions on Robotics and Automation*, 12(5), 816–824.

Yang, J., Li, S., Su, J. et al. (2013). Continuous nonsingular terminal sliding mode control for systems with mismatched disturbances. *Automatica*, 49(7), 2287–2291.

Yang, J., Li, S. & Yu, X. (2012). Sliding-mode control for systems with mismatched uncertainties via a disturbance observer. *IEEE Transactions on Industrial Electronics*, 60(1), 160–169.

Yang, L. & Yang, J. (2011). Nonsingular fast terminal sliding-mode control for nonlinear dynamical systems. *International Journal of Robust and Nonlinear Control*, 21(16), 1865–1879.

Young, K. D., Utkin, V. I. & Ozguner, U. (1999). A control engineer's guide to sliding mode control. *IEEE Transactions on Control Systems Technology*, 7(3), 328–342.

Yu, Q. & Chen, I.-M. (2002). A general approach to the dynamics of nonholonomic mobile manipulator systems. *Journal of Dynamic Systems, Measurement, and Control*, 124(4), 512–521.

Yu, S., Yu, X., Shirinzadeh, B. & Man, Z. (2005). Continuous finite-time control for robotic manipulators with terminal sliding mode. *Automatica*, 41(11), 1957–1964.

Zhang, D., Hu, J., Cheng, J., Wu, Z.-G. & Yan, H. (2024). A novel disturbance observer based fixed-time sliding mode control for robotic manipulators with global fast convergence. *IEEE/CAA Journal of Automatica Sinica*, 11(3), 661–672.

Zhang, H., Zhao, H., Miao, Y., Li, Q. & Zhou, B. (2025). Super-twisting sliding mode- and iterative learning-based synchronization control for 2r1t parallel robots. *IEEE/ASME Transactions on Mechatronics*, 1–12. Early Access.

Zhang, L., Wei, C., Wu, R. & Cui, N. (2018). Fixed-time extended state observer based non-singular fast terminal sliding mode control for a VTVL reusable launch vehicle. *Aerospace Science and Technology*, 82, 70–79.

Zhang, L., Wang, Y., Hou, Y. & Li, H. (2019). Fixed-time sliding mode control for uncertain robot manipulators. *IEEE Access*, 7, 149750–149763.

Zhang, Y., Chen, Z. & Sun, M. (2020). Trajectory tracking control for a quadrotor unmanned aerial vehicle based on dynamic surface active disturbance rejection control. *Transactions of the Institute of Measurement and Control*, 42(12), 2198–2205.

Zhang, Y., Liu, J. & Yang, C. (2023). Neural Network-Based Cooperative Trajectory Tracking Control for a Mobile Dual Flexible Manipulator. *IEEE Transactions on Neural Networks and Learning Systems*.

Zhao, L., Yang, Y., Xia, Y. & Liu, Z. (2015). Active disturbance rejection position control for a magnetic rodless pneumatic cylinder. *IEEE Transactions on Industrial Electronics*, 62(9), 5838–5846.

Zhao, L., Li, Q., Liu, B. & Cheng, H. (2017). Trajectory tracking control of a one degree of freedom manipulator based on a switched sliding mode controller with a novel extended state observer framework. *IEEE Transactions on Systems, Man, and Cybernetics: Systems*, 49(6), 1110–1118.

Zhao, L., Liu, X. & Wang, T. (2019). Trajectory tracking control for double-joint manipulator systems driven by pneumatic artificial muscles based on a nonlinear extended state observer. *Mechanical Systems and Signal Processing*, 122, 307–320.

Zhao, L., Cheng, H. & Wang, T. (2018). Sliding mode control for a two-joint coupling nonlinear system based on extended state observer. *ISA Transactions*, 73, 130–140.

Zhong, G., Kobayashi, Y., Hoshino, Y. & Emaru, T. (2013). System modeling and tracking control of mobile manipulator subjected to dynamic interaction and uncertainty. *Nonlinear Dynamics*, 73(1), 167–182.

Zuo, Z. (2015). Non-singular fixed-time terminal sliding mode control of non-linear systems. *IET Control Theory & Applications*, 9(4), 545–552.